THE WAVEGUIDE DESIGN FOR WIDE BAND $Ti : LiNbO_3$ MACH-ZEHNDER INTENSITY MODULATORS

by
Geng Peng, B.Eng.

Department of Electrical Engineering
McGill University
Montreal, Quebec

January 1998

A thesis submitted to the Faculty of Graduate Studies and Research in partial fulfillment of the requirements for the degree of Master of Engineering

0-612-44101-6

Abstract

In this thesis, the waveguide design characterization for wide-band $Ti : LiNbO_3$ Mach-Zehnder electro-optical interferometric intensity modulators (Z-cut substrate) has been performed using a combination of the effective index method and the 2D finite-difference vectorial beam propation method (FD-VBPM). For the passive aspect of the device, to minimize the propagation loss, the coherent coupling effect of radiation modes has been studied as well as the effectiveness of a cosine-generated Y-branch and a notched Y-branch in comparison with the conventional sharp-bend Y-branch. By making use of the coherent coupling effect on a notched Y-branch structure, a propagation loss figure of 0.145 dB/cm has been achieved. For the active aspect including the electro-optical effect, the minimum seperation of the two waveguide arms in order to achieve an extinction ratio above 20 dB has been decided and the corresponding modulation curve obtained. The best achieved extinction ratio is 21.8 dB with a 15 μm seperation between the inner edges of two branching arms for a 80 GHz electrode design. Two different electrode structures have been design-tested and compared. Tolerance of the alignment between the optical waveguides and the electrodes has also been determined.

Résumé

Dans cette thèse, un modèle de guide d'ondes utilisant des modulateurs d'intensité $Ti : LiNbO_3$ (substrat de coupe Z), à bande passante large, électro-optiques et interférométriques (Mach-Zehnder), a été caractérisé par une combinaison de la méthode de l'index effectif et de la méthode par propagation de faisceaux vectoriels 2D différence finie (FD-VBPM). En ce qui concerne les aspects passifs de cet appareil et afin de minimiser les pertes propagatives, l'effet de couplage cohérent des modes radiatifs à été étudié ainsi que l'efficacité d'une branche en Y cosinus-générée et d'une branche en Y encochée en comparaison avec une branche en Y à courbure prononcée conventionnelle. En utilisant l'effet de couplage cohérent, une perte propagative de 0.145 dB/cm a été réalisée. En ce qui concerne les aspects actifs incluant l'effet electro-optique, la séparation minimale de deux bras du guide d'ondes, afin d'atteindre un ratio d'extinction au dessus de 20 dB, a été choisie et la courbe de modulation y correspondant a été obtenue. Le meilleur ratio d'extinction réalisé est de 21.8 dB et ce ratio correspond à une séparation du bord interne de 15 μm pour un modèle d'électrode à 80 GHz. Deux structures d'électrodes ont été testées et comparées. La tolérance sur l'alignement entre les guides d'ondes et les électrodes a aussi été déterminée.

Acknowledgements

I would like to thank my supervisor, Dr. Gar Lam Yip, for suggesting the thesis topic and for his encouragement and guidance during the course of this research project. His careful correction of the first draft of this thesis is highly appreciated.

I am grateful to my former colleague, Dr. Peter C. Noutsios, currently working at Northern Telecom Inc., for his patient help and for many inspiring discussions during my research work. My gratitude also goes to my former collegue, Mr. Feng-Yuan Gan, for his contribution from a part of his computer programs and for every bit of support he has given to me. I also thank Mr. Fred Mathieu for the French translation of the abstract of this thesis.

An operating grant from the National Sciences and Engineering Research Council of Canada (NSERC) is acknowledged.

Contents

List of Figures

List of Tables

Chapter 1

Introduction

1.1 Background Overview

Optical fiber communication is being widely used nowadays mainly because of the wide bandwidth offered by optical carrier frequencies, the fiber's light weight, low loss over large distances, immunity to electromagnetic interference compared to coaxial cables, etc. To achieve a high performance optical fiber telecommunication system, high speed modulation is an essential part. There are several kinds of modulation techniques including intensity modulation, phase modulation, frequency modulation and polarization modulation in the field of telecommunication. As to the optical implementation, if phase modulation or frequency modulation is to be tried, there will be large amount of dispersion due to the difficulty to get a stable phase and narrow linewidth single mode source as well as extremely high quality single mode fiber [1]. On the other hand, because of its simplicity, commercial optical fiber systems tend to use intensity-modulated source with direct (envelope) detection although it has a relatively low frequency. At the same time, coherent and nonlinear lightwave communications are also being studied widely in order to make use of more efficient modulation techniques [2].

There are two ways of achieving lightwave intensity modulation: by direct modulation of laser source current or by external modulation of the laser beam [3]. In direct modulation, the modulation bandwidth is limited by the presence of relaxation oscillations and parasitic parameters in the laser [4]. Also, an increase in the carrier concentration causes a reduction of the refractive index and so changes the laser mode frequencies, so modulation of the drive current causes the output frequency to vary as well as the power. This phenomena is usually called "chirp" [5]. This broadening of line width will deteriorate the dispersion characteristic of the system [6]. Above two GHz, the laser must be biased well above the threshold, so the stability and lifetime of the laser will be sacrificed.

External modulation has been proved to be a very promising alternative. External modulation generally has the following advantages compared with internal modulation: 1) phase modulation becomes very easy; 2) easy to get 100 % modulation depth; 3) chirp free so that long distance and high bit rate communication is possible; 4) being able to modulate a variety of optical sources including some which can not be intensity-modulated at high frequencies [6]. The disadvantages of external modulation include added complexity, polarization sensitivity and additional insertion loss. Fig. 1.1 shows two RF fiber-optic links using direct modulation and external modulation respectively as an illustration of their different system configurations [7].

There are mainly two kinds of external modulators. Bulk modulators were developed after the invention of laser several decades ago. They were external modultors at an early stage. Diffraction effects prohibit making bulk modulators with both the small lateral dimensions and long interaction length needed to achieve low drive power [8]. Another type is the waveguide version of modulators which use coplanar waveguides to guide the optical wave in the interaction region. Waveguide modulators were developed with the rapid reduction of loss in glass fibers in the late 1960's. They have good compatibility with fibers and have good integration potential. Also, the drive power requirement is reduced compared with bulk modulators. Among the potential materials to serve as substrates of waveguide modulators that can be used to achieve both a wide bandwidth and a low driving power, $Ti : LiNbO_3$ and semiconductors are good candidates. $Ti : LiNbO_3$ optical waveguide modulators are considered to be the best candidate for near-future high-speed transmission systems for the

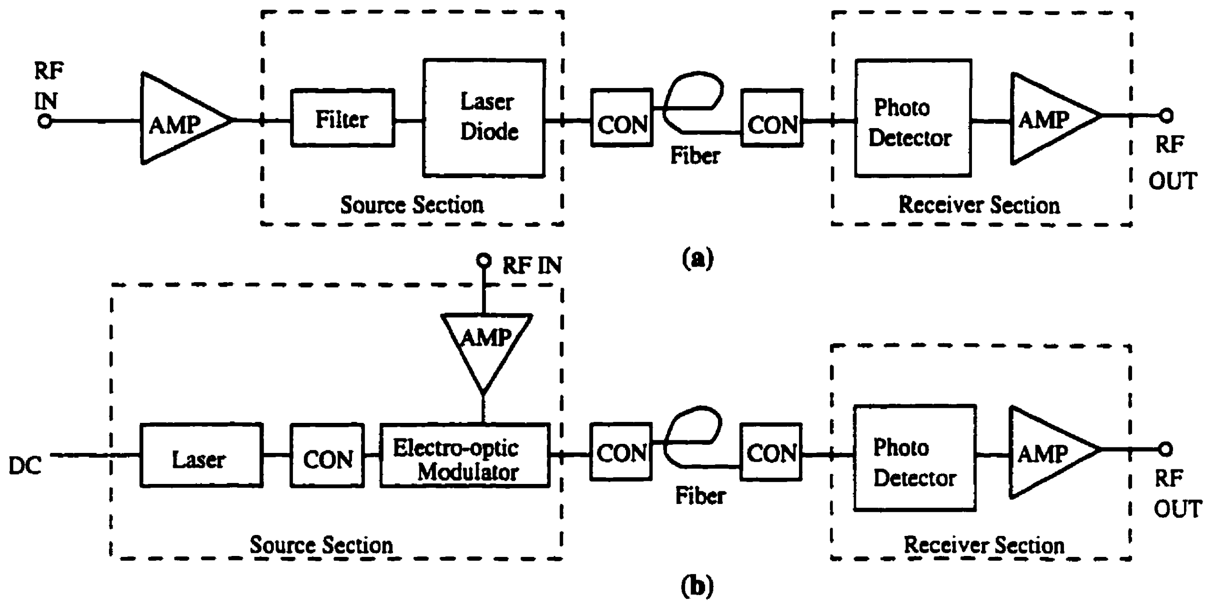

Figure 1.1: RF Fiber-optic links. (a) direct modulation, (b) external modulation.

simplicity in both its structure and fabrication process and low insertion loss. On the other hand, semiconductor optical waveguide modulators have their own attractive features, including the possibility of monolithically integrating modulators and other functional devices [9].

1.2 Mach-Zehnder Interferometric Intensity Modulator Design

The electro-optic Pockels effect of lithium niobate substrate forms the basis of $Ti:LiNbO_3$ modulators. It can be described as a change in a material's (electro-optical crystal) refractive index proportional to the applied external electric field. For anisotropic dielectric crystals, their responses to fields with different orientations or polarizations can differ. Uniaxial crystals like lithium niobate are crystals with one axis of symmetry and an index spheroid. The axis of symmetry is called the optical axis (denoted by Z). Along this axis, the refractive index is called extraordinary index (n_e) in contrast with ordinary index (n_o) on the $X-Y$ plane. In practice, an external electric field is mostly applied (by applying a voltage to the electrodes which are deposited over the crystal surface) along the optical axis (Z) because the electrooptic coefficient is the largest in this direction or along the x or y axis of the coordinate system (z represents the propagation direction of the wave in the coordinate system which should not be confused with the crystal axes).

Channel waveguides are formed in the substrate by titanium in-diffusion to guide optical carrier wave. Planar electrodes can either be placed on either side of the waveguide for X-cut Y-propagating (or Y-cut X-propagating) crystals, or one electrode can be placed directly over the waveguide for Z-cut orientation crystals (which will be the case to be studied in this project). In either case, the crystal orientation is normally chosen to use the largest electrooptic coefficient. In the latter case, a thin S_iO_2 buffer layer is often used to minimize the optical loss and waveguide loading due to the presence of the metal electrodes [10]. Sometimes buffer layers are employed to maintain high electrode impedance. Often, light is chosen to be polarized along the optical axis Z to take advantage of the extraordinary index and the stongest r_{33} electrooptic coefficient. The electrooptically induced index change is [8]:

$$\Delta n_e = -\frac{n_e^3}{2} r_{33} E \tag{1.1}$$

which causes, consequently, a phase shift of the propagating light wave in the crystal:

$$\Delta \beta z = \frac{\omega \Delta n_e}{c} z \tag{1.2}$$

The Y-branch Mach-Zehnder interferometric intensity modulator is like two parallel phase modulators. The input light is splitted into two equal parts and then after passing the so-called "active region", recombined into one beam of light. With no applied voltage, there will be zero phase shift between the two branches and thus the two will add and get the origional light intensity; with an applied voltage strong enough to cause a π relative phase shift the two branches cancel and give zero output; with a relative phase shift between zero and π, the output intensity will be between zero and maximum. So a 100 % modulation depth is possible [11]. A push-pull structure as shown in Fig. 1.2 is often employed to improve efficiency. Since phase shifts for the two branches will have different signs, a $\pi/2$ phase shift for each branch

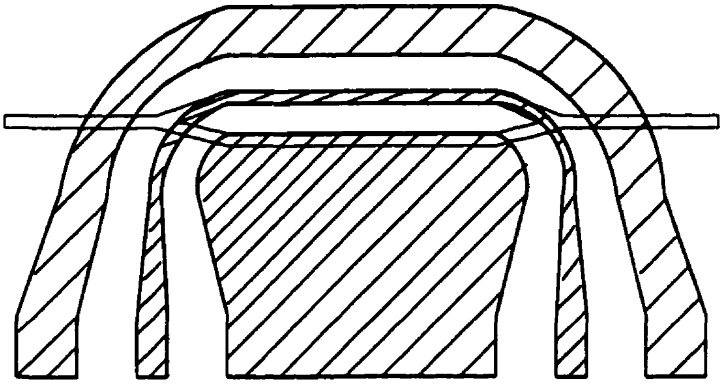

Figure 1.2: Top view of a typical Y-branch M-Z modulator

will be enough to achieve a total output cancellation. The drive voltage requirement is thus reduced by half.

The three-electrode structure as used in Fig. 1.2 is called a CPW (Coplanar Waveguide) electrode configuration. Compared with other two configurations, namely the CPS (Coplanar Strip) and ACPS (Asymmetric Coplanar Strip) which have large unmetalized area, the CPW configuration will have a lower microwave loss [12] [13]. Also, the CPW electrode structure facilitates a good connection to an external microwave circuit (using coaxial cables usually) [14] which is necessary for a travelling wave electrode type (The goal of the traveling-wave electrode is to make the electrodes appear as an extension of the driving transmission line. As such, it should have the same characteristic impedance as the source and cable. In this case, the modulator speed is not limited by the electrode charging time as what happens with a lumped electrode type and limits the potential modulation speed, but rather by the difference in the transit times for the optical and modulating RF waves [8].)

In general, in order to achieve highly efficient integrated optical devices, rigorous computer-aided modelling and simulation has to be conducted because it can minimize time and cost in realizing new designs [15]. For active components like $Ti : LiNbO_3$ M-Z modulators, neither an electrode analysis nor a waveguide analysis can expect to find any closed form analytical solutions. We must resort to using numerical techniques [16] which would yield accurate design results but demand the use of computers to perform extensive calculations.

There are basically four major characteristics of a $Ti : LiNbO_3$ M-Z intensity modulator that have to be optimized during the design process, namely the bandwidth, the drive power, the propagation loss and the extinction ratio. The bandwidth determines the speed limit of the device and thus is the parameter with the most concern. As we know, by using a single-mode fiber at or near the zero dispersion wavelength, the effective bandwidth of the fiber is typically not a limiting factor in link performance [7]. Also for the modulator itself, since the electrooptic effect is an electronic phenomenon that has a subpicosecond response time, the achievable modulation speed depends mainly upon the electrode design [17]. It has been found that the biggest factor that limits the bandwidth of the modulator is the velocity mismatch between the optical waves (carrier) and microwave waves (signal) carried by the travelling-wave electrodes [10] [3]. There are several velocity matching techniques in the literature: 1) thick electrodes with a thick buffer layer [18]; 2) an etched groove into substrate [19]; 3) periodic (phase shifted) electrodes [20]; 4) a shield plane over the electrodes [21]; 5) a ridge structure (with thick electrodes and a buffer layer) [14] [18] [22]. A thorough study and analysis can be found in [23] as the part covering the electrode design for $Ti : LiNbO_3$ Mach-Zehnder modulators done by Mr. F. Y. Gan in our Guided-Wave Photonics Laboratory as his master's project.

For optical waveguide characterization, since 3D waveguides surrounded by different dielectric materials just support two families of hybrid modes (some times called TE-like and TM-like depending upon whether the main electric field component lies in the x or y direction) instead of pure TE and TM modes, the analysis of the waveguides is much more complex than that of planar 2D waveguides, and no exact analytical modal solutions are available. Also, in practical use, optical waveguide devices generally require single-mode waveguides in which light is as strongly confined as possible to minimize the scattering loss due to optical bending or branching [24], which means only the lowest TE-like or TM-like mode exists. Among various numerical techniques in tackling the simulation and design of single-mode 3D optical waveguides, the beam propagation method has been proved to be a very powerful tool to simulate wave propagation in structures of great complexity leading to accurate designs.

The BPM method is very usful because: 1) it handles both the guided and the radiation modes within the same simple formulas; 2) it can analyze devices with structural variations along the propagation direction; 3) it provides detailed information about the optical field. However, a three–dimensional BPM analysis of a typical device usually requires a lot of computation power. It can be reduced by a factor of several hundred if a 2D BPM can provide acceptable results. To perform the 2D BPM analysis of a channel waveguide device, one must transform the 2D transverse refractive index profile of a channel waveguide into a 1D effective index profile. In this project, an effective index method (EIM) based on a Runge–Kutta algorithm is to be used to do this job.

Aiming at lowering the propagation loss and increasing the extinction ratio, an efficient method to simulate $Ti : LiNbO_3$ waveguide from its fabrication parameters will be used in this project, which can be summarized as: (1) a 2D refractive index profile of waveguides is built; (2) the 2D transverse refractive index profile is transformed to a 1D effective index profile and its effective modal field and propagation constant is found using the same EIM method; (3) a 2D beam propagation method with appropriate boundary conditons is applied to the conventional Y-branch to find the output optical field distribution; (4) structural propagation loss is evaluated and optimized by adjusting the local dimensions of the waveguide; (5) other kinds of Y-branch structures will be tested to help further improve loss characteristic; (6) incorporating the electro-optical effects with an externally applied voltage, the 2D refractive index profile is remodelled, and steps 2) through 4) are performed once again to optimize the extinction ratio parameter.

1.3 Chapter Description

In Chapter 2, the refractive index distribution of Ti diffused waveguide in $LiNbO_3$ is first modelled based on the fabrication parameters and under certain approximations. The 1D effective index profile as well as the effective propagation constant and modal field of this resulting slab gradient index waveguide are found using a Effective Index

Method that employs a Runge-Kutta scheme and the Secant root-search method.

Chapter 3 describes the famous "2D Finite-Different Beam Propagation Method" along with the "Transparent Boundary Conditions" and uses them to simulate wave propagation inside the waveguide. Detailed mathematical derivations are presented as appendices. The propagation loss is evaluated and the coherent coupling effect of radiation modes is observed and studied which leads to a non-classical way of optimizing propagation loss.

Chapter 4 explores two types of Y-branches other than the traditional sharp-bend Y-branch: the cosine-generated S-bend Y-branch and the notched Y-branch. The effectiveness of each structure is studied.

Chapter 5 deals with the active aspect of the waveguide design, aiming at optimizing the extinction ratio and on-off voltage by changing the longitudinal waveguide dimensions, electrode types and waveguide/electrode alignment.

Chapter 6 serves as a summary to all the work that has been done in the author's master's project, and suggestions for future implementation are also made.

Bibliography

[1] John Senior, *Optical Fiber Communications: Principles and Practice*, Prentice-Hall, pp. 320, 1985

[2] Milorad Cvijetic, *Coherent and nonlinear lightwave communications*, Artech House, 1996

[3] Weidong Wang, Boyu Wu, Deje Li, Jihu Peng, Keqian Zhang, "Fully Packaged High-Speed $Ti : LiNbO_3$ Waveguide Mach-Zehnder Intensity Modulator," *Fiber and Integrated Optics*, vol. 12, pp. 83–88, 1993

[4] A. H. Gnauck, T. E. Darcie and G. E. Bodeep, "Comaprison of Direct and External Modulation for CATV Lightwave Transmission at 1.5 μm Wavelength", *Electronics Letters*, vol. 28, No. 20, pp. 1875–1876, 1992

[5] John Gowar, *Optical Communication Systems*, Prentice-Hall, pp. 404,544, 1993

[6] Roger L. Jungerman, *et al.*, "High-Speed Optical Modulator for Application in Instrumentation," *J. of Lightwave Technology*, vol. 8, no. 9, pp. 1363–1370, 1990

[7] W. E. Stephens, T. R. Joseph, "System Characteristics of Direct Modulated and Externally Modulated RF Fiber-Optic Links", *Journal of Lightwave Technology*, vol. LT-5, No. 3, pp. 380–387, 1987

[8] R. C. Alferness, "Waveguide Electrooptic Modulators," *IEEE Transactions on Microwave Theory and Techniques*, vol. MTT–30, No. 8, pp. 1121–1137, 1982

[9] Kenji Kawano, "High-Speed $Ti : LiNbO_3$ and Semiconductor Optical Modulators", *IEICE Trans. Electron.*, vol. E76-C, No. 2, pp. 183–190, 1993

[10] Haeyang Chung, William S. C. Chang, Eric L. Adler, "Modeling and Optimization of Traveling-Wave $LiNbO_3$ Interferometric Modulators," *IEEE J. of Quantum Electronics*, vol. 27, no. 3, pp. 608–617, 1991

[11] Simon Ramo, John R. Whinnery, Theodore Van Duger, *Fields and Waves in Communication Electronics*, John Willey & Sons, pp. 689–703, 1984

[12] Ganesh K. Gopalakrishnan, *et al.*, "Performance and Modeling of Broadband $LiNbO_3$ Traveling Wave Optical Intensity Modulators," *J. of Lightwave Technology*, vol. 12, no. 10, pp. 1807–1891, 1994

[13] G. K. Gopalakrishnan, W. K. Burns, C. H. Bulmer, "Electrical Loss Mechanics in Traveling Wave $LiNbO_3$ Optical Modulators," *Electronic Letters*, vol. 28, no. 2, pp. 207–209, 1992

[14] Kazuto Noguchi, Osamu Mitomi, Hiroshi Miyazawa, Shunji Seki, "A Broadband $Ti : LiNbO_3$ Optical Modulator with a Ridge Structure," *J. of Lightwave Technology*, vol. 13, no. 6, pp. 1164–1168, 1995

[15] K. T. Koai and P. L. Liu, "Modeling of $Ti : LiNbO_3$ Waveguide Devices: Part I — Directional Couplers", *J. of Lightwave Tech.*, Vol. 7, No. 3, pp. 533-539, 1989

[16] D. Marcuse, *Theory of Dielectric Optical Waveguides*, Academic Press, 1991, Chapter 8. Approximate and Numerical Methods

[17] R. C. Alferness, *Guided-Wave Optoelectronics: 4. Titanium-Diffused Lithium Niobate Waveguide Devices*, Springer-Verlag, pp. 145–211, 1988

[18] K. Noguchi, O. Mitomi, K. Kawano, M. Yanagibashi, "Highly Efficient 40-GHz Bandwidth $Ti : LiNbO_3$ Optical Modulator Employing Ridge Structure," *IEEE Photonics Technology Letters*, vol. 5, no. 1, pp. 52–54, 1993

[19] H. Haga, M. Izutsu, T. Sueta, "$LiNbO_3$ Traveling-Wave Light Modulators/Switch with an Etched Groove," *IEEE J. of Quantum Electronics*, vol. QE-22, no. 6, pp. 902–906, 1986

[20] J. H. Schaffner, R. Hayes, "Velocity-Matching in Millimeter Wave Integrated Optic Modulators with Periodic Electrodes," *J. of Lightwave Technology*, vol. 12, no. 3, pp. 503–511, 1994

[21] K. Kawano, T. Kitoh, H. Jumonji, T. Nozawa, M. Yanagibashi, "New Traveling-Wave Electrode Mach-Zehnder Optical Modulator with 20 GHz Bandwidth and 4.7v Driving Voltage at 1.52 μm Wavelength," *Electronics Letters*, vol. 25, no. 20, pp. 1382–1383, 1989

[22] K. Noguchi, K. Kawano, "Proposal for $Ti : LiNbO_3$ Optical Modulator with Modulation Bandwidth of More Than 150 GHz," *Electronics Letters*, vol. 28, no. 18, pp. 1759–1761, 1992

[23] F. Y. Gan, *Traveling Wave Electrode Design For High Speed $LiNbO_3$ Intensity Modulators*, Master's Thesis, McGill University, 1996

[24] M. Born and E. Wolf, *Principles of Optics*, Pergamon, NY, pp. 665–681, 1980

Chapter 2

Modelling of a $Ti : LiNbO_3$ Waveguide by the Effective Index Method

To better outline the schemes used to model the $Ti : LiNbO_3$ waveguide in a Mach–Zehnder intensity modulator, a schematic diagram of the cross–sectional view of such a device is given for its active region (see Fig. 2.1). A coordinate system with z as the propagation direction and y the depth direction is chosen. The device to be studied uses a Z-cut $LiNbO_3$ substrate, and the externally applied electric field passes through the waveguides in the depth direction along the optical axis. Therefore, the extraordinary refractive index is seen by the electric field. Also, the optical field is polarized along the depth (y) direction.

In the following descriptions, we will first assume that we are dealing with an isotropic substrate with a bulk refractive index n_e (the extraordinary refractive index of $LiNbO_3$, which is actually an anisotropic material). The formulas for anisotropic medium are derived in *Section 3.3.2* as a reference, which shows that for a reduced dimension case (from 3D to 2D) and a TE_0 mode, there will be no risk in making the above assumption because the simplifications lead to exactly the same formulas as those for an isotropic case.

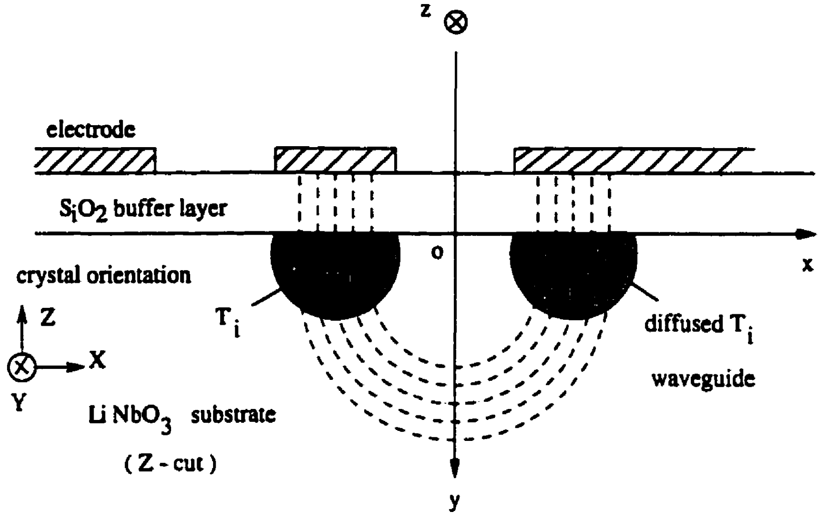

Figure 2.1: A schematic diagram of the cross–sectional view of a Mach–Zehnder $Ti : LiNbO_3$ waveguide intensity modulator on a Z-cut substrate

2.1 Modelling of Ti-diffused Channel Waveguide in $LiNbO_3$

To relate the refractive index profile of a $Ti : LiNbO_3$ waveguide with fabrication conditions and parameters, we have to start with the in–diffused titanium concentration distribution. In most single mode $Ti : LiNbO_3$ waveguides, the maximum titanium concentration is less than 2 percent of that of the pure titanium metal [4]. The titanium concentration distrubution of the active part (with two parralel waveguides) in a M–Z modulator can be expressed as (formed by diffusing two titanium strips with a width w, a thickness τ, and a small gap d, into the substrate as shown in Fig. 2.2) [5]:

$$C(x, y) = G(x - \frac{w}{2} - \frac{d}{2}, y) + G(x + \frac{w}{2} + \frac{d}{2}, y) \qquad (2.1)$$

where

$$G(x, y) = \frac{C_0}{2} e^{-(\frac{y}{D_B})^2} [erf(\frac{w/2 + x}{D_S}) + erf(\frac{w/2 - x}{D_S})] \qquad (2.2)$$

$G(x, y)$ represents the transverse distribution profile of titanium in a single waveguide and is called a double error function. D_S and D_B are the surface and bulk diffusion lengths, respectively. $C_0 = 2\alpha\tau/\sqrt{\pi} \cdot D_B$ is the normalization coefficient derived from

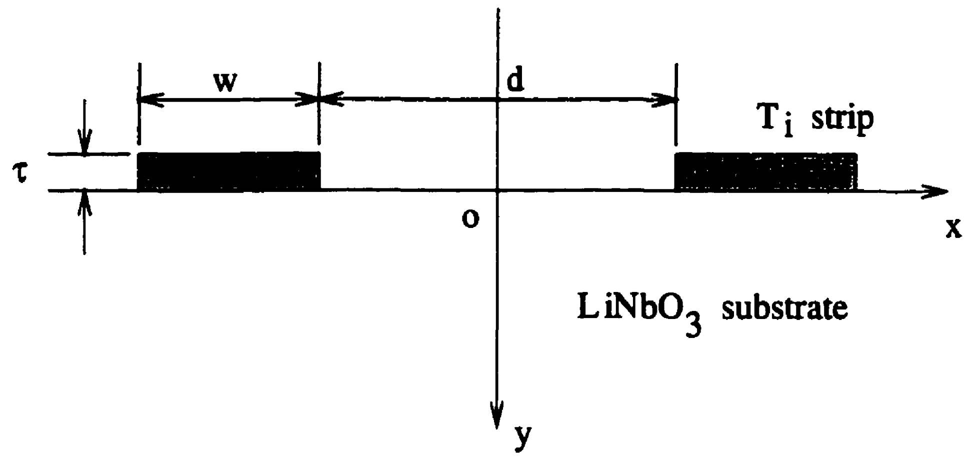

Figure 2.2: Geometry of Ti strips used to fabricate a $Ti : LiNbO_3$ M–Z modulator (the active part)

the law of conservation of matter [6] [7] [8], where α is the atomic density of the Ti film [6]. The diffusion lengths D_B and D_S can be calculated from:

$$D_{B,S} = 2\sqrt{D_{TB,TS}t} \tag{2.3}$$

where t denotes the diffusion time and D_{TB} and D_{TS} are the surface and bulk diffusion coefficients which are drawn from literature [4] [9] to be $D_{TB} = 2.18 \times 10^{-12}cm^2s^{-1}$ and $D_{TS} = 1.36 \times 10^{-12}cm^2s^{-1}$ under the fabrication condition of $1050°C$, 5 hours, and $500Å$ strip thickness.

The corresponding transverse profiles for the extraordinary refractive indices can be described by:

$$n_e(x, y, \lambda) = n_{eb}(\lambda) + \Delta n_e(x, y, \lambda) \tag{2.4}$$

where $n_{eb}(\lambda)$ is the bulk refractive index, and $\Delta n_e(x, y, \lambda)$ is the change of refractive index induced by the titanium diffusion. Measured wavelength dispersion of the bulk refractive indices can be found in literature [10] [11], where at $\lambda = 1.3\mu m$, $n_e = 2.146$, and $n_o = 2.2205$ (interpolated from [11]).

It has been found that the extraordinary index change Δn_e at a fixed wavelength varies almost linearly with the titanium concentration [5] [10]:

$$\Delta n_e(x, y, \lambda) = \alpha_e(C_0, \lambda)C(x, y) \tag{2.5}$$

where $\alpha_e(C_0, \lambda)$ represents a coefficient which is a near-linear function of wavelength and C_0. Inconsistant results have been reported in the literature about the coefficient α_e at a particular C_0 and λ. The inconsistency could have resulted from variations in the crystal quality, sample preparation, diffusion process, density variations of the deposited titanium films, and calibration procedures. Some efforts have been made to get an interpolation formula to describe the dispersion of α_e [9] [10], and in [10] the linear relation has also been modified in the higher wavelength region (1.3–1.6 μm) which is of great interest in optical communications. However, the accuracy and generality of these formulae have to be further proved though they are not very complicated. Hence, in the initial design stage, the following simple refractive index distribution will be used:

$$n(x, y) = n_b + \Delta n_s f(y) g(x) \tag{2.6}$$

where $f(y)$ is a Gaussian function and $g(x)$ is a double error function which has different forms in different regions of the M-Z waveguide, both of which form the expression of $C(x, y)$ (Eq. (2.1)). Δn_s is the refractive index change at the crystal surface. Strictly speaking, we have $\Delta n_s = \alpha_e(C_0, \lambda) \times C_0$. A good approximation of this relation (especially at not too long a wavelength) can be found in many papers to be $\Delta n_s = 0.66 \times C_0/\alpha$ [5]. From the law of conservation we can obtain the relationship between C_0/α and the fabrication parameters as $C_0/\alpha = 2\tau/\sqrt{\pi} \cdot D_B$, and the bulk diffusion depth D_B is given by $D_B = 2\sqrt{D_{TB}t}$. So, for $\tau = 500\mathring{A}$, $t = 5hrs$, and $1050°C$, $C_0/\alpha = 0.01424$ and $\Delta n_s = 0.0094$; for $\tau = 600\mathring{A}$ and with other conditions remaining the same, we get $C_0/\alpha = 0.0156$ and $\Delta n_s = 0.0103$. Hence, a conclusion could be drawn that under usual fabrication conditions, Δn_s is always around 0.01, more or less. Since our main focus will be on finding the structural effect rather than changing fabrication conditions, an approximation of $\Delta n_s = 0.01$ will be applied during the computations that follow.

It could be found from later derivations that $n^2(x, y)$ is used more often than $n(x, y)$, so the following approximation is usually used (since $\Delta n_s \ll n_b$)

$$\begin{aligned} n^2(x, y) &= n_b^2 + 2n_b \Delta n_s f(y) g(x) + \Delta n_s^2 f^2(y) g^2(x) \\ &\approx n_b^2 + 2n_b \Delta n_s f(y) g(x) \end{aligned} \tag{2.7}$$

With a perturbation introduced by an external electric field based on the electro-optical effect along the optical axis, the refractive index distribution will become

$$n(x,y) = n_b + \Delta n_s f(y) g(x) - \frac{n_b^3}{2}\gamma_{33} E(x,y) \tag{2.8}$$

$$n^2(x,y) \approx n_b^2 + 2n_b \Delta n_s f(y) g(x) - n_b^4 \gamma_{33} E(x,y) \tag{2.9}$$

To get the expression of $g(x)$ for different longitudinal sections, we divide the whole M–Z waveguide into seven regions where only the first four are significant and the last three are simply some kinds of duplicates of the first three due to the device symmetry. In Fig. 2.3, the first four sections and relating parameters are shown (some typical parameters are chosen for computation simplicity from literature), where l_1 denotes the input or output region, l_{21} denotes the taper region, l_{22} denotes the branching region, and l_3 denotes the active region with two parallel waveguides. The width of a single waveguide w and the seperation between the two parallel ones d are chosen in accordance with the electrode design which has already been performed in our laboratory in previous thesis [12].

As for the expression of distribution function $g(x)$ along the horizontal direction, for the input and output region:

$$g(x) = \frac{1}{2}[erf(\frac{w/2+x}{D_S}) + erf(\frac{w/2-x}{D_S})] \tag{2.10}$$

For the taper region (from $z = l_1$ to $l_1 + \frac{wl_2}{2d'}$, where $d' = (w+d)/2$):

$$g(x) = \frac{1}{2}[erf(\frac{\frac{w}{2} + (z-l_1)\frac{d'}{l_2} + x}{D_S}) + erf(\frac{\frac{w}{2} + (z-l_1)\frac{d'}{l_2} - x}{D_S})] \tag{2.11}$$

For the branching region (from $z = l_1 + \frac{wl_2}{2d'}$ to $l_1 + l_2$):

$$\begin{aligned} g(x) \;\; = \;\; & \tfrac{1}{2}\{erf(\tfrac{\frac{w}{2}+x-(z-l_1)\frac{d'}{l_2}}{D_S}) + erf(\tfrac{\frac{w}{2}-x+(z-l_1)\frac{d'}{l_2}}{D_S}) \\ & +erf(\tfrac{\frac{w}{2}+x+(z-l_1)\frac{d'}{l_2}}{D_S}) + erf(\tfrac{\frac{w}{2}-x-(z-l_1)\frac{d'}{l_2}}{D_S})\} \end{aligned} \tag{2.12}$$

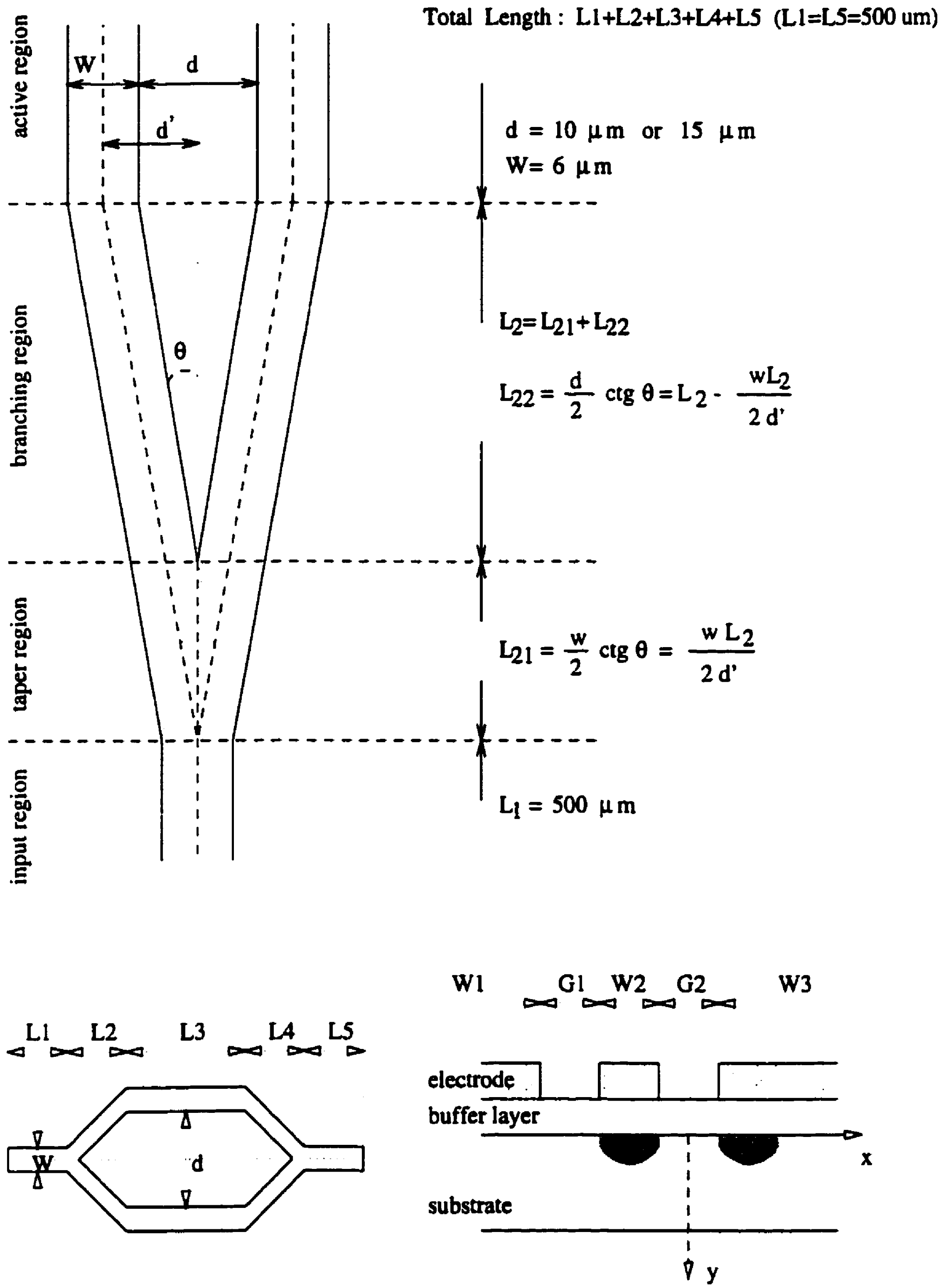

Figure 2.3: Schematic diagrams of the waveguide structure of a M-Z intensity modulator

For the active region:

$$g(x) = \frac{1}{2}[erf(\frac{x - d/2}{D_S}) + erf(\frac{w - x + d/2}{D_S}) + erf(\frac{w + x + d/2}{D_S}) + erf(\frac{-x - d/2}{D_S})] \quad (2.13)$$

The unique characteristic of the above modelling is that the taper and the branching region are treated seperately with different expressions of the x-direction distribution, not like that in reference [13] where they are treated as a whole and unfortrunately discontinuity occured at the point where input region meets taper region. By using the above modelling, the refractive index distribution along the propagation direction is continuous and smooth (but the maximum value will not be constant), so that any simulation afterwards based on it will surely be more accurate and making more sense.

First things first, before anything further could be done, we must find error function values. The definition of an error function is:

$$erf(x) = \frac{2}{\sqrt{\pi}} \int_0^x e^{-t^2} dt \quad (2.14)$$

with a series expansion form of:

$$erf(x) = \frac{2}{\sqrt{\pi}}(x - \frac{x^3}{1!3} + \frac{x^5}{2!5} - \frac{x^7}{3!7} + \cdots) \quad (2.15)$$

which shows that the error function is odd and only numerical methods could be used to get its discrete values. In this paper, the Simpson's integration rule is applied with a step size 0.001 and symmetry of the function itself is used. In case the integration's upper limit is less than 0.001, or when an extra region is left at the upper end because of the special requirement of the Simpson's rule that the number of internal points should be even, a trapezoidal rule is applied. The accuracy should not deteriorate very much since the integration region covered by the trapezoidal rule is so small. Tests prove that this combination is a farely fast way of obtaining error function values.

2.2 Effective Index Method Using a Runge-Kutta Algorithm

In an early paper published in 1970 [1], Knox and Toulios first developed the effective index method (on rectangular waveguides), which is difficult to derive as an approximation of an inherently exact mathematical procedure, but which has an obvious intuitive appeal [2]. Comparisons of the results of the effective index method with exact methods, in cases where such comparisons are possible, often show that the effective index method is more accurate than might have been expected. Since their work, essentially the same technique has been extended to optical waveguides with an arbitrary transverse index distribution. However, in both [2] and [3], it has been pointed out that even though the effective index method yields a very accurate value for the modal propagation constant, it gives distorted values for the modal field. Hence, we only use this method to calculate the 1D effective index distribution of a transversely 2D channel waveguide before implementing a 2D FD–VBPM to find out the field distribution.

2.2.1 General Methodology Description

Starting from the very original Maxwell's equations, the following Helmholtz vector wave equations for the electric field and for the magnetic field could be obtained

$$\nabla^2\vec{E} + \nabla(\vec{E} \cdot \frac{\nabla n^2}{n^2}) + k_0^2 n^2 \vec{E} = 0 \tag{2.16}$$

$$\nabla^2\vec{H} + \frac{1}{n^2}(\nabla n^2) \times (\nabla \times \vec{H}) + k_0^2 n^2 \vec{H} = 0 \tag{2.17}$$

where $k_0^2 = \omega^2\mu_0\epsilon_0$. If the second term in (2.16) and (2.17) are neglected, they become scalar wave equations. With pactical systems, this will introduce little error, especially when the variation of the dielectric constant is small in distances of the order of the wavelength (this is almost always true, particularly for optical beams). However, since we are going to use the vectorial beam propagation method in the next stage of our waveguide design, in order to maintain enough accuracy so as not to ruin the accuracy of the VBPM later on, we keep the second term here.

If we consider the evolution of the transverse electric field in a channel waveguide (in the case of a Z-cut M-Z intensity modulator on $LiNbO_3$, if the Cartesian coordinate system is chosen so that y is along the depth direction, the optical field will always be polarized and lauched in y direction, so only the E_y component will be considered like that in a TM mode) in space and time of the form

$$\vec{E_t} = \vec{\psi_t} e^{-jk_0 n_0 z} \tag{2.18}$$

And the y component is:

$$E_y = \psi_y e^{-jk_0 n_0 z} \tag{2.19}$$

Since our aim is to find the local effective index distribution of a channel waveguide, we assume now that the only z dependent term of E_y is the propagation term and that ψ_y depends on x and y only (we will not make this assumption when the VBPM formulas are derived). Hence, writing out the y component of (2.16) and make use of (2.19) and the above assumpsion, we have

$$\frac{\partial^2 \psi_y}{\partial x^2} + \frac{\partial^2 \psi_y}{\partial y^2} + [k_0^2 n^2 - \beta^2]\psi_y + \frac{\partial}{\partial y}[\frac{1}{n^2}\frac{\partial n^2}{\partial y}\psi_y] = 0 \tag{2.20}$$

Let [14]

$$\psi_y(x, y) = F(x, y)G(x) \tag{2.21}$$

and assuming that $F(x, y)$ is a slowly varying function of x. Substituting (2.21) into (2.20), we have

$$F\frac{\partial^2 G}{\partial x^2} + G\frac{\partial^2 F}{\partial x^2} + 2\frac{\partial F}{\partial x}\frac{\partial G}{\partial x} + G\frac{\partial^2 F}{\partial y^2} + [k_0^2 n^2 - \beta^2]FG + G\frac{\partial}{\partial y}[\frac{1}{n^2}\frac{\partial n^2}{\partial y}F] = 0 \tag{2.22}$$

Defining $n_{eff}(x)$ such that

$$\frac{\partial^2 G}{\partial x^2} + [k_0^2 n_{eff}^2(x) - \beta^2]G = 0 \tag{2.23}$$

$$F\frac{\partial^2 G}{\partial x^2} + [k_0^2 n_{eff}^2(x) - \beta^2]FG = 0 \tag{2.24}$$

Substract (2.22) by (2.24), we have

$$G\frac{\partial^2 F}{\partial x^2} + 2\frac{\partial F}{\partial x}\frac{\partial G}{\partial x} + G\frac{\partial^2 F}{\partial y^2} + [k_0^2 n^2(x, y) - k_0^2 n_{eff}^2(x)]FG + G\frac{\partial}{\partial y}[\frac{1}{n^2}\frac{\partial n^2}{\partial y}F] = 0 \tag{2.25}$$

which can be reduced to a 1D problem in y direction for $F(x,y)$ (with x as a parameter) by assuming that most of the variation in x is taken by $G(x)$ and that the first and second terms in (2.25) are negligible. Cancelling G in each of the remaining terms, (2.25) becomes

$$\frac{\partial^2 F}{\partial y^2} + \frac{\partial}{\partial y}[\frac{1}{n^2}\frac{\partial n^2}{\partial y}F] + [k_0^2 n^2(x,y) - k_0^2 n_{eff}^2(x)]F = 0 \tag{2.26}$$

By solving (2.26), the local effective index $n_{eff}(x)$ (along with $F(x,y)$) is found for all the values of x and substituted into (2.23) (also a 1D waveguide problem) to yield $G(x)$ and the effective propagation constant β of the channel waveguide.

If the original two dimensional waveguide has an arbitrary refractive index profile $n(x,y)$ or $n(x,y)$ is not one of the several forms which are known to lead to analytical solutions, a numerical method must be applied and the effective index profile $n_{eff}(x)$ must be determined pointwise from (2.26), i.e., for each point x_i, $n_{eff}(x_i)$ has to be calculated numerically [14] [15].

From equation (2.26), it can be seen that for each x_i, the problem is the same as solving for the effective propagation constant $\beta_d = k_0 n_{eff}(x_i)$ for a (TM_0) wave travelling in a one-dimensional (y) slab waveguide having an inhomogeneous refractive index profile $n(x_i, y)$ (which is Gaussian in the depth direction). After a pointwise distribution of the effective index has been obtained along the x axis, the problem changes to a (TE_0) wave travelling in a one-dimensional (x) slab waveguide having a symmetric gradient refractive index profile $n_{eff}(x_i)$. A diagram (Fig. 2.4) is drawn to illustrate the physical meaning of such a process.

To solve the one variable second-order ordinary differential equation like (2.26) for the effective index distribution or (2.23) for propagation constant and field distribution, quite a few methods could be used including the Rayleigh–Ritz variational procedure with Hermite–Gaussian basis functions [14], Vessell's matrix formulism [15], and the WKB method [16] [17] [18]. Here, we use the method presented by Kaul, Hosain and Thyagrajan in [19] and Mishra and Shama in [20]. This method consists of transforming the second-order differential equation into a first order differential equation

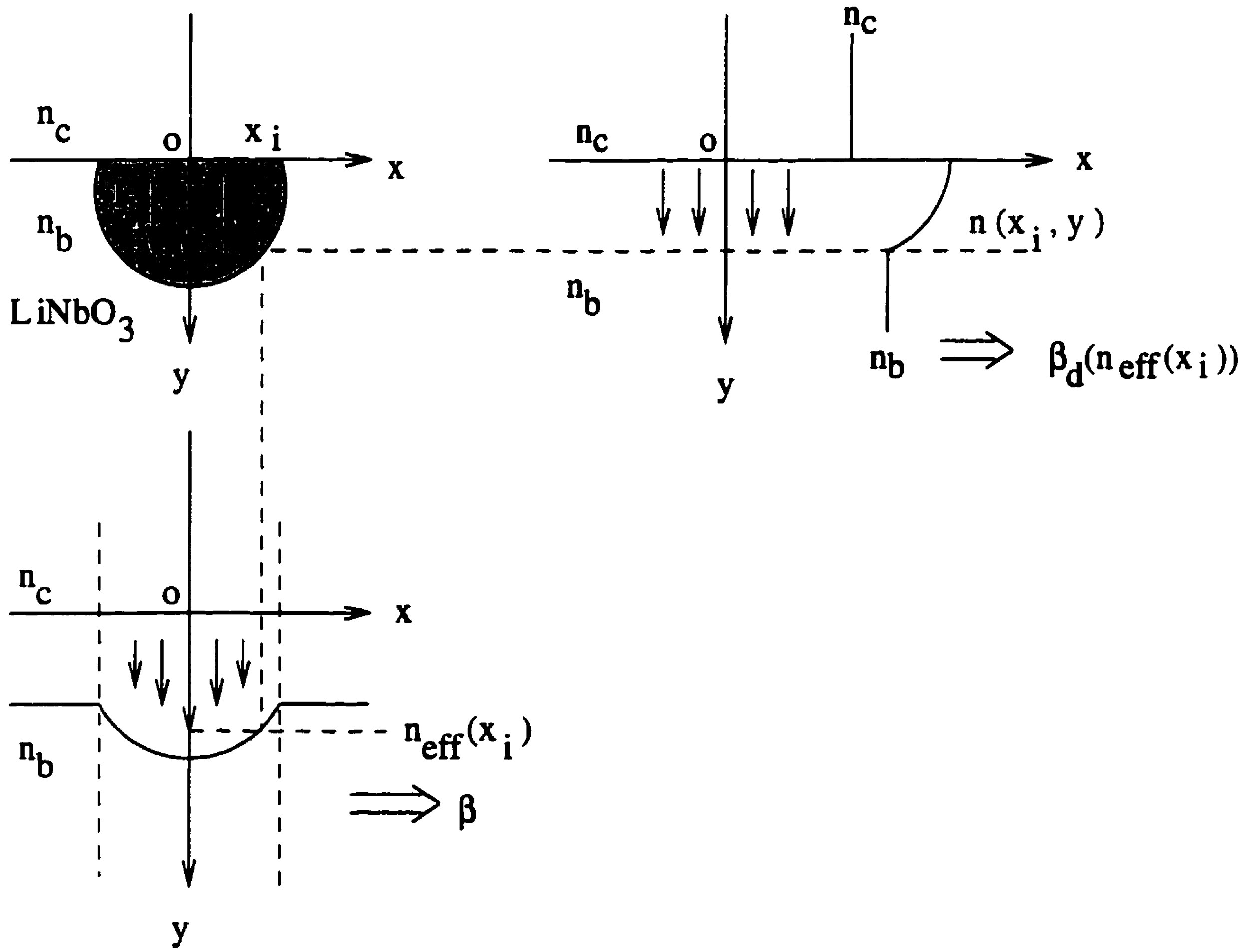

Figure 2.4: A schemetic representation of the present method to determine the propagation constant of the modes in a two dimensional waveguide with arbitrary cross-sectional shape and refractive index profile.

by a suitable substitution, and then solving it by a Runge–Kutta algorithm [21].

For a Z-cut M–Z intensity modulator, in a coordinate system with y as the depth direction, the input optical field is always polarized in the y direction in order to coincide with the externally applied electric field and the optical axis of $LiNbO_3$. Thus, equation (2.26) has to be solved for TM_0 (as we will allow only single mode in the waveguide). Since $\psi_y(x,y) = F(x,y)G(x)$, the function F will have all the same distribution characteristics and fulfill the same boundary conditions as ψ_y or E_y.

For a TM_0 mode in a slab waveguide, at the dielectric interface, the boundary conditions demand the continuity of H_x (and thereby of ϵE_y) and of $(1/n^2)(\partial H_x/\partial y)$ (and thereby of E_z) [22]. In order to use these conditions to solve (2.26), for each x_i, let

$$\phi(x_i, y) = n(x_i, y)F(x_i, y) \tag{2.27}$$

and (2.26) can be transformed into (for each x_i)

$$\frac{d^2\phi}{dy^2} + \{k_0^2 n^2(x_i, y) + \frac{1}{2n^2}\frac{d^2n^2}{dy^2} - \frac{3}{4}(\frac{1}{n^2}\frac{dn^2}{dy})^2 - k_0^2 n_{eff}^2(x_i)\}\phi = 0 \tag{2.28}$$

The above equation is once again transformed, by defining

$$K(\rho) = \frac{1}{\phi}\frac{d\phi}{d\rho} \tag{2.29}$$

with $\rho = y/a$ (a the effective depth of diffusion, $a = D_B$), to

$$\frac{dK}{d\rho} = -K^2 - a^2k_0^2[n^2(x_i, \rho) - n_{eff}^2(x_i)] + \frac{3}{4}(\frac{1}{n^2}\frac{dn^2}{d\rho})^2 - \frac{1}{2n^2}\frac{d^2n^2}{d\rho^2} \tag{2.30}$$

where

$$n^2(x_i, \rho) \simeq n_b^2 + 2n_b\Delta n f(\rho) \tag{2.31}$$

without electric field perturbation;

$$n^2(x_i, \rho) \simeq n_b^2 + 2n_b\Delta n f(\rho) - r_{33}n_b^4 E_y(x_i, a\rho) \tag{2.32}$$

with electric field perturbation; and

$$\Delta n = \Delta n_s g(x_i) \tag{2.33}$$

$$f(\rho) = e^{-\rho^2} \tag{2.34}$$

For $y \leq 0$, equation (2.28) becomes:

$$\frac{d^2\phi}{d\rho^2} - k_0^2 a^2 [n_{eff}^2 - n_c^2]\phi = 0 \tag{2.35}$$

with general solution:

$$\phi(x_i, \rho) = C_1 exp(k_0 a\sqrt{n_{eff}^2 - n_c^2}\rho) + C_2 exp(-k_0 a\sqrt{n_{eff}^2 - n_c^2}\rho) \tag{2.36}$$

where n_c is the index of the cover region, for silicon dioxide its value is the square root of 3.9, for air its value is 1.0. Since the modal field must vanish away from the surface, i.e. when $\rho \to -\infty$, $\phi \to 0$, the second solution must be rejected, making

$$\phi(x_i, \rho) \propto exp(W_c \rho), \quad \rho \leq 0 \tag{2.37}$$

where

$$W_c = a\sqrt{\beta_d^2 - k_0^2 n_c^2} = ak_0\sqrt{n_{eff}^2 - n_c^2} \tag{2.38}$$

From (2.29), we know the solution of K in the cover region is

$$K(\rho) = W_c, \quad \rho \leq 0 \tag{2.39}$$

For a large distance away from the surface into the substrate, say at $\rho = \rho_s$, the profile varies very slowly and the index is almost constant and equal to the substrate index n_b. Therefore, beyond this point we can assume that the solution of (2.28) is

$$\phi(x_i, y) \sim exp(-W_b \rho), \quad \rho \geq \rho_s \tag{2.40}$$

where

$$W_b = a\sqrt{\beta_d^2 - k_0^2 n_b^2} = ak_0\sqrt{n_{eff}^2 - n_b^2} \tag{2.41}$$

and

$$K(\rho) = -W_b, \quad \rho \geq \rho_s \tag{2.42}$$

The solutions in the three different regions, i.e., $\rho < 0$, $0 < \rho < \rho_s$, and $\rho > \rho_s$ are connected through the boundary conditions mentioned above. For TM_0 mode

$$\phi = nF \sim nE_y \sim \frac{H_x}{n} \tag{2.43}$$

$$E_z \sim \frac{1}{n^2}\frac{\partial H_x}{\partial y} \sim \frac{1}{n^2}\frac{\partial(n\phi)}{\partial y} \tag{2.44}$$

Hence, the continuity of H_x and E_z means

$$n\phi \quad and \quad \frac{1}{n^2}\frac{d(n\phi)}{d\rho} \tag{2.45}$$

are continuous.

$$\frac{1}{n^2}\frac{d(n\phi)}{d\rho}|_{\rho=0_+} = \frac{1}{n^2}\frac{d(n\phi)}{d\rho}|_{\rho=0_-}$$

$$\frac{1}{n^2}\frac{d(n\phi)}{d\rho} = \frac{1}{n^2}(n\frac{d\phi}{d\rho}+\phi\frac{dn}{d\rho}) = \frac{1}{n}\frac{d\phi}{d\rho}+\frac{\phi}{n^2}\frac{dn}{d\rho} = \frac{1}{n}\frac{d\phi}{d\rho}+\frac{\phi}{2n^3}\frac{dn^2}{d\rho} = \frac{n\phi}{n^2}(\frac{1}{\phi}\frac{d\phi}{d\rho}+\frac{1}{2n^2}\frac{dn^2}{d\rho})$$

Hence,

$$\frac{n\phi}{n^2}(\frac{1}{\phi}\frac{d\phi}{d\rho} + \frac{1}{2n^2}\frac{dn^2}{d\rho})|_{\rho=0_+} = \frac{n\phi}{n^2}(\frac{1}{\phi}\frac{d\phi}{d\rho} + \frac{1}{2n^2}\frac{dn^2}{d\rho})|_{\rho=0_-}$$

Since

$$n\phi|_{\rho=0_+} = n\phi|_{\rho=0_-}$$

$$K|_{\rho=0_+} = \frac{1}{\phi}\frac{d\phi}{d\rho}|_{\rho=0_+}$$

$$\frac{1}{n^2}|_{\rho=0_+} = \frac{1}{n_s^2 + 2n_s\Delta n} = \frac{1}{n_m^2}$$

$$\frac{1}{2n^2}\frac{dn^2}{d\rho}|_{\rho=0_+} = \frac{1}{2n_m^2}\frac{dn^2}{d\rho}|_{\rho=0_+}$$

$$\frac{1}{n^2}|_{\rho=0_-} = \frac{1}{n_c^2}$$

$$K|_{\rho=0_-} = \frac{1}{\phi}\frac{d\phi}{d\rho}|_{\rho=0_-} = W_c \quad (from\ (2.39))$$

$$\frac{1}{2n^2}\frac{dn^2}{d\rho}|_{\rho=0_-} = \frac{1}{2n_c^2}\cdot 0 = 0$$

Thus,

$$\frac{1}{n_m^2}(K|_{\rho=0_+} + \frac{1}{2n_m^2}\frac{dn^2}{d\rho}|_{\rho=0_+}) = \frac{W_c}{n_c^2}$$

$$K|_{\rho=0_+} = \frac{n_m^2}{n_c^2} W_c - \frac{1}{2n_m^2} \frac{dn^2}{d\rho}|_{\rho=0_+} \tag{2.46}$$

with $n_m = n\ |_{\rho=0_+}$, namely, the peak refractive index at the surface of the waveguide.

Similarly, from boundary continuities at $\rho = \rho_s$, we get

$$K|_{\rho=\rho_{s-}} = -\frac{n_f^2}{n_b^2} W_b - \frac{1}{2n_f^2} \frac{dn^2}{d\rho}|_{\rho=\rho_{s-}} \tag{2.47}$$

with $n_f = n\ |_{\rho=\rho_{s-}}$, namely, the refractive index at $\rho = \rho_{s-}$.

Hence, we have obtained the initial and final values of $K(\rho)$. Thus the transcendental equation to be solved is

$$K(\rho)|_{\rho=\rho_s} = -\frac{n_f^2}{n_b^2} W_b - \frac{1}{2n_f^2} \frac{dn^2}{d\rho}|_{\rho=\rho_{s-}} \tag{2.48}$$

and $K(\rho)|_{\rho=\rho_s}$ is obtained by solving (2.30) with the initial conditions (2.46), where a Runge–Kutta method could be used. Boundary conditions and expanded expressions involving n for situations with and without an electric field perturbation are listed in the following two subsections.

Before solving the transcendental equation, one has to choose a value of ρ_s and an initial guess value (or two initial guess values if the Secant method is to be used to find the root) of n_{eff} (or β_d). The following steps can be followed:

1. Choose a ρ_s, depending on the V value (smaller ρ_s for larger V values), say $\rho_s =$ 1 or 1.2, and two guess values of n_{eff} (between n_b and $n_b + \Delta n$). Use a Runge–Kutta method to get $K(\rho)$ at $\rho = \rho_s$ and thus $K(\rho)\ |_{\rho=\rho_s} + \frac{n_f^2}{n_b^2} W_b + \frac{1}{2n_f^2} \frac{dn^2}{d\rho}|_{\rho=\rho_{s-}}$ for each initial guess to see if they are close to 0.
2. Use the classic Secant root searching method to find a new value for n_{eff} which is used as one of the two new guesses (the other one from the previous guesses).
3. Increase ρ_s by a small step (this increase should be small enough to ensure the whole convergency, and should differ according to difference cover materials; in most of the computation a step size of 0.025 has been applied for SiO_2 cover), and plug the two new guesses into Step 1. for better accuracy.

4. The process from Step 1 to Step 3 is continued until the desired accuracy in n_{eff} is reached and further increase in the value of ρ_s does not change the n_{eff} value significantly.

Here, the classical fourth-order Runge–Kutta method is used:

$$K_{n+1} = K_n + \frac{1}{6}(k_1 + 2k_2 + 2k_3 + k_4)$$
$$k_1 = h\Gamma(\rho_n, K_n)$$
$$k_2 = h\Gamma(\rho_n + \frac{h}{2}, K_n + \frac{k_1}{2})$$
$$k_3 = h\Gamma(\rho_n + \frac{h}{2}, K_n + \frac{k_2}{2})$$
$$k_4 = h\Gamma(\rho_n + h, K_n + k_3)$$
$$n = 0, 1, \ldots, \frac{\rho_s}{h} - 1$$

where $\Gamma(\rho, K)$ represents the right hand side of (2.30) [21] and h is the step size. The associated truncation error is $\sim h^5$ to $\sim h^4$ when the whole process is convergent (which is not necessarily true under certain situations when ρ_s has been chosen too large initially). It has been found through practice that a proper step size h can affect the running speed very dramatically, and also this value should differ according to different cover material in order to ensure convergence (in most of the computation a step size of 0.025 has been applied for SiO_2 cover).

Fig. 2.5 shows the 3D distribution of the effective index distributions for both the taper and the branching region obtained by the above described method. The computation window is $40\mu m$ and the x step size is 0.1 μm.

2.2.2 Boundary Conditions Without an Applied Voltage

When there are no applied voltage, the boundary condtions for *Section 2.2.1* are

$$n_m^2 = n_b^2 + 2n_b\Delta n \tag{2.49}$$

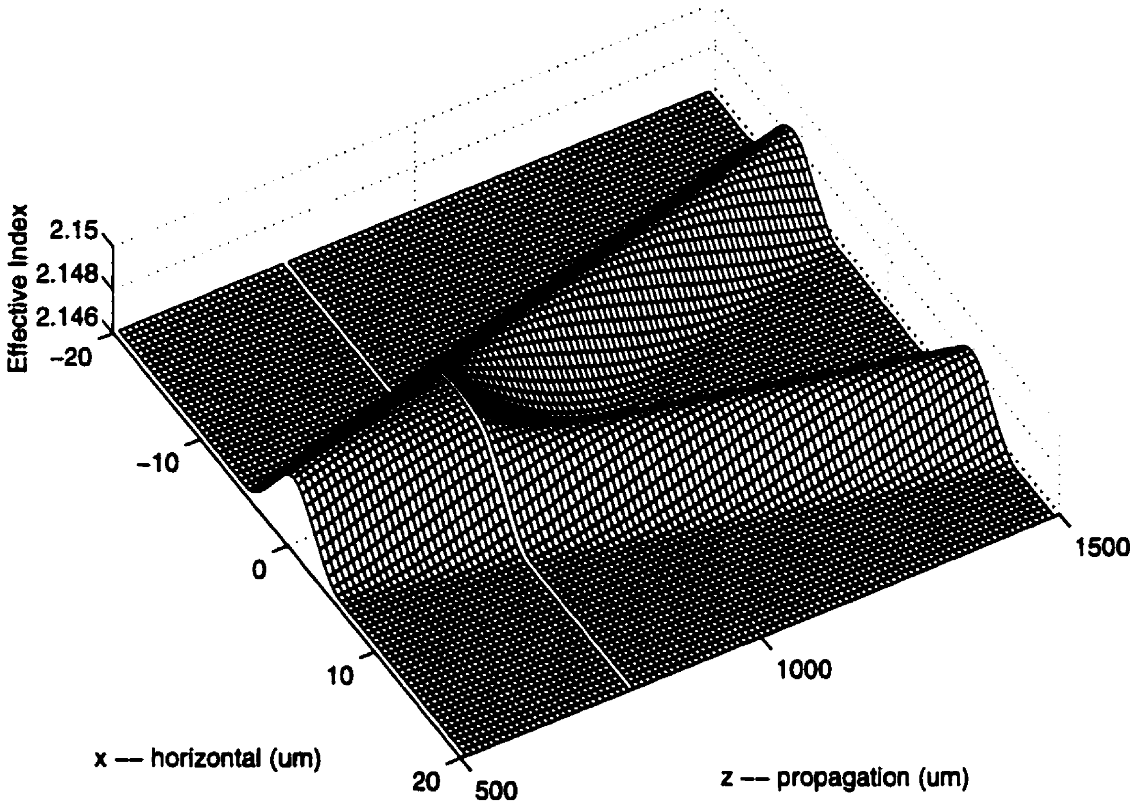

Figure 2.5: 3D effective index distribution of the Y-branch alone (S_iO_2 covered)

$$\frac{dn^2}{d\rho}\mid_{\rho=0_+}= -4n_b\Delta n\rho e^{-\rho^2}\mid_{\rho=0_+}=0 \tag{2.50}$$

$$n_f^2 = n_b^2 + 2n_b\Delta n e^{-\rho^2}\mid_{\rho=\rho_{s-}} \tag{2.51}$$

$$\frac{dn^2}{\rho}\mid_{\rho=\rho_{s-}} = -4n_b\Delta n\rho e^{-\rho^2}\mid_{\rho=\rho_{s-}} \tag{2.52}$$

$$\frac{3}{4}(\frac{1}{n^2}\frac{n^2}{d\rho})^2 = \frac{12n_b^2(\Delta n)^2\rho^2 exp(-2\rho^2)}{[n_b^2+2n_b\Delta n exp(-\rho^2)]^2} \tag{2.53}$$

$$-\frac{1}{2n^2}\frac{d^2n^2}{d\rho^2} = \frac{2n_b\Delta n(1-2\rho^2)exp(-\rho^2)}{n_b^2+2n_b\Delta n exp(-\rho^2)} \tag{2.54}$$

2.2.3 Boundary Conditions With an Applied Voltage

When there is an applied voltage, the boundary conditions for *Section 2.2.1* are

$$n_m^2 = n_b^2 + 2n_b\Delta n - r_{33}n_b^4E_y(x_i,0) \tag{2.55}$$

$$\frac{dn^2}{d\rho}\mid_{\rho=0_+}= -r_{33}n_b^4E_y'\mid_{\rho=0} \tag{2.56}$$

$$n_f^2 = n_b^2 + 2n_b\Delta n e^{-\rho_s^2} - r_{33}n_b^4E_y(x_i,\rho_s) \tag{2.57}$$

$$\frac{dn^2}{d\rho}\mid_{\rho=\rho_s}= -4n_b\Delta n\rho_s e^{-\rho_s^2} - r_{33}n_b^4E_y'\mid_{\rho=\rho_s} \tag{2.58}$$

$$\frac{3}{4}(\frac{1}{n^2}\frac{dn^2}{d\rho})^2 = \frac{3}{4}(\frac{4n_b\Delta n\rho e^{-\rho^2}+r_{33}n_b^4E_y'(x_i,a\rho)}{n_b^2+2n_b\Delta n e^{-\rho^2}-r_{33}n_b^4E_y(x_i,a\rho)})^2 \tag{2.59}$$

$$\frac{1}{2n^2}\frac{d^2n^2}{d\rho^2} = \frac{8n_b\Delta n\rho^2e^{-\rho^2}-4n_b\Delta n e^{-\rho^2}-r_{33}n_b^4E_y''(x_i,a\rho)}{2n_b^2+4n_b\Delta n e^{-\rho^2}-2r_{33}n_b^4E_y(x_i,a\rho)} \tag{2.60}$$

2.3 Effective Propagation Constant and Modal Field Distribution

2.3.1 Effective Propagation Constant

After reducing the 2D cross–sectional refractive index distribution into a 1D (x–horizontal) effective index profile $n_{eff}(x_i)$ using techniques described in Section 2.2.1, while making the step size Δx enough small, we can apply the same technique again to further find the propagation constant of this effective slab waveguide confined in the x-direction with a refractive index distribution of $n_{eff}(x)$. Though the subscript i here has been eliminated because there are enough points obtained, during further calculation, a pointwise numerical approarch will still be used.

Because the optical field is to be launched along the y-direction, we have to solve the wave equation for TE_0 mode now, instead of for TM_0 mode as it was the case in the last section. The process will be easier because the wave equation for TE_0 mode is simple compared to that for TM_0 mode. The wave equation to be solved is:

$$\frac{d^2G}{dx^2} + [k_0^2 n_{eff}^2(x) - \beta^2]G = 0 \tag{2.61}$$

where β is the propagation constant of the slab waveguide, which could be regarded as a very good representation of the propagation constant of the original channel waveguide. Also, we define $n_0 = \beta/k_0$, which will serve as the reference refractive index in the FD–VBPM method that follows. To find n_0 and β, we use the same technique described in Section 2.2.1.

Let the two edge points be called x_L and x_R where the effective index goes to the substrate index (strictly speaking, n_{eff} will approach n_b as x goes to infinity, but in numerical simulation, we have to set $n_{eff} = n_b$ once their difference is small enough. In the program which calculates the effective index distribution, if Δx is set to be 0.01, we have $x_R = 5.16\mu m$ and $x_L = -5.16\mu m$.

For $x \leq x_L$, (2.61) becomes

$$\frac{d^2G}{dx^2} + k_0^2(n_b^2 - n_0^2)G = 0 \tag{2.62}$$

General solution of the above equation is

$$G(x) = C_1 e^{k_0\sqrt{n_0^2-n_b^2}(x+x_L)} + C_2 e^{-k_0\sqrt{n_0^2-n_b^2}(x+x_L)} \tag{2.63}$$

Since when $x \to -\infty$, $G \to 0$, it must be

$$G(x) \sim e^{k_0\sqrt{n_0^2-n_b^2}(x+x_L)} \tag{2.64}$$

Let

$$J(x) = \frac{1}{G}\frac{dG}{dx} \tag{2.65}$$

From (2.64) we obtain

$$J(x) \mid_{x=x_L} = k_0\sqrt{n_0^2 - n_b^2} \tag{2.66}$$

and also (2.61) becomes

$$\frac{dJ}{dx} = -J^2 - k_0^2(n_{eff}^2(x) - n_0^2) \tag{2.67}$$

Similarly, for $x \geq x_R$,

$$G(x) \sim e^{-k_0\sqrt{n_0^2-n_b^2}(x-x_R)} \tag{2.68}$$

$$J(x) \mid_{x=x_R} = -k_0\sqrt{n_0^2 - n_b^2} \tag{2.69}$$

Now that the two boundary conditions for solving (2.67) are known, we are ready to solve for n_0 and consequently $J(x)$ and $G(x)$ from (2.67) and (2.61) respectively. Here, we slightly modify the steps described in Section 2.2.1. Instead of setting the upper boundary initially at a low value for the Runge–Kutta method and later relaxing it during each step within the Secant root searching, we directly use x_L as the lower boundary and x_R as the upper boundary because we know the exact upper boundary in this case. To keep the Runge–Kutta process convergent, initial guesses of n_0 has to be chosen very carefully and deliberately. After some test run, the following reference index has been found using double precision: $n_0 = 2.1475504268534$. All the significant figures have been kept for best accuracy.

2.0.1 Effective Modal Field Distribution

To compute modal field $G(x)$, notice that the value of G at an arbitrary value of x can be written as [19]

$$G(x) = exp[\int_0^x J(\xi)d\xi] \tag{2.70}$$

Once n_0 is determined, the quantity $\int_0^x J(\xi)d\xi$ is computed numerically, where the integrand $J(\xi)$ is obtained from the numerical solution of (2.67). Thus, the modal field $G(x)$ can be plotted as a function of x, and compared with the Gaussian distribution which is sometimes used as an approximation of the excitation field. It is known that loss will occur from the adjustment of light from a Gaussian distribution to the TE_0 modal field distribution. This loss will have nothing to do with the branching structure of the waveguide and should be excluded either by getting P_{in} from a distance away from $z = 0$ after BPM program has been run, or by using the modal field directly as the initial excitation.

Also the running time could be saved if symmetry of the field distribution is used. In fact, we could start from x_L and use the Runge–Kutta method to compute $J(x)$ from x_L to 0 with a step size of 0.01 and get the other half (from 0 to x_R) using the symmetry (J(x) is in fact an odd function). Further, since G(x) is an even function, we need to compute only half of the region (say, from 0 to x_R) and get the other half by symmetry. The distribution of $G(x)$ beyond the boundary points can be obtained using the exponentially decaying relation. The step sizes for computing $J(x)$ and $G(x)$ are 0.01 and 0.04 respectively.

It has been found (see following figure) that a Gaussian distribution with a $1/e$

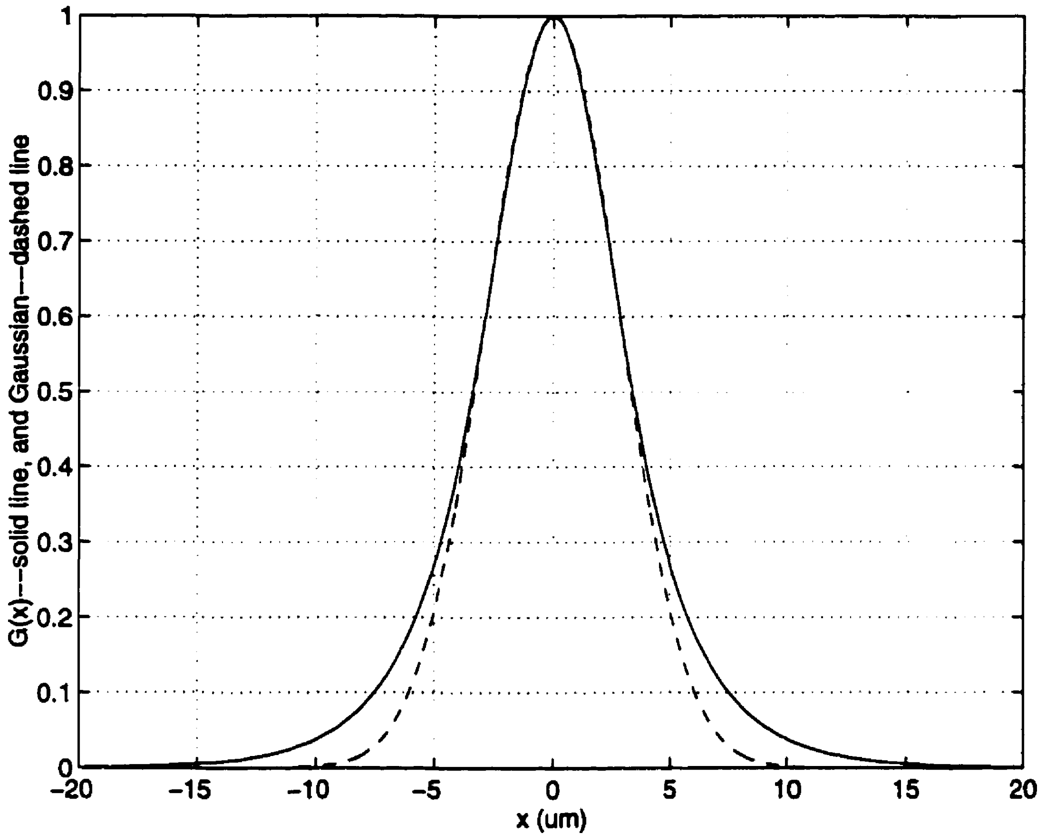

Figure 2.6: Comparison between modal field G(x) and Gaussian approximation with a $1/e$ intensity diameter of $8\mu m$

intensity diameter of $8\mu m$, i.e., $exp[-(x/4.0)^2]$, is very similar to the actual modal distribution especially near the central region of the waveguide ($W = 6\mu m$), and thus may be used as an approximation under certain circumstances. Also, according to [23] and [24], the near field intensity profile of a Corning $8\mu m$ core single mode fiber at $\lambda = 1.3\mu m$ has a $7\mu m$ $1/e$ intensity diameter, which is very close to the value obtained by the above computation for a $6\mu m$ wide $Ti : LiNbO_3$ waveguide. Thus, this width is proved to be appropriate both to ensure a single-mode (according to literature) and good coupling.

Bibliography

[1] R. M. Knox and P. P. Toulios, "Integrated Circuits for the Millimeter through Optical Frequency Range", *Proc. MRI Symp. Submillimeter Waves*, J. Fox, Ed., New York: Polytechnic Press, 1970

[2] D. Marcuse, *Theory of Dielectric Optical Waveguides*, Academic Press, 1991, Chapter 8. Approximate and Numerical Methods

[3] H. Nishihara, M. Haruna and T. Suhara, *Optical Integrated Circuits*, McGraw Hill, 1989

[4] M. Fukuma and J. Noda, "Optical Properties of Titanium-Diffused $LiNbO_3$ Strip Waveguides and Their Coupling–to–a–Fiber Characteristics", *Applied Optics*, Vol. 19, No. 4, pp. 591–597, 1980

[5] K. T. Koai and P. L. Liu, "Modeling of $Ti : LiNbO_3$ Waveguide Devices: Part I — Directional Couplers", *J. of Lightwave Tech.*, Vol. 7, No. 3, pp. 533-539, 1989

[6] R. V. Schmidt and I. P. Kaminov, "Metal-Diffused Optical Waveguides in $LiNbO_3$", *Applied Physics Letters*, Vol. 25, pp. 458-460, 1974

[7] F. S. Chu, P. L. Liu, and J. E. Barau, "Fabrication Tolerance of $Ti : LiNbO_3$ Waveguides", *J. of Lightwave Tech.*, Vol. 8, No. 5, pp. 784–788, 1990

[8] F. S. Chu and P. L. Liu, "Simulation of $Ti : LiNbO_3$ Waveguide Modulators — A Comparison of Simulation Techniques", *J. of Lightwave Tech.*, Vol. 8, No. 10, pp. 1492–1496, 1990

[9] J. Ctyroky, *et al.*, "3–D Analysis of $LiNbO_3 : T_i$ Channel Waveguides and Directional Couplers", *IEEE J. of Quantum Electronics*, QE–20, No. 4, pp. 400–409, 1984

[10] S. Fouchet, *et al.*, "Wavelength Dispersion of T_i Induced Refractive Index Change in $L_iN_bO_3$ as a Function of Diffusion Parameters", *J. of Lightwave Tech.*, Vol. LT–5, NO. 5, pp. 700–708, 1987

[11] C. J. G. Kirkby, "Refractive Index of Lithium Niobate, Wavelength Dependence: Tables", in *Properties of Lithium Niobate, EMIS Data Review Series*, No. 5, pp. 92–124, 1988

[12] F. Y. Gan, *Traveling Wave Electrode Design For High Speed $LiNbO_3$ Intensity Modulators*, Master's Thesis, McGill University, 1996

[13] P. Danielsen, "Two–Dimentional Propagating Beam Analysis of an Electrooptic Waveguide Modulator", *IEEE J. of Quantum Electronics*, Vol. QE–20, No. 9, pp. 1093–1097, 1984

[14] J. Albert and G. L. Yip, "Wide Single-Mode Channels and Directional Coupler by Two-Step Ion-Exchange in Glass", *J. of Lightwave Tech.*, Vol. 6, No. 4, pp. 552–563, 1988

[15] K. Van de Velde, H. Thienpont, and R. V. Green, "Extending the Effective Index Method for Arbitrarily Shaped Inhomogeneous Optical Waveguides", *J. of Lightwave Tech.*, Vol. 6, No. 6, pp. 1153–1159, 1988

[16] G. B. Hocker and W. K. Burns, "Modes in Diffused Optical Waveguides of Arbitrary Index Profile", *J. of Quantum Electronics*, QE–11, No. 6, pp. 270–276, 1975

[17] G. B. Hocker and W. K. Burns, "Mode Dispersion in Diffused Channel Waveguides by the Effective Index Method", *Applied Optics*, Vol. 16, No. 1, pp. 113–118, 1977

[18] K. S. Chiang, "Simplified Universal Dispersion Curves for Graded-Index Planar Waveguides Based on the WKB Method", *J. of Lightwave Tech.*, Vol. 13, No. 2, pp. 158–162, 1995

[19] A. N. Kaul, S. I. Hosain, and K. Thyagarajan, "A Simple Numerical Method for Studying the Propagation Characteristics of Single-Mode Graded-Index Planar Optical Waveguides", *IEEE Trans. on Microwave Theory and Techniques*, MTT–34, No. 2, pp. 288–292, 1986

[20] Prasanna K. Mishra and Anurag Sharma, "Analysis of Single Mode Inhomogeneous Planar Waveguides", *Journal of Lightwave Technology*, Vol. LT–4, No. 2, pp. 204–211, 1986

[21] G. G. Bach, *Numerical Analysis*, class notes, Mechanical Engineering Dept., McGill University, 1982

[22] T. Tamir, Ed., *Integrated Optics*, New York: Springer-Verlag, 1977, Chap. 2 Theory of Dielectric Waveguides, H. Kogelnik

[23] P. G. Suchoski and R. V. Ramaswamy, "Minimum–Mode–Size Low–loss T_i : $L_iN_bO_3$ Channel Waveguides for Efficient Modulator Operation at 1.3 μm", *IEEE Journal of Quantum Electronics*, Vol. QE–23, No. 10, pp. 1673–1679, 1987

[24] D. Marcuse, *Light Transmission Optics*, New York: Van Nostrand Reinhold, 2nd ed., 1991

Chapter 3

BPM Simulation and Design Optimization of Propagation Loss

3.1 2D Finite-Difference Beam Propagation Method

3.1.1 General Methodology Description

In a pioneering paper [1], Feit and Fleck first proposed the beam propagation method (BPM), also called the propagating beam method. This method has become the most basic and powerful simulation technique in integrated optics for its good applicability to the modeling of varies kinds of devices.

The BPM method was restricted by the conditions that reflected waves can be neglected and that all refractive index differences are small [2]. It was concluded in [2] and [3] that the BPM does not work well in cases where reflection of waves plays a significant role (like a Y–branch with big angle); and its application is also limited to weakly guiding structures where the polarization of waves can be neglected. However, with the development of vectorial BPM (VBPM) ([4]–[9]) the latter limitation has already been broken. Also, by using a time domain BPM which is described in [10]–[13], and takes into account the reflected waves, the first limitation can also be overcome.

In the original BPM scheme, the wave propagtion is modelled as a spectrum of plane waves in the spectral domain and the effect of inhomogeneity in the medium is accounted for as a phase correction in the spatial domain at each propagation step. The Fast Fourier Transform (FFT) is used to provide the link between the spatial and spectral domains. Hence, the method is named FFT–BPM [3]. The beam propagation method that solves the paraxial wave equations (both scalar and vector) in either a homogeneous or an inhomogeneous medium (even anisotropic [14]) using the finite–difference method, called the finite–difference beam propagation method (FD–BPM), has also been developed and assessed [4]–[6] [15]. For both high accuracy and simplicity in our computations, the 2D standard (compared with other improved methods) FD–VBPM scheme will be chosen in this project. In comparison with the FFT–BPM the FD–VBPM is computationally more efficient and more robust as well [5].

The applicability of the various BPM schemes has been discussed in great details by several authors like in [3] [4] and [15]. Further, these schemes have been applied to many waveguiding structures like electrooptic waveguide modulators [16], waveguide crossings [17], directional couplers [5] [8] [18], polarizers [19], mode splitters [20], ridge waveguide linear-mode confinement modulators [21], and gratings [3] etc.

A lot of work has also been done in improving the standard BPM method. A modified finite–difference beam-propagation method based on the Douglas scheme was proposed in [8] which could reduce the truncation error to $(\Delta x)^4$ in the transverse direction, whereas the error in the conventional FD–BPM is typically $(\Delta x)^2$. A couple of explicit finite–difference schemes have also been developed in [22] and [23]. Although explicit methods are much easier to implement, it has the risk of instability under certain conditions (especially a strict requirement on the step-size Δz along the propagation direction, thus not feasible for long devices like a modulator). A couple of refined BPM schemes especially dedicated to wide-angle applications can also be found in [24] [25].

3.1.2 Paraxial-Wave Vector Helmholtz Equations

Starting from the basic Maxwell's equations, we can obtain the paraxial vetor Helmholtz equations (all details in *Section 3.3.1*)

$$\nabla^2 \vec{E} + n^2 k_0^2 \vec{E} = -\nabla(\nabla \ln \epsilon \cdot \vec{E}) \tag{3.1}$$

If the refractive index varies slowly along z-axis and so does $\vec{E}$, then only the transverse field components are of interest and (3.1) becomes

$$\nabla^2 \vec{E_t} + n^2 k_0^2 \vec{E_t} = -\nabla_t(\nabla_t \ln n^2 \cdot \vec{E_t}) \tag{3.2}$$

where $\vec{E_t} = E_x \hat{i} + E_y \hat{j}$ and $\nabla_t = \frac{\partial}{\partial x}\hat{i} + \frac{\partial}{\partial y}\hat{j}$. Seperating (3.2) into x and y components, we have

$$\nabla^2 E_x + n^2 k_0^2 E_x = -\frac{\partial}{\partial x}(\frac{\partial \ln n^2}{\partial x} E_x) - \frac{\partial}{\partial x}(\frac{\partial \ln n^2}{\partial y} E_y) \tag{3.3}$$

$$\nabla^2 E_y + n^2 k_0^2 E_y = -\frac{\partial}{\partial y}(\frac{\partial \ln n^2}{\partial x} E_x) - \frac{\partial}{\partial y}(\frac{\partial \ln n^2}{\partial y} E_y) \tag{3.4}$$

Now assume that these transverse fields can be represented by plane waves travelling in a homogeneous medium where n_0 is a reference refractive index.

$$\vec{E_t} = \vec{\psi_t} e^{-jk_0 n_0 z} \tag{3.5}$$

Making use of the slowly varying envelope approximation:

$$|\frac{\partial^2 \psi_x}{\partial z^2}| \ll 2k_0 n_0 |\frac{\partial \psi_z}{\partial z}| \tag{3.6}$$

We have:

$$j\frac{\partial \psi_x}{\partial z} = \frac{1}{2n_0 k_0}[\frac{\partial^2 \psi_x}{\partial y^2} + (n^2 - n_0^2)k_0^2 \psi_x + \frac{\partial}{\partial x}(\frac{1}{n^2}\frac{\partial}{\partial x}(n^2 \psi_x)) + \frac{\partial}{\partial x}(\frac{1}{n^2}\frac{\partial}{\partial y}(n^2 \psi_y)) - \frac{\partial^2 \psi_y}{\partial x \partial y}] \tag{3.7}$$

$$j\frac{\partial \psi_y}{\partial z} = \frac{1}{2n_0 k_0}[\frac{\partial^2 \psi_y}{\partial x^2} + (n^2 - n_0^2)k_0^2 \psi_y + \frac{\partial}{\partial y}(\frac{1}{n^2}\frac{\partial}{\partial y}(n^2 \psi_y)) + \frac{\partial}{\partial y}(\frac{1}{n^2}\frac{\partial}{\partial x}(n^2 \psi_x)) - \frac{\partial^2 \psi_x}{\partial x \partial y}] \tag{3.8}$$

When TM-like or TE-like waves are studied, which means either the y component or the x component is zero ($\psi_x \neq 0, \psi_z \neq 0, \psi_y = 0$ or $\psi_y \neq 0, \psi_z \neq 0, \psi_x = 0$), the above two paraxial-wave Helmholtz equations in isotropic media could be simplified to

$$j\frac{\partial \psi_x}{\partial z} = \frac{1}{2n_0k_0}[\frac{\partial^2 \psi_x}{\partial y^2} + (n^2 - n_0^2)k_0^2\psi_x + \frac{\partial}{\partial x}(\frac{1}{n^2}\frac{\partial}{\partial x}(n^2\psi_x))] \tag{3.9}$$

$$j\frac{\partial \psi_y}{\partial z} = \frac{1}{2n_0k_0}[\frac{\partial^2 \psi_y}{\partial x^2} + (n^2 - n_0^2)k_0^2\psi_y + \frac{\partial}{\partial y}(\frac{1}{n^2}\frac{\partial}{\partial y}(n^2\psi_y))] \tag{3.10}$$

In a 3-D problem like diffused channel waveguides, the above n should be written as $n(x, y, z)$. If we use the Effective Index Method to reduce a 3-D problem to a 2-D problem, the above two Helmholtz equations could be further simplified (assuming that the coordinates are chosen so that y is the depth direction and $\partial/\partial y = 0$ by the nature of the lateral index distribution):

$$j\frac{\partial \psi_x}{\partial z} = \frac{1}{2n_0k_0}[(n_{eff}^2(x,z) - n_0^2)k_0^2\psi_x + \frac{\partial}{\partial x}(\frac{1}{n_{eff}^2(x,z)}\frac{\partial}{\partial x}(n_{eff}^2(x,z)\psi_x))] \tag{3.11}$$

$$j\frac{\partial \psi_y}{\partial z} = \frac{1}{2n_0k_0}[\frac{\partial^2 \psi_y}{\partial x^2} + (n_{eff}^2(x,z) - n_0^2)k_0^2\psi_y] \tag{3.12}$$

An important issue related to the implementation of the FD–VBPM is the choice of the reference refractive index n_0. In the case of single–mode waveguides, the reference index n_0 can be chosen as the effective index of the guided–mode (local guided mode) $n_0 = \beta/k$, where β is the propagation constant of the fundamental mode of the waveguide, which could be obtained by using the EIM method described in the previous section.

A more rigorous formulism which has taken into consideration the anisotropic nature of the $LiNbO_3$ crystal has been included in *Section 3.3.2*. For TE-like 2D ($n(x, z)$) waveguides, the simplified wave equations will be identical whether derived as in *Section 3.3.2* or through the process shown above (Equation (3.12) is the same as the last equation in *Section 3.3.2*). This proves that it is safe to treat the $LiNbO_3$ substrate as an isotropic medium having refractive index of n_e (along y direction) when TE-like 2D waveguides are studied.

3.1.3 Finite-Difference Scheme

An implicit weighted finite–difference scheme for solving the above derived wave equations has been employed (details in *Section 3.3.3*). Since in our particular case, only the y component of the field is concerned, only the FD solution of equation (3.12) in Section 3.1.2 will be derived in full detail. This corresponds to a TE_0 mode in a 2D problem with an effective refractive index profile $n_{eff}(x,z)$. Discretize a window in the xz surface into a mesh and let the step size in the x and z direction be Δx and Δz and use m and l as the index in x and z coordinate grid respectively, the scheme can be described by

$$A_m^{l+1}\psi_y^{l+1}(m) + A_{m+1}^{l+1}\psi_y^{l+1}(m+1) + A_{m-1}^{l+1}\psi_y^{l+1}(m-1)$$

$$= A_m^{l}\psi_y^{l}(m) + A_{m+1}^{l}\psi_y^{l}(m+1) + A_{m-1}^{l}\psi_y^{l}(m-1) \tag{3.13}$$

where

$$A_m^{l+1} = 1 - j\frac{\omega\Delta z}{2n_0k_0}\{\frac{2}{(\Delta x)^2} - [n^2(m,l+1) - n_0^2]k_0^2\}$$

$$A_{m\pm1}^{l+1} = j\frac{\omega\Delta z}{2n_0k_0(\Delta x)^2}$$

$$A_m^{l} = 1 + j\frac{(1-\omega)\Delta z}{2n_0k_0}\{\frac{2}{(\Delta x)^2} - [n^2(m,l) - n_0^2]k_0^2\}$$

$$A_{m\pm1}^{l} = -j\frac{(1-\omega)\Delta z}{2n_0k_0(\Delta x)^2}$$

The stability criteria, the numerical dissipation and dispersion of the finite–difference schemes have been analyzed in detail in [4], which could be used as a guidance when the algorithm is implemented. According to the analyses, it is very important to choose a good ω and a small enough Δz in order to fulfill the requirements of stability, numerical dissipation and numerical dispersion. In computation afterwards, the relaxation constant w is taken to be 0.51, while the step sizes along two directions are $\Delta z = 2\mu m$ and $\Delta x = 0.1\mu m$ respectively. They are decided after various values of these three variables have been tested and compared, not only to enssure stability, enough accuracy, but also to restrict the computation time to a reasonable and feasible limit.

For the initial input field, although sometimes Gaussian approximation can be used (the field distribution inside a fiber is Gaussian [29] and the modal field of a 3D channel waveguide can be approximated by a Hermite-Gaussian function [26]), to ensure unnecessary numerical loss, the modal field of the effective 2D waveguide (which is to accommodate the TE_0 mode) obtained by the EIM has been used. Strictly speaking, even the exact eigenmode of the waveguide has to adjust itself at the initial stage of the propagation in order to become the eigenmode of the discretized structure. During this process, nonphysical radiation loss may occur, causing power attenuation at the initial stage of propagation. To avoid this problem, either a sufficient fine mesh over the transverse cross section should be used or one has to substract the transient loss from the final results [4]. In the computations that follow, the field at about the 10th step after the initial input is taken to serve as the "real" modal field of the discretized structure.

3.1.4 Transparent Boundary Conditions

We can see that the 2D-FD-VBPM scheme results in the solution of a tridiagonal matrix (a pentadiagonal matrix for a 3D problem) with a known initial field distribution. This requires the pre-knowledge of the first and last elements because the number of elements in the very first and very last equation is one less than that in other equations. In other words, not only do we have to set a finite computation window, but we also have to determine the values of the two edge points of the window at each step before the matrix can be solved. Since virtually all the branching structures studied for photonics applications scatter considerable amounts of radiation towards the boundaries [28], the radiation tends to reflect from the problem boundaries back into the solution region where it causes unwanted interference. In this project, a so-called transparent boundary condition algorithm proposed by Hadley will be implemented which simulates a nonexistent boundary. Radiation is allowed to freely escape the problem boundary without appreciable reflection, whereas radiation flux back into the problem region is also prevented [27] [28]. In contrast to the old absorber method, where artificial absorption regions adjacent to the pertinent boundaries are inserted, this transparent boundary condition (TBC) employs no adjustable parameters, and is thus problem independent. In addition, it is easily incorporated into a standard Crank–Nicholson (or a weighted) finite–difference scheme in both two and three dimensions. It has been shown that this TBC is both accurate and robust for both 2D and 3D problems compared with the absorber method, and it also saves the running time and storage space.

This transparent boundary method is based on the assumpsion that the field dependence near the boundary of interest is a complex exponential, i.e., the field amplitude should satisfy ($e^{-j\omega t}$ time dependence assumed here for deriving the TBC)

$$\psi_y = \psi_{y0} e^{jk_x x} \tag{3.14}$$

or in the finite difference form

$$\psi_y^{l+1}(M) = \psi_y^{l+1}(M-1) e^{jk_x \Delta x} \tag{3.15}$$

where ψ_{y0} and k_x are complex. It has been shown in [27] and [28] that as long as the real part of k_x is positive, the radiative energy can only flow out of the problem region. The transverse wave vector k_x is computed from the previous step by calculating the ratio $\psi_y^l(M-1)/\psi_y^l(M-2)$. Prior to the application of the above equation, the real part of k_x must be restricted to be positive. If not, it has to be reset to zero.

This method is extended to two more general but complicated TBC schemes in [28]. k_x is computed after the completion of the nth step, using various internal points near the boundary (not restricted to the two immediate adjacent points), and then apply this same value of k_x to the *(n+1)th* step. The determination of the two points depend on the angle at which the wavefront impinges on the boundary and the relative mesh spacing (refer to Fig. 1 of [28]). If the step-size Δz is too large, the simple method may lead to unwanted oscillations. Then, the complicated and complete algorithms may be implemented.

3.1.5 Visualization of BPM Simulations

By implementing the above-stated BPM method to a straight $Ti : LiNbO_3$ channel waveguide whose refractive index has already been reduced to 2D by the EIM method, the field propagation pattern as shown in Fig. 3.1 was obtained. By using the method described in Section 3.2.1 to evaluate propagation loss, the loss curve of a straight guide has also been obtained and shown in Fig. 3.2. This figure reveals the numerical loss introduced by the BPM method itself. Since the BPM method involves only the information of the step by step change of the refractive index along the z-direction, as long as there is no variation of refractive index along the z-direction, ideally, the BPM should produce unchanged field distributions at each step and gives zero loss. Physical losses due to scattering and absorption can not be shown by the BPM. Hence, any loss from computations must be numerical loss. It can be seen that after a certain distance, the numerical loss becomes stable in the range of $4 \times 10^{-7} dB$ range. Compared with a typical propagation loss of 0.3 dB for a conventional M-Z waveguide structure, this value is small enough to be neglected. Fig. 3.3 through Fig. 3.11 are some simulation results of wave propagation inside M-Z waveguide structures of different arm seperations and different lengths of taper/branching regions (shorter length corresponds to larger branching angles).

Fig. 3.3 to Fig. 3.7 are beam propagation patterns for structures with an arm seperation of 10 μm. Five differnt taper/branching lengths have been used in the simulations: 400 μm, 600 μm, 1000 μm, 1200 μm and 1500 μm, corresponding to full branching angles ranging from 2.29° to 0.62°. Fig. 3.8 to Fig. 3.11 are beam propagation patterns for structures with an arm seperation of 15 μm. Four different taper/branching lengths have been used in the simulations: 500 μm, 1000 μm, 1500 μm and 2000 μm, corresponding to full branching angles ranging from 2.4° to 0.6°. Qualitatively, we see that the bigger the branching angle (which means more significant longitudinal variation of refractive index), the worse the propagation. For a taper/branching length of around 500 μm (or a full branching angle of around 2°), most of the input power can not get to the output waveguide. The radiation of energy is very significant. For a taper/branching length that is greater than 1000 μm (or a full branching angle of less than 1°), most of the input power can be transported to the output waveguide, though there is still obvious beating of modes during propagation. An interesting thing is that below 1°, any further decrease of the full branching angle does not necessarily cause a smoother propagation pattern. In other words, the tendancy of having a lower loss with a smaller angle is not monotonical. This can be verified to be true and explained by the coherent coupling effect of radiation modes which will be discussed in the following sections.

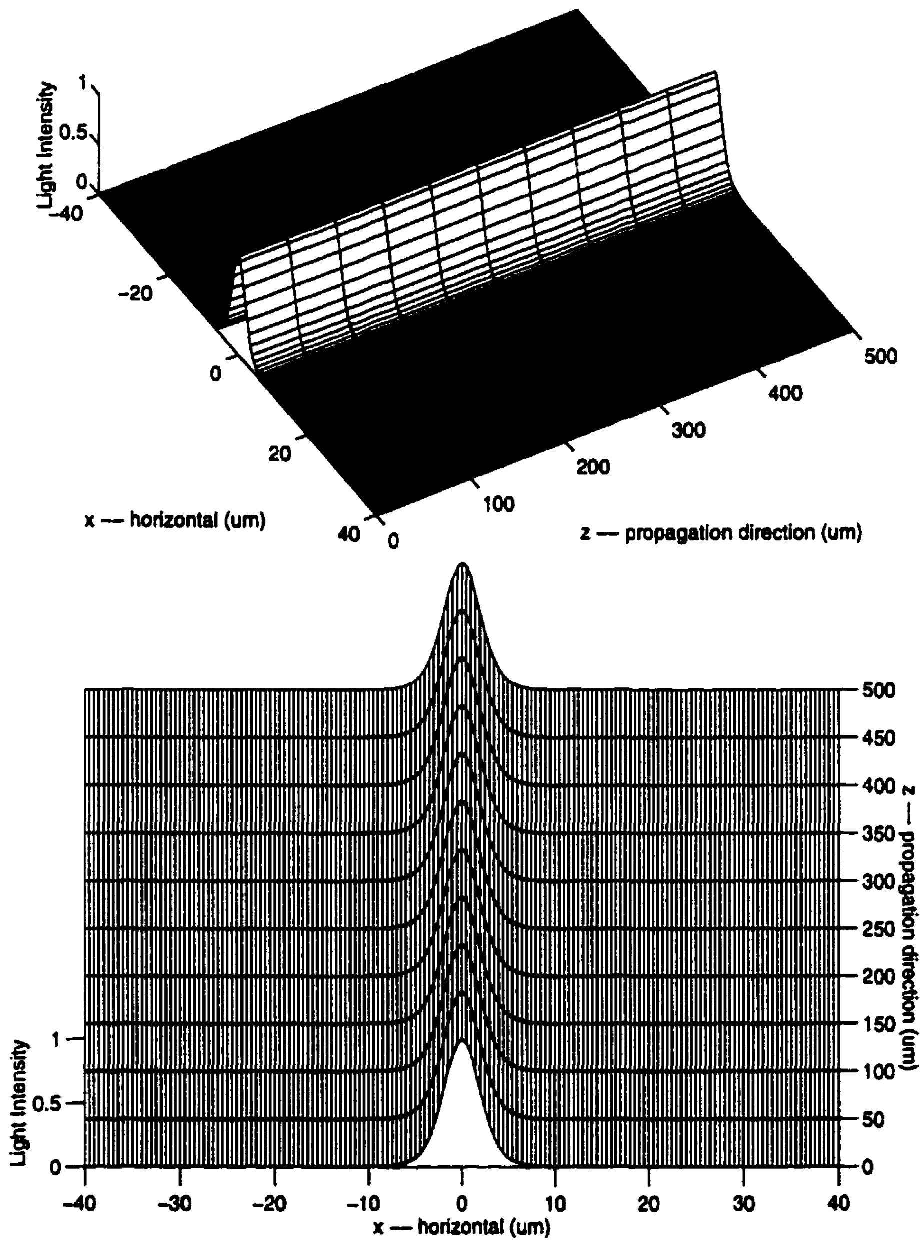

Figure 3.1: Beam propagation inside a straight Ti diffused waveguide

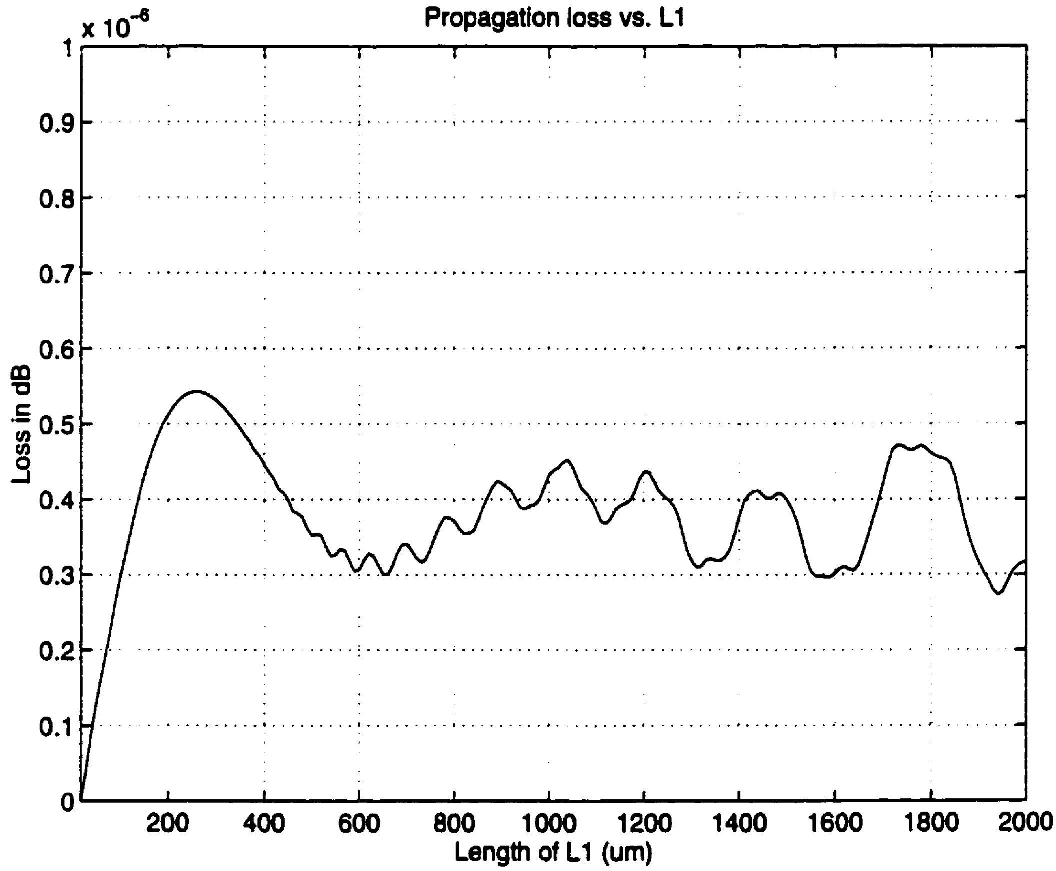

Figure 3.2: Numerical loss of the 2D-FD-VBPM vs. propagation length in a straight guide

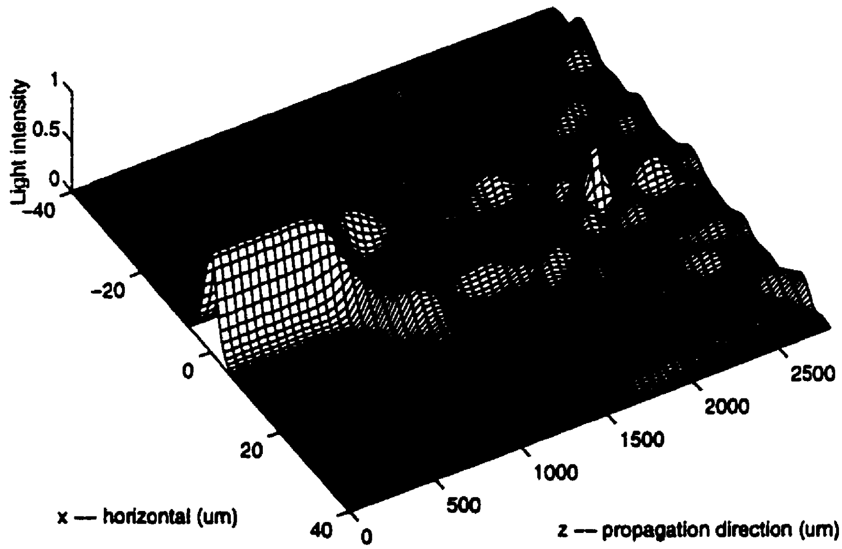

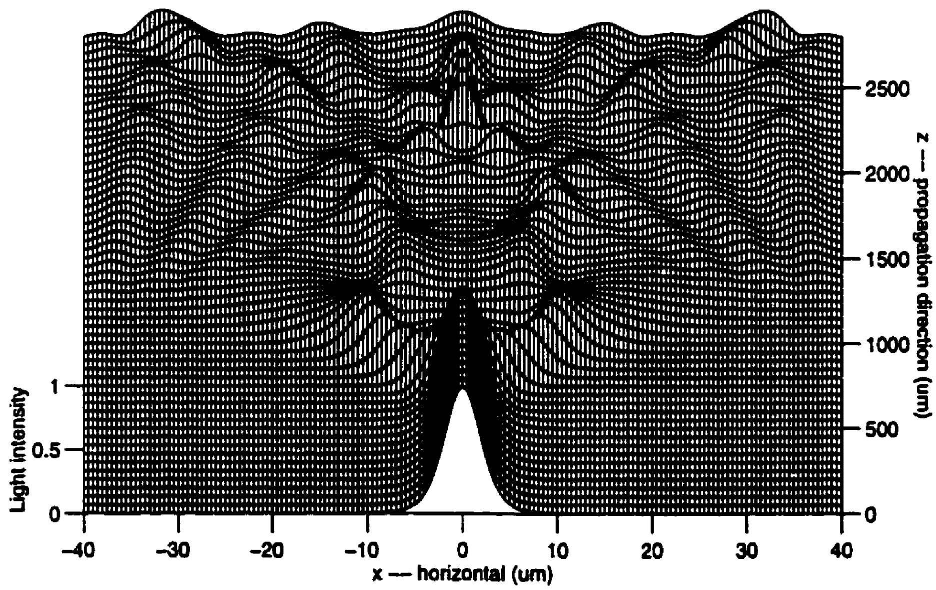

Figure 3.3: Beam propagation along a structure of L1=L5=500 μm, L2=L4=400 μm, L3=1000 μm, W=6 μm and d=10 μm, $2\theta = 2.29°$

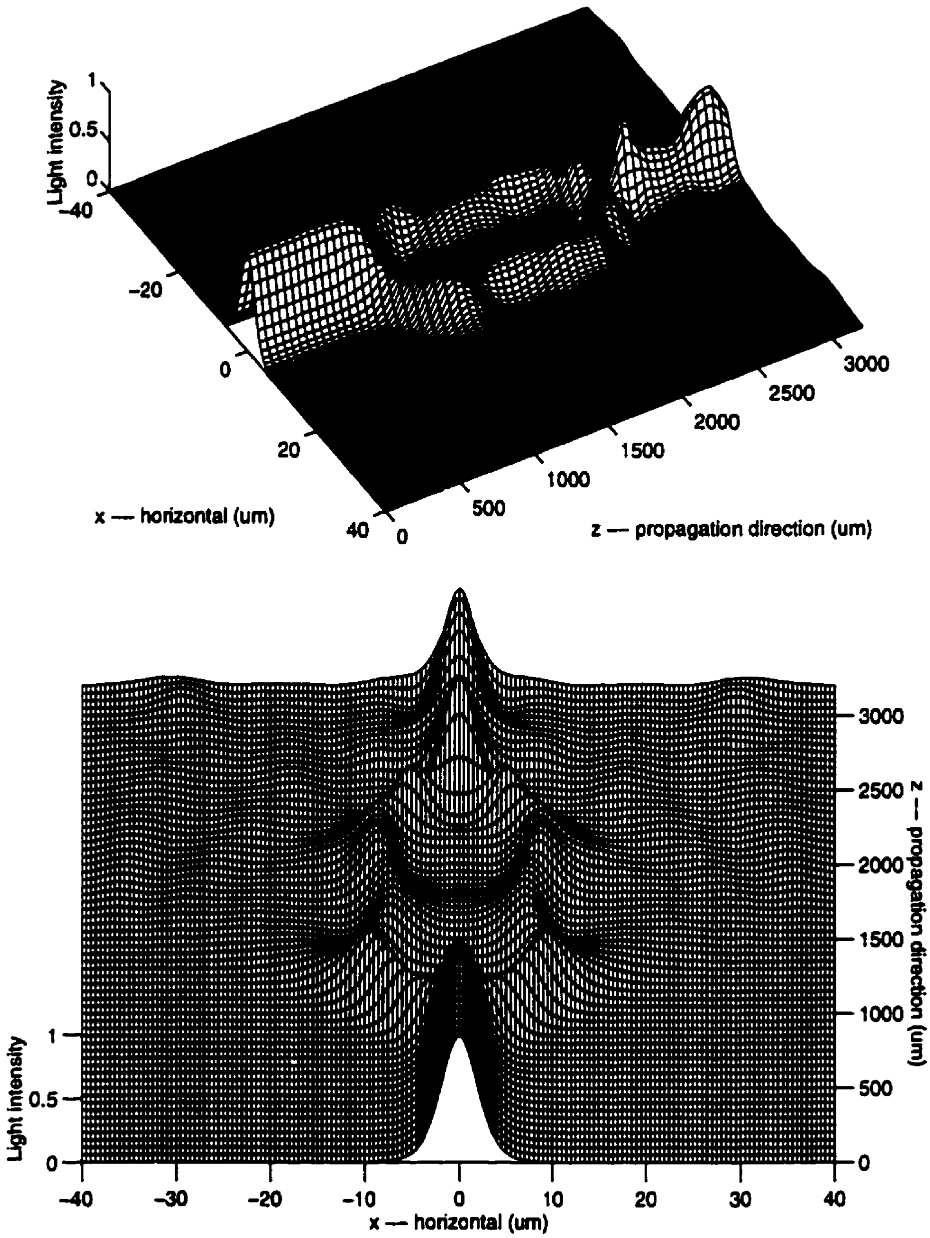

Figure 3.4: Beam propagation along a structure of L1=L5=500 μm, L2=L4=600 μm, L3=1000 μm, W=6 μm and d=10 μm, $2\theta = 1.53°$

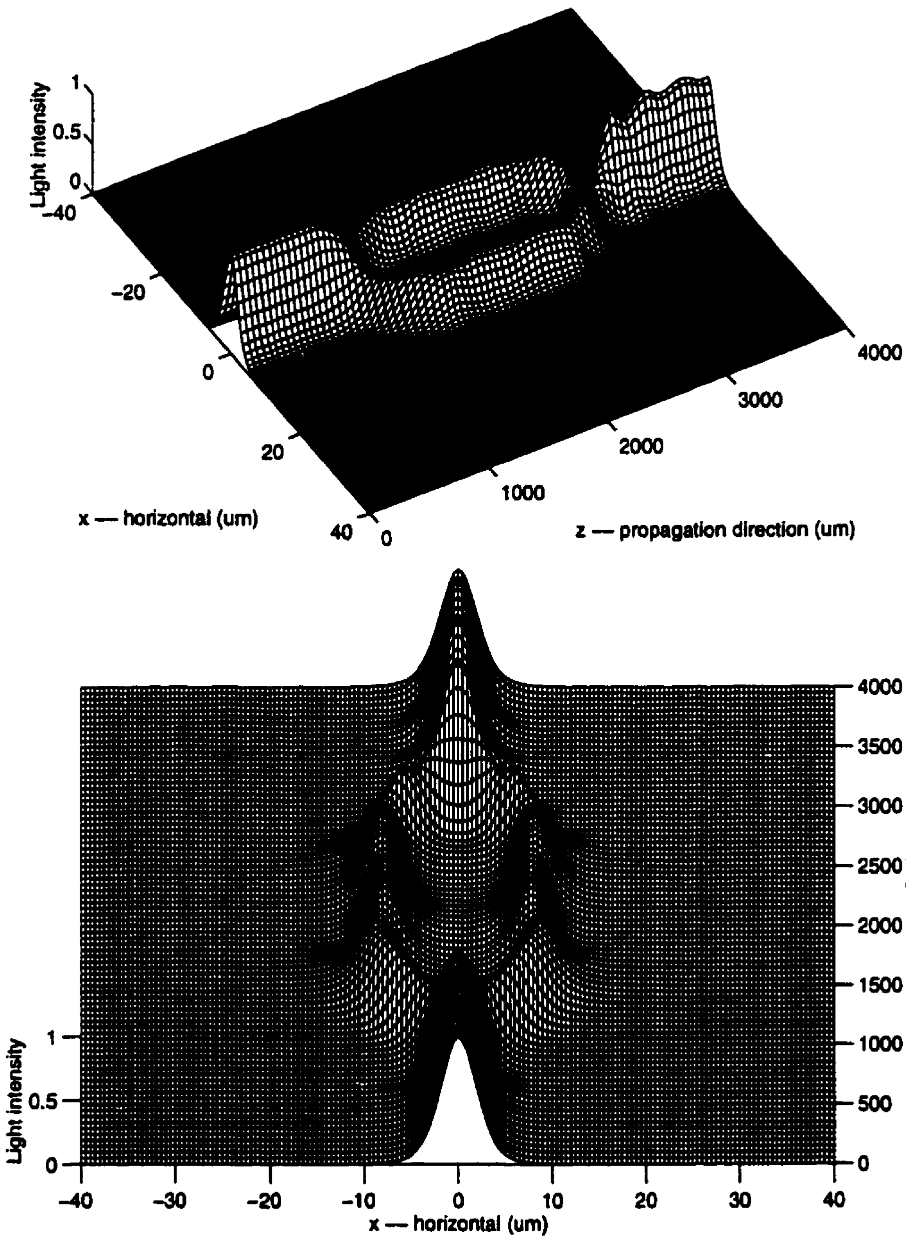

Figure 3.5: Beam propagation along a structure of L1=L5=500 μm, L2=L4=1000 μm, L3=1000 μm, W=6 μm and d=10 μm, $2\theta = 0.92°$

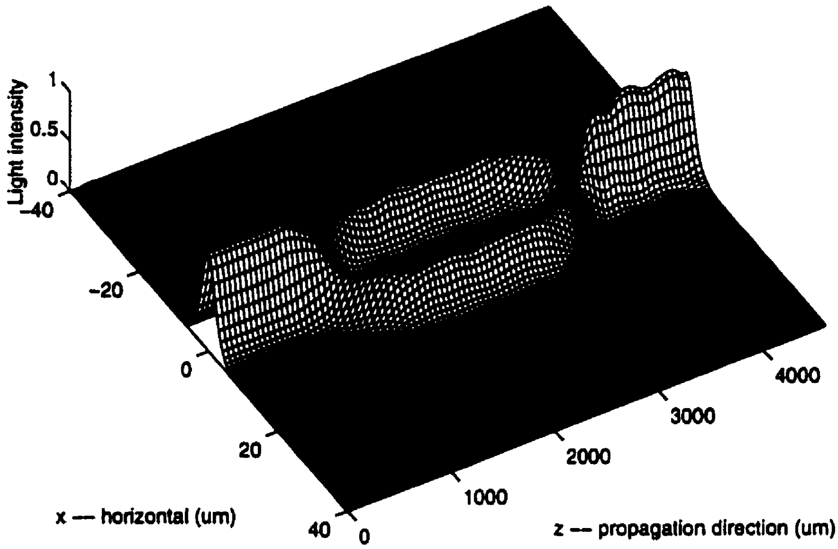

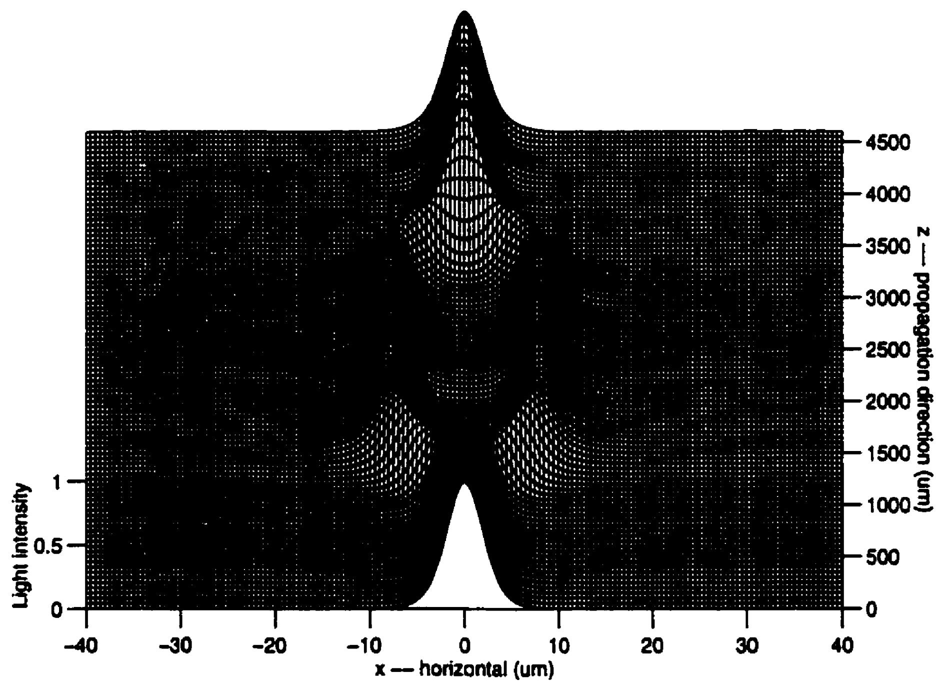

Figure 3.6: Beam propagation along a structure of L1=L5=500 μm, L2=L4=1200 μm, L3=1200 μm, W=6 μm and d=10 μm, $2\theta = 0.76°$

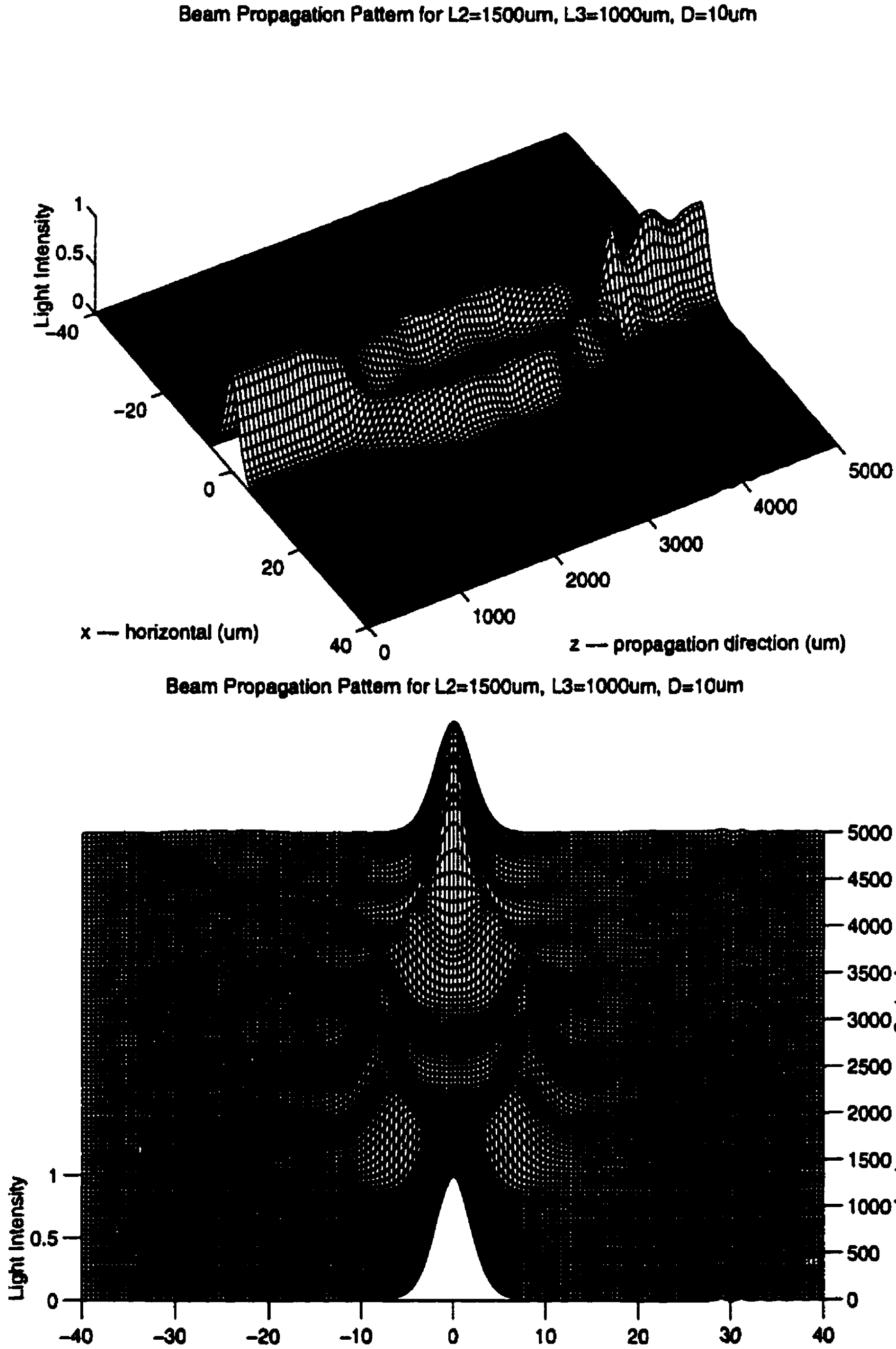

Figure 3.7: Beam propagation along a structure of L1=L5=500 μm, L2=L4=1500 μm, L3=1000 μm, W=6 μm and d=10 μm, $2\theta = 0.62°$

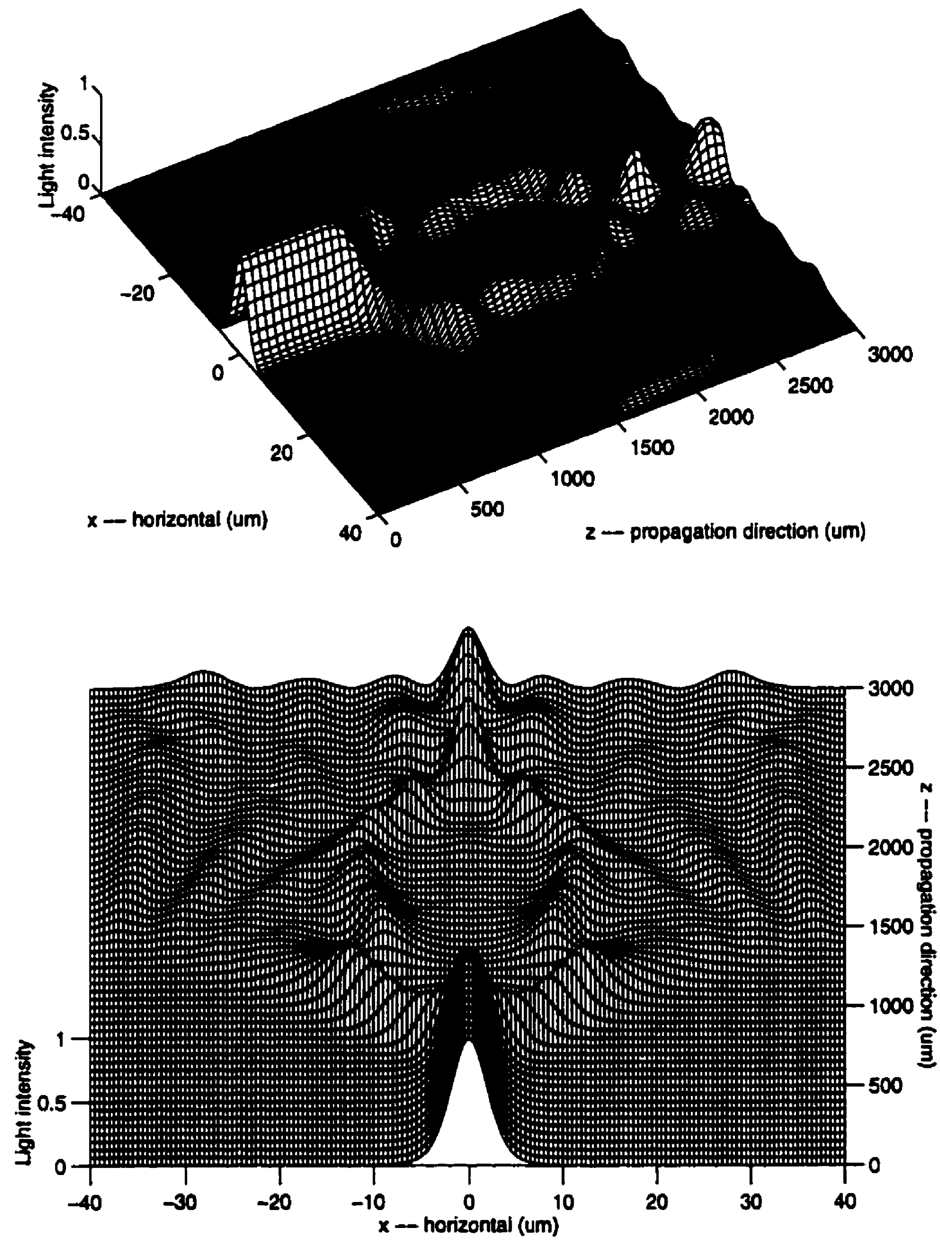

Figure 3.8: Beam propagation along a structure of L1=L5=500 μm, L2=L4=500 μm, L3=1000 μm, W=6 μm and d=15 μm, $2\theta = 2.4°$

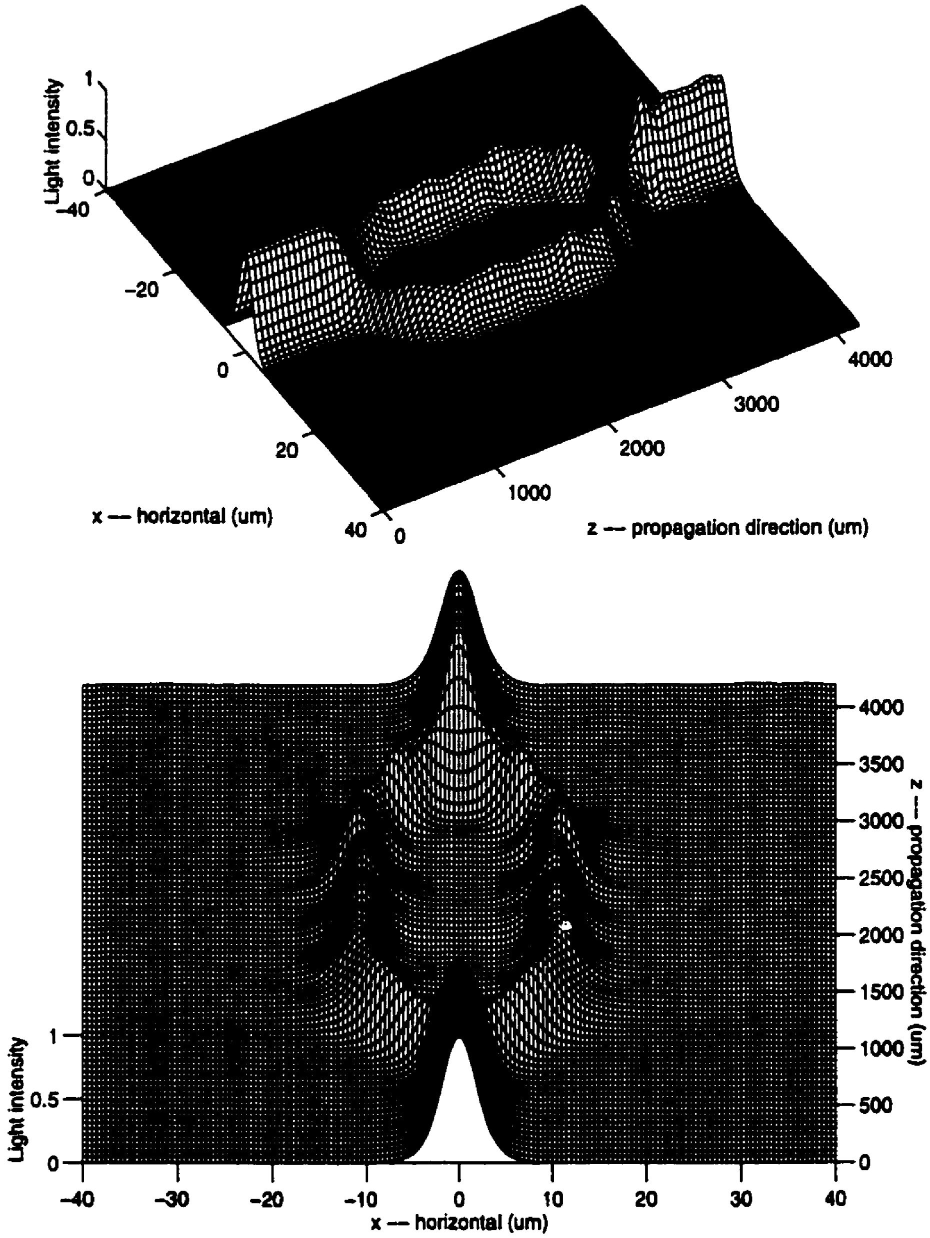

Figure 3.9: Beam propagation along a structure of L1=L5=500 μm, L2=L4=1000 μm, L3=1200 μm, W=6 μm and d=15 μm, $2\theta = 1.2°$

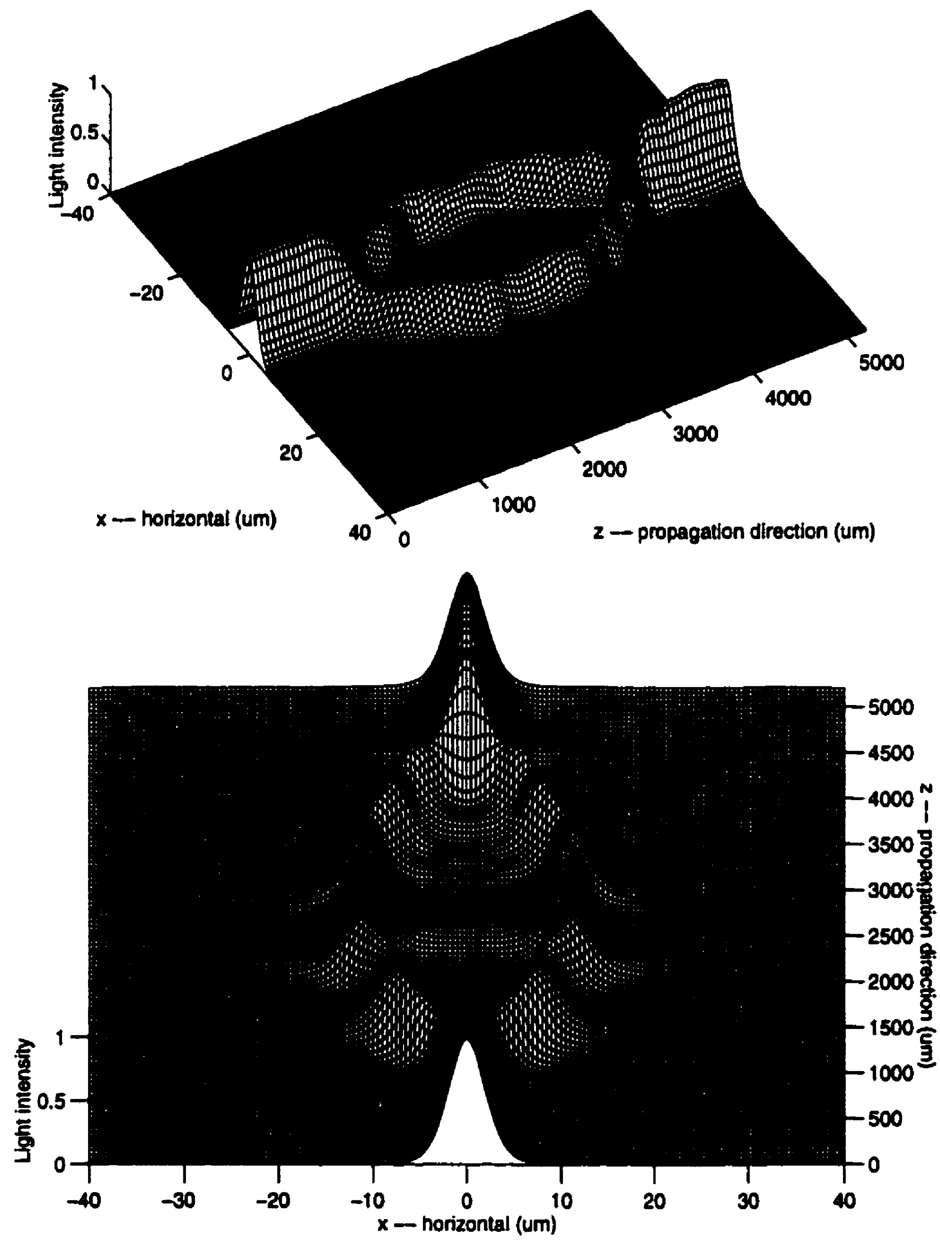

Figure 3.10: Beam propagation along a structure of L1=L5=500 μm, L2=L4=1500 μm, L3=1200 μm, W=6 μm and d=15 μm, $2\theta = 0.8°$

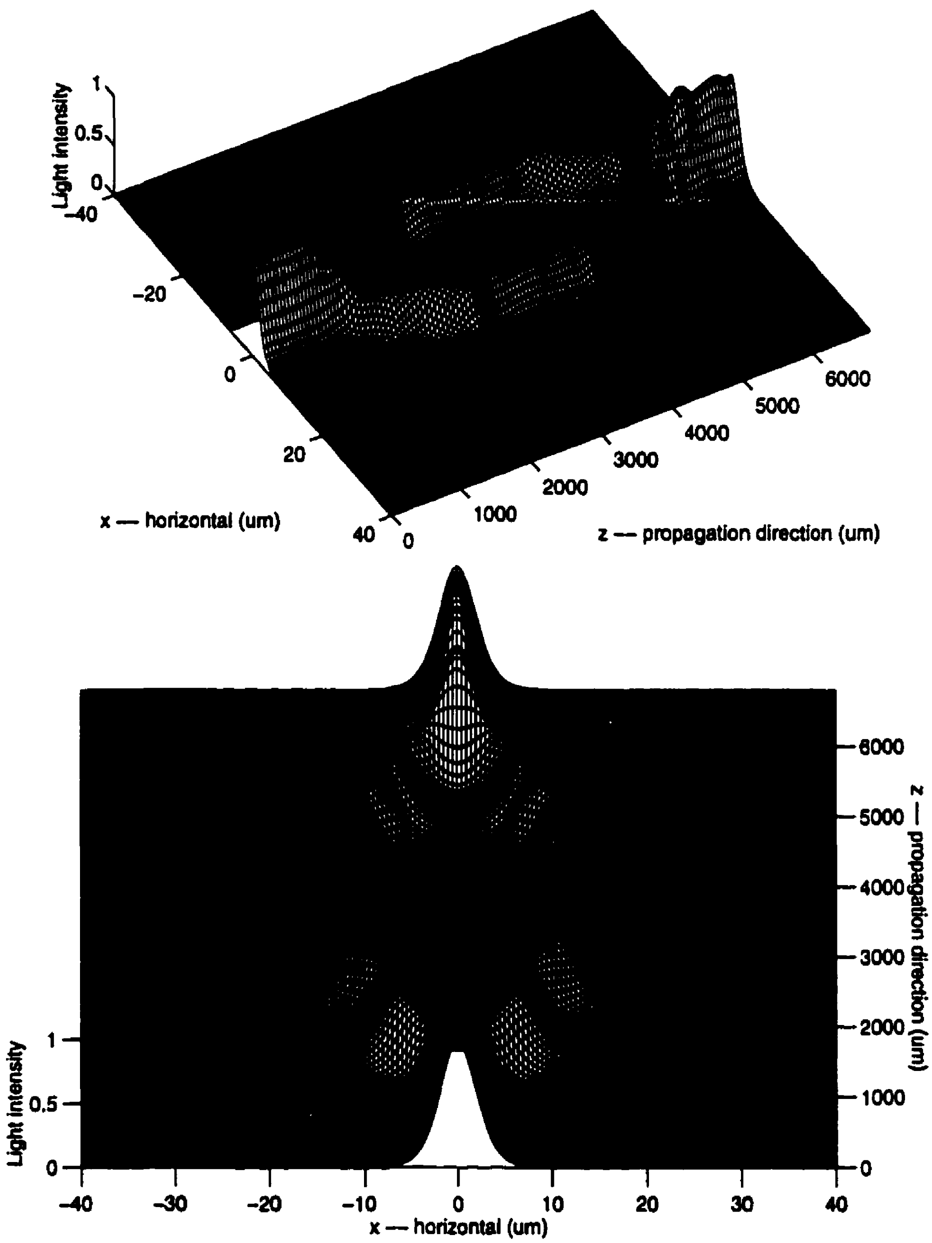

Figure 3.11: Beam propagation along a structure of L1=L5=500 μm, L2=L4=2000 μm, L3=1800 μm, W=6 μm and d=15 μm, $2\theta = 0.6°$

3.2 Design Optimization of Propagation Loss

3.2.1 Evaluation of Propagation Loss

There are three primary loss components contributing to the fiber–$Ti : LiNbO_3$ waveguide throughput loss: 1) Fresnel loss due to reflections of the optical field at the input and output interfaces, 2) propagation loss in the $LiNbO_3$ waveguide, and 3) mode mismatch loss due to the single–mode fiber and the channel waveguide having different mode sizes and shapes. These three kinds of losses can be isolated and estimated seperately [29]. From the output field distribution obtained by a combination of the EIM and FD–VBPM, the propagation loss can be calculated.

To calculate the propagation loss which is defined as $Loss = -10log(P_{out}/P_{in})$, we must find the output optical power and normalize it to the input optical power. The accurate way of calculating output power can be expressed as [30] [31]

$$P_{out} = \frac{\mid \int \psi_y^*(x,0)\psi_y(x,z)dx \mid^2}{(\int \mid \psi_y(x,0) \mid^2 dx)(\int \mid \psi_y(x,z) \mid^2 dx)} \tag{3.14}$$

where $\psi_y(x,0)$ is the eigen mode of the 2D single waveguide found by the effective index method and $\psi_y(x,z)$ represents the field distribution at the output end. It is obvious that using this formula, the input power is unity already which means the normalization is done simultaneously during the evaluation of the output power.

Although outside the scope of this project, it is worth mentioning that while the structure of the Y–branch can affect the propagation loss greatly, the waveguide fabrication parameters also play an important role in controlling both the propagation losses and coupling losses. This is studied in Ref. [32]. It is concluded that factors influencing waveguide optical losses are Ti-strip thickness, strip width, diffusion temperature, diffusion time, and crystal anisotropy. The Ti thickness changes the refractive index proportionally. A large refractive index change is preferable for obtaining high optical confinement in the waveguide. However, the diffusible Ti thickness is restricted by diffusion conditions, and non-diffused residual TiO_2 film on the waveguide causes a large scattering loss. The diffusible Ti thickness at $1000-1050°C$ for 5h is $400-600\mathring{A}$.

The diffusion temperature severely affects optical losses and is a most useful factor for controlling waveguide parameters. The strip width factor is effective in controlling the mode number. Total coupling losses are mostly influenced by vertical misalignment in the near–field pattern. Optimum fabrication parameters for achieving the lowest propagation and coupling losses for both Z-cut and Y-cut $LiNbO_3$ are summarized in [32].

3.2.2 Coherent Coupling Effect of Radiation Modes

In an ideal case, only the fundamental guided mode will exist inside the waveguide of the interferometer and any higher order modes and radiation modes can be ignored. Consequently, the propagation loss should increase monotonically with the decrease of L_2 and does not have much to do with the variation of L_3. But in fact, since the optical guiding is relatively weak, any small axial variation in the structure results in a coupling of a great amount of energy to the radiation modes. The radiation modes may be coupled coherently to the guided modes at another optical discontinuity, resulting in a reduction, or an increase, of the structure losses depending on the phase conditions satisfied at the second discontinuity [36]. This kind of coupling effect between the radiation modes and the guided mode has been studied in [33]–[36]. Among them, [36] is especially dedicated to M-Z electrooptic modulators in GaAs, although the data are less complete and the modulation characterization is much less accurate compared to what have been reported in this thesis.

Here, in this project, the coherent coupling of radiation modes is studied by using the 2D-FD-VBPM method for a $Ti : LiNbO_3$ M-Z modulator. Since the BPM is a non-modal technique which takes into account the propagation of both the radiation and guided modes, it is expected to give satisfactory results. Unlike [36] which only considered the effect of the length of the active region L_3 in computing the total propagation loss, both variations of L_2 and L_3 have been taken into consideration in this thesis with sufficient data to show more thoroughly that this coupling occurs both in the branching region and in the active region.

Fig. 3.12 and Fig. 3.13 give a rough idea about how the coupling of radiation modes can affect the output power through a small variation of L_3 from $9600\mu m$ to $9800\mu m$ for a structure of $L_1 = L_5 = 500\mu m$, $L_2 = L_4 = 1000\mu m$, $W = 6\mu m$ and $d = 15\mu m$. For $L_3 = 9600\mu m$, the total propagation loss is $0.1dB$, while for $L_3 = 9800\mu m$, the total propagation loss is $0.58dB$. From Fig. 3.13. we can see clearly that near the entrance of the second Y-branch, a bigger portion of energy is lost than what happens in Fig. 3.12. While it can not affect significantly either the bandwidth or the driving power of the device, a $200\mu m$ change in the length of the active region will give rise to a big difference in the propagation loss.

From Fig. 3.12–3.13 and those 3D figures listed in the previous subsection, it can be seen that the maximum of the electric field oscillates about the center of the waveguide in both the two-arm section and the branching section of the interferometer. As the coupling length of the interferometer arms is in the order of centimeters, this oscillatory behavior could not be attributed to the coupling between the two arms. This oscillation could be explained by the interference between the guided mode and a group of higher-order asymmetric radiation modes in each guide. These modes could be treated as an effective asymmetric mode [36]. According to the length of L_2 and L_3, the phase condition at the input of the second Y junction may favor the excitation of the guided or the radiation modes of the output guide. Therefore, the losses of the interferometer are expected to be an oscillatory function of the length L_3 and L_2.

Extensive computation has proved the above explanation. Two different seperation distances $d = 10\mu m$ and $d = 15\mu m$ were chosen. For each structure, different L_2 lengths were studied when for each length of L_2. the length of L_3 was varied from $1000\mu m$ to $20000\mu m$. A mathematical mean value was calculated for each L_2 in this L_3 variation range. This value was taken as the average propagation loss for a specific L_2 length. Tables 3.1 and 3.2 show the average propagation losses and minimum achievable losses for each of the two structures, respectively. Detailed loss data for the $d = 15\mu m$ structure is attached in Table 3.3 and Table 3.4 shows the relation between L_2 and branching angle. The data for the $d = 10\mu m$ structure is of less importance and has not been included because from the work done in Chapter 5,

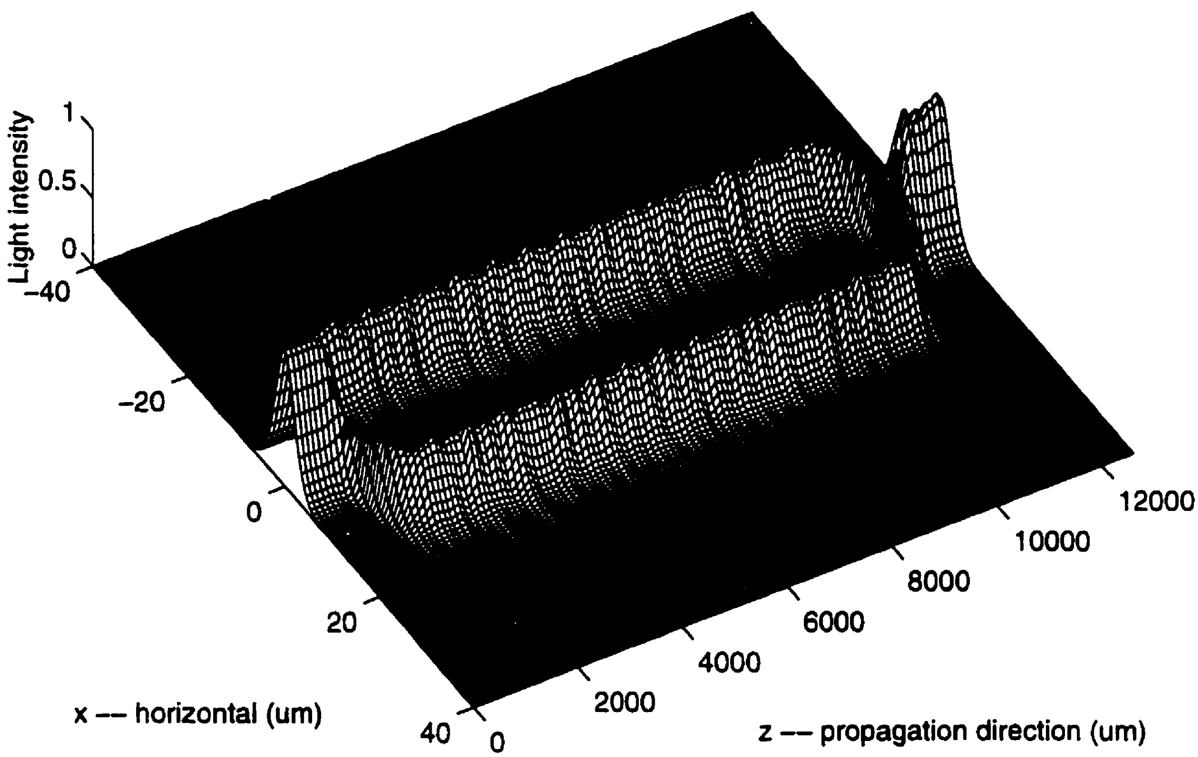

Figure 3.12: Beam propagation along a structure of L1=L5=500 μm, L2=L4=1000 μm, L3=9600 μm, W=6 μm and d=15 μm

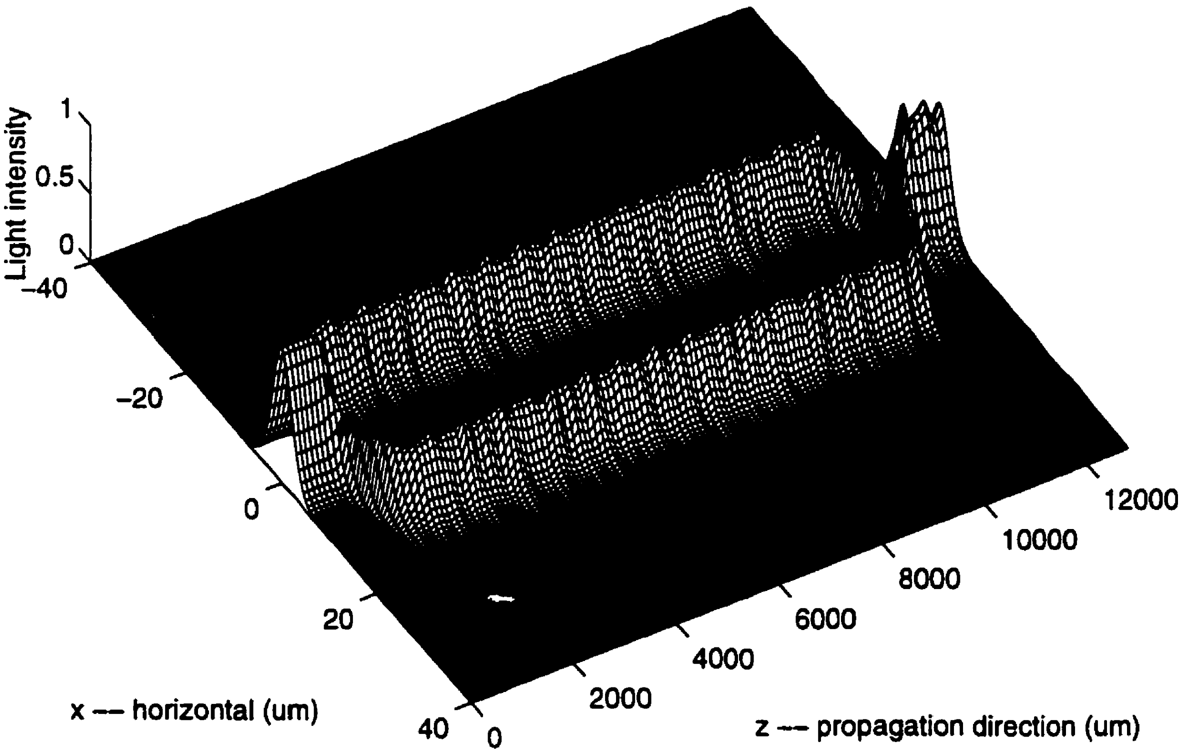

Figure 3.13: Beam propagation along a structure of L1=L5=500 μm, L2=L4=1000 μm, L3=9800 μm, W=6 μm and d=15 μm

it has been shown that this seperation is not sufficient to give good extinction ratio and thus can not be used in any future design.

Fig. 3.14 to 3.21 follow show that the fluctuation of loss with regard to L_3 is severe and has a large value for a small L_2 which corresponds to a big branching angle. This fluctuation tends to become smaller and less significant with the increase of L_2. However, this change is not monotonic. When L_2 reaches a certain value (for $d = 15\mu m$ this value is approximately $1000\mu m$ and for $d = 10\mu m$ this value is approximately $1200\mu m$), the average loss rises with the increase of L_2 until it reaches a maximum, and starts to decrease again with a further increase in L_2. Hence, it shows that the loss with L_2 is also a oscillatory function (Fig. 3.22 to 3.24).

The above-discussed results provide us with a special way to design a device with both a short transition length and small propagation loss. As can be seen from both the figures and the tables, for a structure with $d = 15\mu m$, a length $L_2 = 2000\mu m$ can offer a propagation loss of less than $0.1dB$ no matter how L_3 is chosen. However, in case a short device length is desired, which is usually the case when designing integrated optical circuits, we can also choose $L_2 = 1000\mu m$ and by delibrately setting a good L_3 length, a propagation loss of around $0.1dB$ can also be obtained without much difficulty and effect on other design characteristics. From Fig. 3.22 and Fig. 3.23, it can be seen that the minimum achievable loss is much smaller than the average loss for any value of L_2.

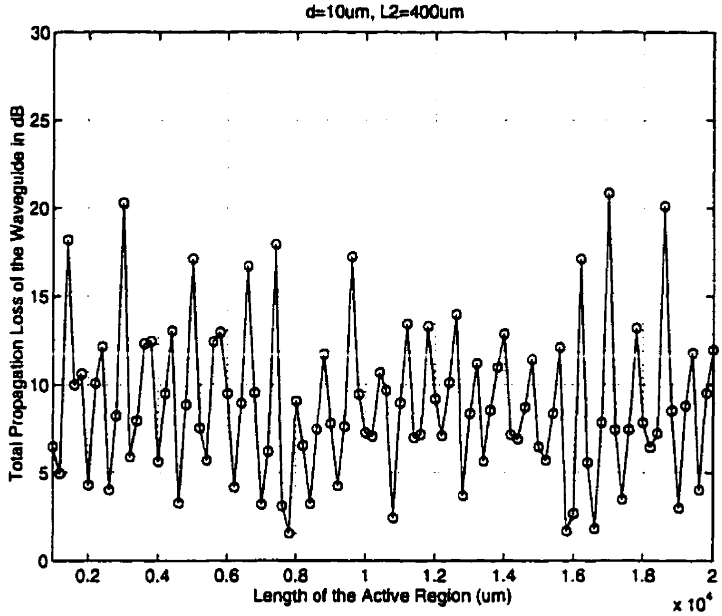

Figure 3.14: Propagation loss vs. L3 in a structure of L1=L5=500 μm, L2=L4=400 μm, W=6 μm and d=10 μm

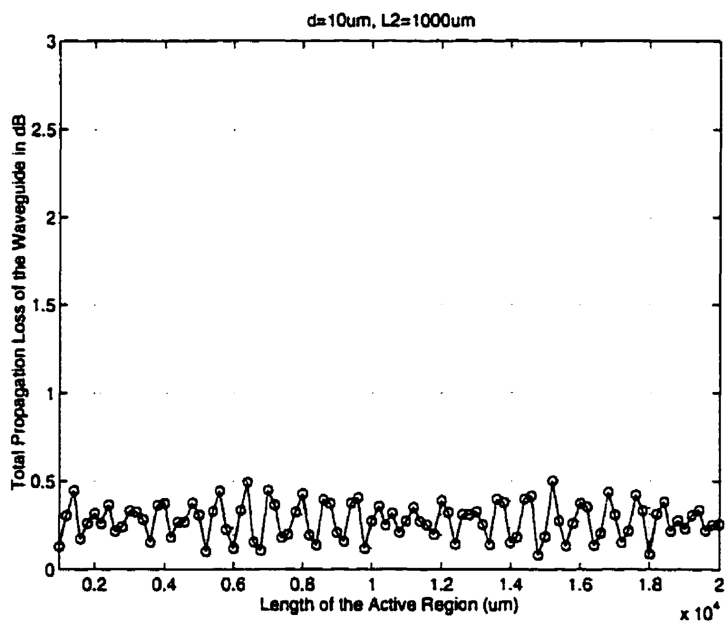

Figure 3.15: Propagation loss vs. L3 in a structure of L1=L5=500 μm, L2=L4=1000 μm, W=6 μm and d=10 μm

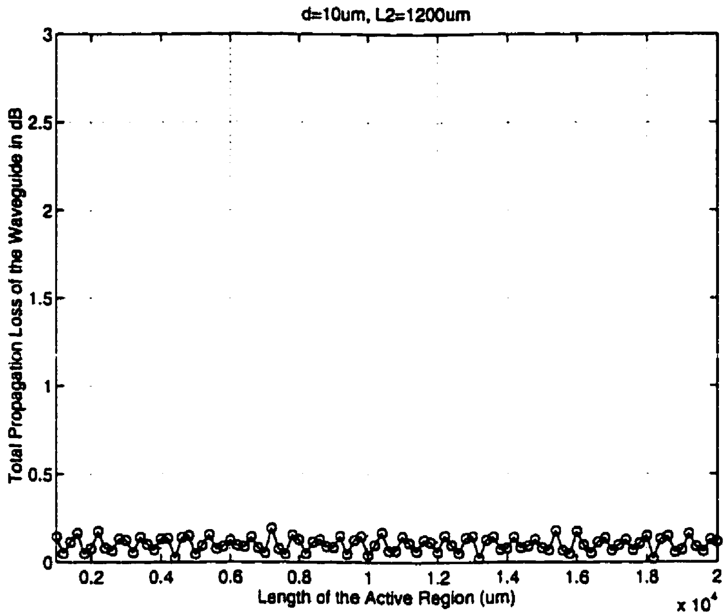

Figure 3.16: Propagation loss vs. L3 in a structure of L1=L5=500 μm, L2=L4=1200 μm, W=6 μm and d=10 μm

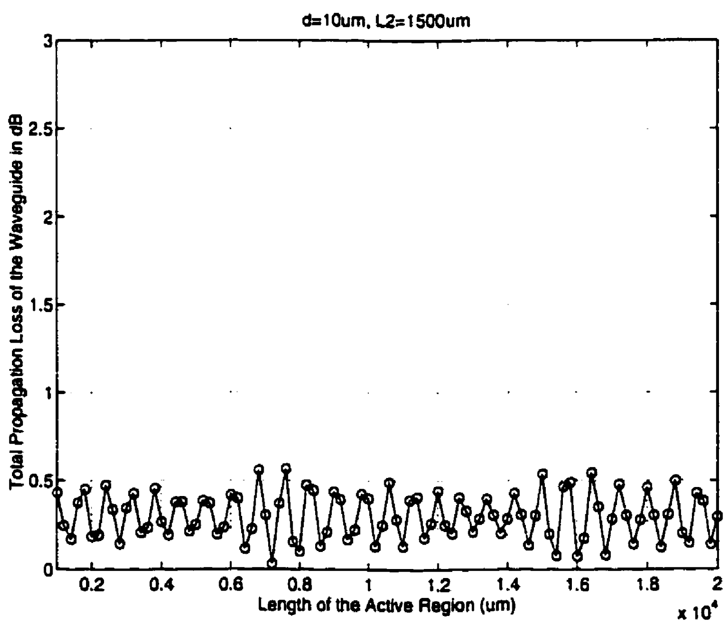

Figure 3.17: Propagation loss vs. L3 in a structure of L1=L5=500 μm, L2=L4=1500 μm, W=6 μm and d=10 μm

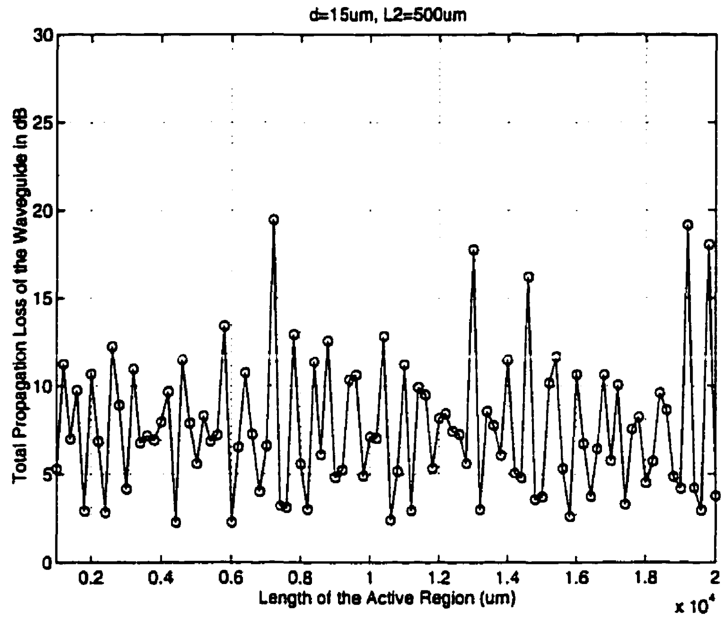

Figure 3.18: Propagation loss vs. L3 in a structure of L1=L5=500 μm, L2=L4=500 μm, W=6 μm and d=15 μm

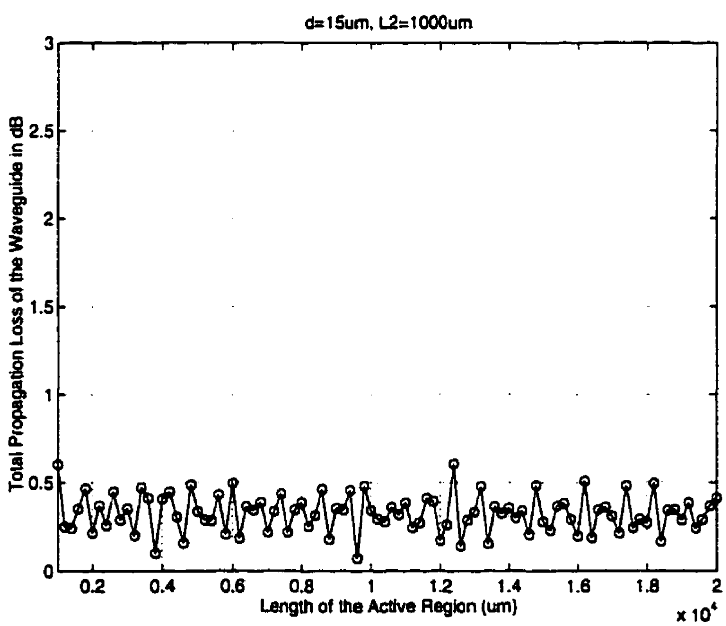

Figure 3.19: Propagation loss vs. L3 in a structure of L1=L5=500 μm, L2=L4=1000 μm, W=6 μm and d=15 μm

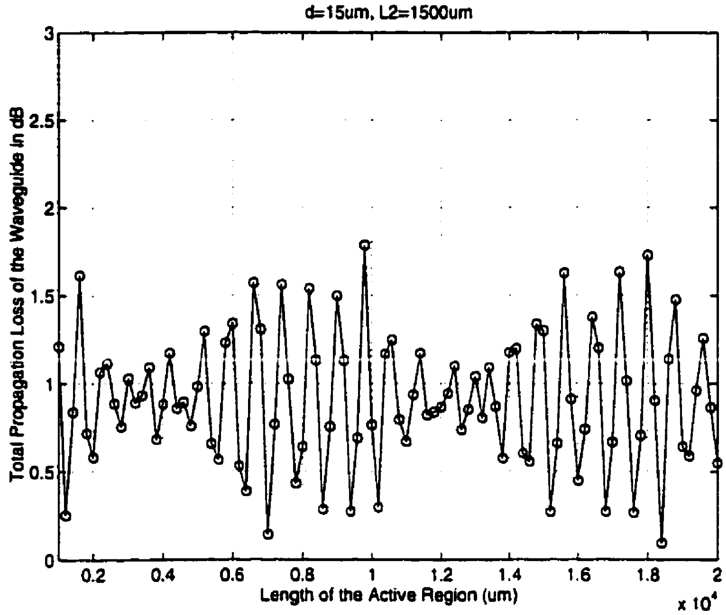

Figure 3.20: Propagation loss vs. L3 in a structure of L1=L5=500 μm, L2=L4=1500 μm, W=6 μm and d=15 μm

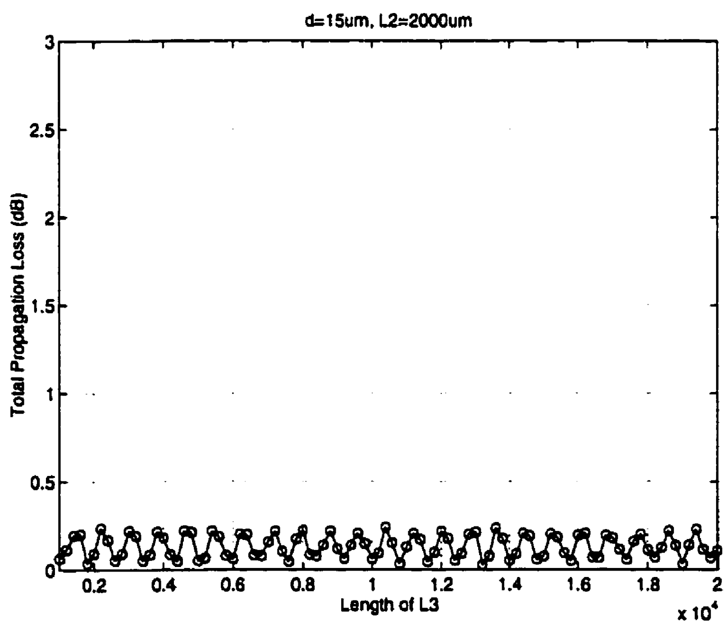

Figure 3.21: Propagation loss vs. L3 in a structure of L1=L5=500 μm, L2=L4=2000 μm, W=6 μm and d=15 μm

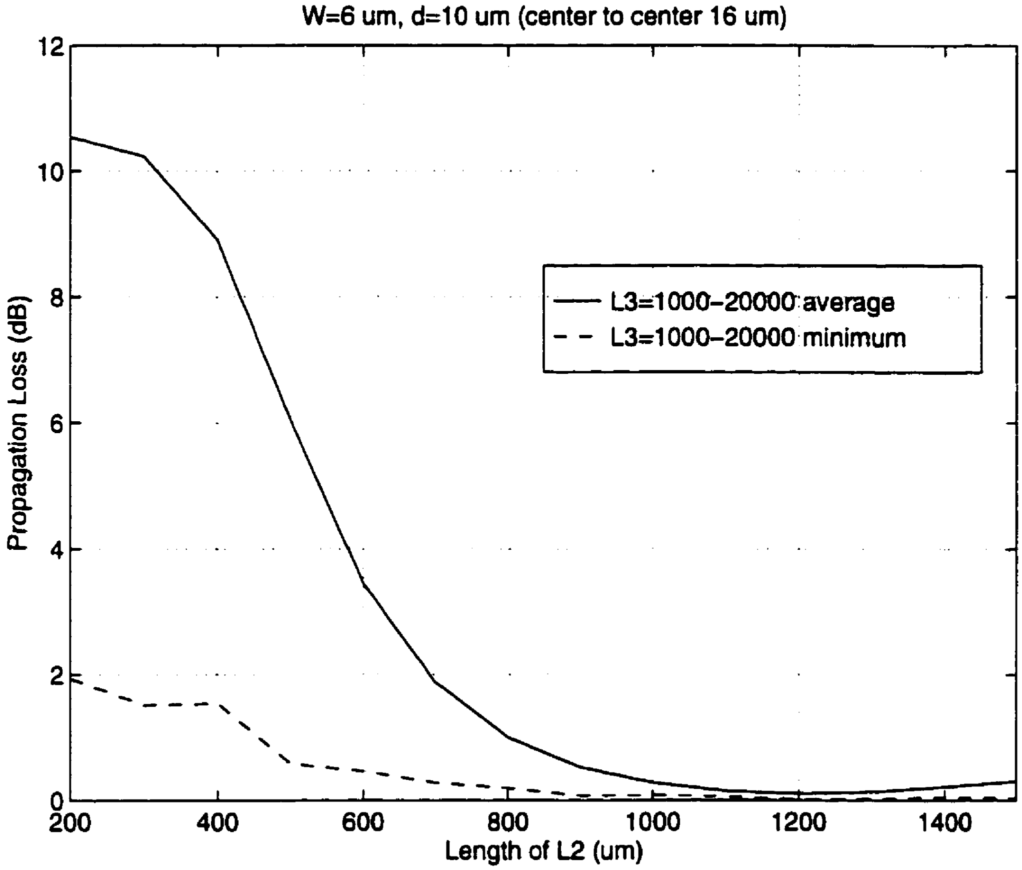

Figure 3.22: Average and minimum propagation loss (L3=1000 μm to 20000 μm) for different L2 lengths in a structure of L1=L5=500 μm, W=6 μm and d=10 μm

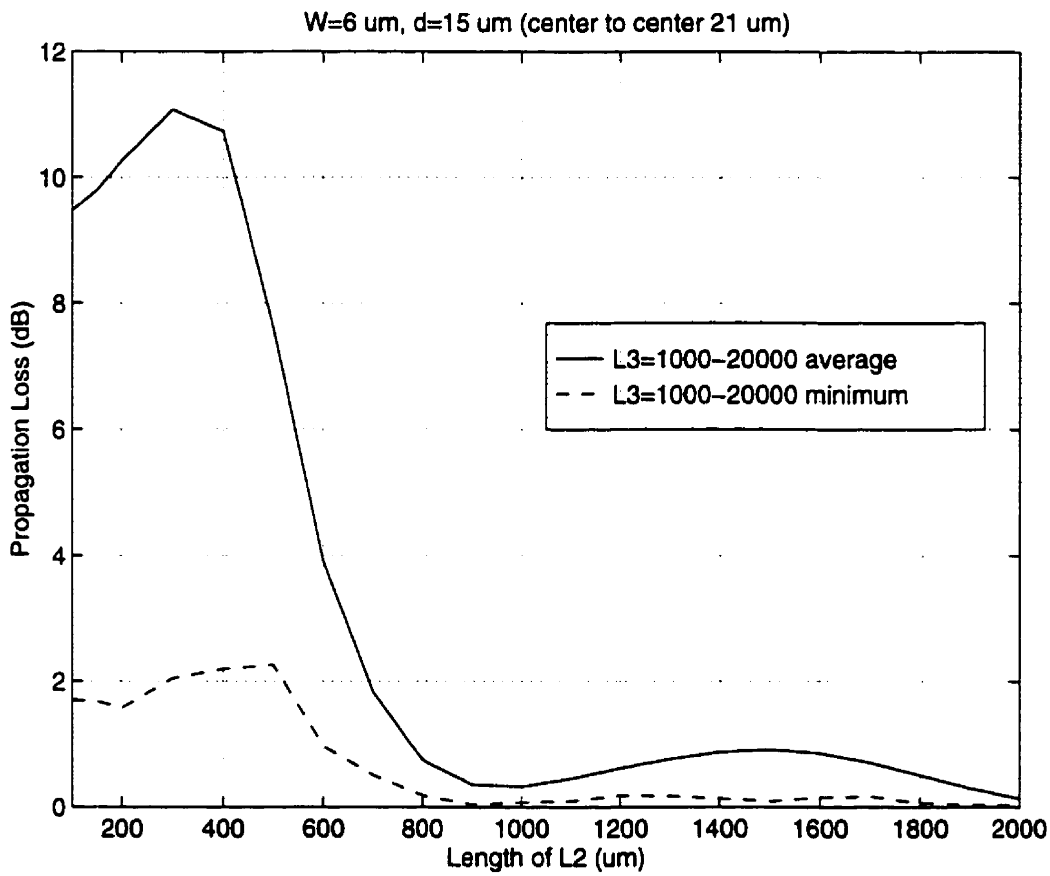

Figure 3.23: Average and minimum propagation loss (L3=1000 μm to 20000 μm) for different L2 lengths in a structure of L1=L5=500 μm, W=6 μm and d=15 μm

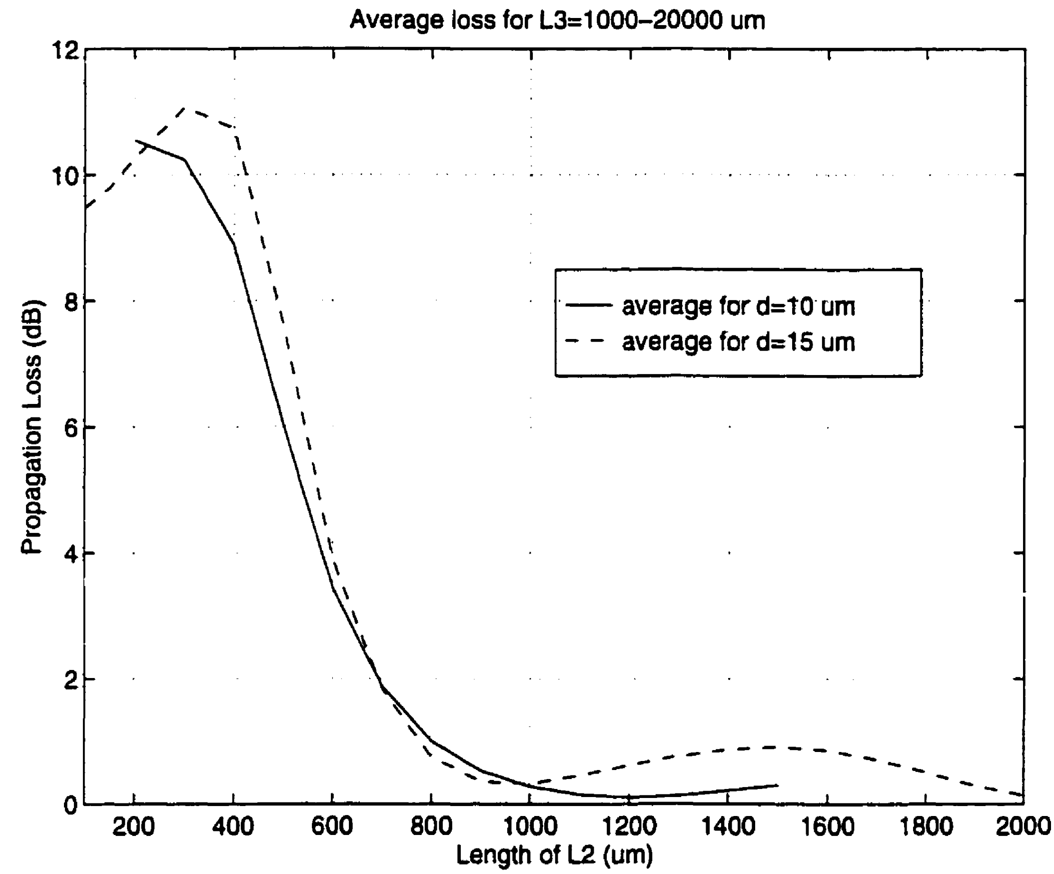

Figure 3.24: Comparison of average propagation losses (L3=1000 μm to 20000 μm) for different L2 lengths between d=10 μm and d=15 μm in structures of L1=L5=500 μm, W=6 μm

Table 3.1: Average and minimum achievable losses for different L2's with L3 from 1000 μm to 20000 μm (L1=L5=500 μm, W=6 μm and d=10 μm)

L2 (um)	Average Loss (dB)	Minimum Achievable Loss (dB)
200	10.543	1.934
300	10.229	1.512
400	8.890	1.539
500	6.027	0.581
600	3.445	0.463
700	1.872	0.278
800	1.001	0.195
900	0.526	0.067
1000	0.277	0.080
1100	0.147	0.055
1200	0.102	0.019
1300	0.134	0.022
1400	0.215	0.045
1500	0.300	0.030

Table 3.2: Average and minimum achievable losses for different L2's with L3 from 1000 μm to 20000 μm (L1=L5=500 μm, W=6 μm and d=15 μm)

L2 (um)	Average Loss (dB)	Minimum Achievable Loss (dB)
100	9.476	1.698
150	9.799	1.677
200	10.270	1.576
300	11.073	2.045
400	10.730	2.195
500	7.623	2.256
600	3.906	0.966
700	1.830	0.504
800	0.746	0.181
900	0.355	0.041
1000	0.327	0.071
1100	0.453	0.100
1200	0.618	0.186
1300	0.763	0.175
1400	0.872	0.135
1500	0.912	0.094
1600	0.854	0.157
1700	0.704	0.170
1800	0.502	0.061
1900	0.296	0.036
2000	0.133	0.027

Table 3.3: Propagation loss (dB) vs. different L2's and L3's for L1=L5=500 μm, W=6 μm, and d=15 μm

L3\L2	100	150	200	300	400	500	600
1000	8.810	8.308	8.991	18.303	9.213	5.293	3.666
1200	9.448	13.061	13.961	9.133	16.036	11.265	3.931
1400	8.208	7.483	7.107	9.634	9.575	6.987	4.916
1600	7.195	8.188	10.343	16.728	30.747	9.744	3.747
1800	11.611	13.854	19.761	13.302	6.253	2.918	1.799
2000	19.235	19.699	17.440	8.383	7.102	10.688	7.497
2200	12.798	10.104	7.700	7.900	10.144	6.859	2.566
2400	7.245	7.767	8.065	5.658	3.509	2.818	2.700
2600	6.421	5.241	4.512	5.387	10.753	12.252	6.024
2800	4.883	5.191	6.952	14.767	23.534	8.908	3.119
3000	6.846	7.933	8.866	10.498	7.684	4.158	2.688
3200	7.647	8.336	7.856	7.037	9.101	10.995	6.412
3400	7.645	8.110	8.845	12.192	15.554	6.783	2.945
3600	9.107	9.797	10.039	11.232	9.694	7.173	3.662
3800	12.464	16.862	22.054	50.508	13.394	6.937	3.605
4000	27.603	25.403	19.226	20.706	13.274	7.975	5.521
4200	18.875	21.582	31.696	13.994	18.082	9.665	3.271
4400	17.237	14.568	12.133	7.563	4.092	2.256	1.832
4600	12.065	9.962	7.493	5.343	8.007	11.488	6.749
4800	8.354	7.893	8.467	9.644	13.225	7.882	3.501
5000	7.813	8.116	8.756	10.442	9.025	5.587	3.068
5200	8.971	10.144	12.027	11.828	8.486	8.295	4.949
5400	11.028	9.594	8.027	10.379	18.060	6.869	2.780
5600	7.846	8.970	11.577	17.716	11.418	7.209	4.833
5800	11.802	13.624	17.259	22.490	25.232	13.401	4.961
6000	18.494	19.639	19.885	13.135	5.980	2.277	0.966
6200	25.567	19.153	12.732	6.065	5.066	6.531	5.616
6400	12.740	9.353	7.796	7.929	12.769	10.747	4.800
3600	7.754	7.153	6.720	7.557	9.067	7.263	3.514
6800	6.542	7.524	10.918	16.810	7.910	4.019	2.116
7000	10.616	11.455	11.061	9.733	8.344	6.613	4.521
7200	8.363	8.185	8.520	11.521	14.985	19.456	6.453
7400	6.993	7.981	8.314	6.728	4.972	3.194	1.569
7600	5.994	5.394	4.795	5.018	4.709	3.099	2.494
7800	4.262	4.840	6.149	5.727	7.024	12.928	7.883
8000	3.662	3.468	3.576	5.476	7.037	5.572	2.222
8200	2.623	3.266	2.879	2.045	2.195	3.010	3.634
8400	1.698	1.677	1.576	3.692	12.135	11.386	4.029
8600	1.791	2.804	4.522	13.775	13.136	6.098	2.967
8800	4.230	6.647	10.380	20.852	21.778	12.563	6.445
9000	7.418	9.090	12.117	20.312	9.175	4.820	2.497
9200	11.390	14.545	11.199	7.955	7.154	5.231	3.164
9400	8.432	8.877	9.221	10.725	18.172	10.352	4.776
9600	7.162	7.499	8.280	13.892	18.887	10.638	4.799
9800	7.283	9.393	12.985	12.892	7.859	4.890	3.035
10000	9.923	9.996	8.925	7.954	9.594	7.126	3.043
10200	7.423	7.461	7.720	16.141	12.016	7.047	4.912

L3\L2	100	150	200	300	400	500	600
10400	7.177	11.246	18.149	13.301	17.142	12.828	4.975
10600	9.760	10.003	10.770	9.355	5.224	2.384	1.174
10800	9.096	9.048	7.476	4.355	3.714	5.160	5.833
11000	5.724	4.939	4.425	4.814	9.268	11.239	3.698
11200	3.506	3.787	3.596	3.561	4.006	2.913	2.116
11400	2.775	3.374	4.171	5.728	9.318	9.923	5.607
11600	4.452	5.358	7.404	19.284	17.173	9.517	3.785
11800	7.685	9.913	10.320	11.586	10.792	5.330	2.684
12000	7.562	8.159	9.737	12.528	11.149	8.159	4.936
12200	11.424	13.231	15.248	18.323	22.384	8.437	3.916
12400	14.254	14.398	17.047	19.609	12.643	7.424	3.858
12600	20.618	24.253	28.364	32.577	16.101	7.235	3.164
12800	24.494	27.408	25.367	18.728	10.002	5.599	3.927
13000	28.879	27.471	22.573	12.144	12.968	17.760	5.148
13200	19.507	13.286	9.637	7.092	5.020	2.993	1.943
13400	10.812	9.092	7.684	7.018	8.335	8.568	5.409
13600	10.934	11.118	10.572	11.410	17.909	7.750	3.135
13800	9.784	9.781	11.260	14.353	10.175	6.071	3.750
14000	12.568	14.591	15.849	15.695	16.563	11.484	5.621
14200	16.366	17.883	19.085	20.789	12.129	5.027	1.879
14400	17.161	17.044	17.365	12.225	7.801	4.787	3.019
14600	26.373	20.072	17.133	16.139	11.594	16.237	8.224
14800	18.266	19.452	12.410	6.727	5.821	3.568	1.541
15000	9.898	7.845	6.415	4.794	3.874	3.710	2.964
15200	7.562	6.868	5.869	6.959	15.543	10.185	4.697
15400	5.854	6.698	7.959	14.559	22.092	11.685	5.778
15600	6.876	8.941	12.306	13.694	9.695	5.305	2.393
15800	9.144	10.073	9.861	6.741	4.616	2.594	1.770
16000	7.294	7.122	7.859	6.582	5.784	10.659	7.739
16200	5.852	5.525	4.011	3.575	7.191	6.714	3.248
16400	2.615	3.011	3.912	5.589	5.580	3.713	2.256
16600	3.445	4.308	5.396	6.306	6.093	6.444	4.928
16800	3.886	4.223	4.697	6.101	14.273	10.646	3.400
17000	3.002	3.314	4.106	6.822	7.789	5.755	4.481
17200	3.513	4.471	5.732	9.878	23.602	10.052	4.036
17400	6.049	8.647	15.077	14.942	7.242	3.274	1.352
17600	11.839	12.762	15.004	12.847	7.548	7.549	6.389
17800	11.500	13.143	11.840	7.386	9.307	8.235	3.881
18000	7.896	6.707	6.078	5.627	5.490	4.511	2.691
18200	5.717	5.774	6.341	9.410	10.636	5.735	3.066
18400	5.926	7.407	9.700	12.800	13.056	9.592	5.465
18600	6.505	7.553	10.011	10.165	11.695	8.639	4.317
18800	6.822	6.410	5.970	7.592	8.117	4.860	2.137
19000	5.767	6.807	9.108	10.050	5.664	4.185	3.501
19200	7.115	7.455	7.053	6.863	11.404	19.150	6.635
19400	4.679	5.098	5.912	6.586	6.710	4.203	1.611
19600	4.161	4.469	4.788	3.735	2.455	2.963	3.882
19800	3.698	3.124	2.356	3.426	9.296	18.041	4.848
20000	2.394	2.855	3.447	5.961	6.974	3.750	2.015

L3\L2	700	800	900	1000	1100	1200	1300
1000	1.861	0.626	0.421	0.602	0.673	0.736	1.044
1200	1.661	0.795	0.372	0.249	0.411	0.703	0.742
1400	2.653	0.965	0.345	0.239	0.303	0.238	0.222
1600	1.269	0.472	0.297	0.351	0.428	0.727	1.125
1800	1.456	1.010	0.529	0.466	0.725	0.964	1.128
2000	3.044	0.804	0.257	0.213	0.356	0.494	0.414
2200	0.782	0.319	0.225	0.368	0.379	0.336	0.560
2400	2.106	1.255	0.665	0.256	0.344	0.770	1.047
2600	2.700	0.765	0.176	0.448	0.778	0.869	0.957
2800	0.789	0.202	0.288	0.287	0.342	0.517	0.569
3000	2.034	1.184	0.552	0.352	0.364	0.366	0.521
3200	2.679	0.955	0.259	0.200	0.356	0.776	1.169
3400	1.242	0.431	0.329	0.471	0.832	0.899	0.702
3600	1.674	0.714	0.433	0.410	0.232	0.275	0.597
3800	1.867	0.973	0.352	0.100	0.384	0.748	0.940
4000	2.814	0.831	0.294	0.406	0.508	0.611	0.622
4200	1.010	0.440	0.379	0.446	0.615	0.702	0.880
4400	1.569	0.907	0.520	0.305	0.297	0.571	0.829
4600	2.803	0.893	0.103	0.156	0.482	0.652	0.643
4800	1.295	0.516	0.464	0.486	0.471	0.542	0.808
5000	1.985	1.076	0.536	0.334	0.477	0.744	0.748
5200	1.924	0.558	0.125	0.287	0.464	0.541	0.832
5400	1.086	0.489	0.396	0.282	0.420	0.766	0.877
5600	3.122	1.380	0.498	0.430	0.485	0.419	0.471
5800	1.542	0.399	0.255	0.206	0.371	0.699	0.917
6000	0.679	0.480	0.323	0.496	0.639	0.714	0.853
6200	2.888	1.222	0.452	0.183	0.298	0.579	0.840
6400	2.160	0.711	0.307	0.362	0.532	0.605	0.558
6600	1.354	0.563	0.315	0.343	0.380	0.482	0.581
6800	1.160	0.706	0.473	0.386	0.564	0.807	1.281
7000	2.753	1.026	0.294	0.218	0.386	0.754	0.749
7200	2.232	0.640	0.243	0.336	0.535	0.330	0.175
7400	0.700	0.473	0.550	0.436	0.234	0.505	1.049
7600	2.156	1.220	0.318	0.218	0.699	1.076	1.143
7800	2.594	0.488	0.195	0.346	0.429	0.480	0.568
8000	0.896	0.613	0.452	0.387	0.390	0.428	0.408
8200	2.601	1.271	0.505	0.251	0.292	0.490	0.856
8400	1.388	0.290	0.114	0.313	0.714	1.143	1.341
8600	1.548	0.741	0.428	0.462	0.490	0.441	0.399
8800	2.833	1.103	0.481	0.177	0.180	0.296	0.412
9000	1.209	0.488	0.193	0.355	0.495	0.736	1.068
9200	1.588	0.728	0.432	0.344	0.671	0.970	1.041
9400	2.316	0.854	0.391	0.456	0.423	0.427	0.604
9600	1.912	0.806	0.258	0.071	0.215	0.448	0.393
9800	1.594	0.646	0.409	0.480	0.564	0.573	0.870
10000	1.417	0.722	0.412	0.343	0.525	1.037	1.393
10200	2.663	0.952	0.298	0.294	0.562	0.503	0.273

L3\L2	700	800	900	1000	1100	1200	1300
10400	1.579	0.406	0.242	0.278	0.136	0.201	0.444
10600	1.010	0.936	0.555	0.359	0.583	0.875	1.200
10800	3.318	1.017	0.339	0.318	0.539	0.849	0.934
11000	0.903	0.181	0.091	0.385	0.568	0.499	0.481
11200	1.497	1.011	0.652	0.245	0.100	0.281	0.531
11400	2.972	1.103	0.285	0.272	0.590	0.859	1.087
11600	1.123	0.233	0.217	0.412	0.608	0.830	0.932
11800	1.464	0.790	0.490	0.392	0.444	0.423	0.390
12000	2.498	1.014	0.320	0.171	0.145	0.366	0.811
12200	1.780	0.640	0.299	0.261	0.660	0.990	0.917
12400	1.742	0.650	0.391	0.605	0.556	0.489	0.686
12600	1.324	0.754	0.391	0.141	0.314	0.664	0.868
12800	2.558	0.916	0.274	0.286	0.393	0.468	0.517
13000	1.666	0.581	0.315	0.333	0.503	0.694	0.899
13200	1.377	0.815	0.558	0.478	0.533	0.694	0.858
13400	2.412	0.776	0.153	0.152	0.359	0.574	0.618
13600	1.167	0.422	0.322	0.364	0.462	0.530	0.816
13800	2.406	1.204	0.572	0.326	0.382	0.693	0.745
14000	2.191	0.702	0.177	0.353	0.602	0.585	0.682
14200	0.504	0.184	0.339	0.299	0.337	0.677	0.950
14400	2.380	1.321	0.465	0.339	0.516	0.570	0.651
14600	2.748	0.770	0.287	0.207	0.302	0.561	0.734
14800	0.632	0.318	0.286	0.483	0.661	0.683	0.641
15000	1.777	0.910	0.483	0.277	0.286	0.525	0.984
15200	2.340	0.853	0.286	0.228	0.540	0.851	0.901
15400	2.294	0.732	0.247	0.367	0.397	0.347	0.242
15600	0.897	0.543	0.498	0.381	0.452	0.573	0.906
15800	1.650	0.908	0.377	0.291	0.421	0.860	1.208
16000	2.822	0.805	0.143	0.198	0.600	0.655	0.463
16200	1.194	0.451	0.464	0.507	0.268	0.236	0.483
16400	1.664	1.106	0.462	0.187	0.416	0.771	0.926
16600	2.246	0.533	0.186	0.346	0.587	0.768	1.074
16800	1.134	0.467	0.303	0.359	0.487	0.685	0.647
17000	2.808	1.345	0.544	0.308	0.275	0.186	0.245
17200	1.471	0.400	0.208	0.212	0.372	0.771	1.126
17400	0.811	0.546	0.331	0.482	0.760	0.904	1.032
17600	3.059	1.126	0.470	0.243	0.287	0.454	0.521
17800	1.657	0.586	0.192	0.291	0.367	0.384	0.441
18000	1.312	0.626	0.437	0.271	0.392	0.666	0.896
18200	1.783	0.791	0.396	0.494	0.695	0.904	1.250
18400	2.327	0.829	0.234	0.166	0.330	0.569	0.463
18600	1.828	0.622	0.336	0.342	0.387	0.222	0.201
18800	1.079	0.687	0.472	0.347	0.307	0.708	1.331
19000	2.361	1.064	0.335	0.287	0.792	1.086	0.973
19200	2.045	0.368	0.151	0.384	0.315	0.254	0.310
19400	0.728	0.676	0.504	0.242	0.295	0.439	0.616
19600	3.094	1.256	0.468	0.290	0.397	0.707	1.028
19800	1.335	0.249	0.041	0.367	0.779	0.993	1.017
20000	1.098	0.643	0.546	0.412	0.301	0.285	0.348

L3\L2	1400	1500	1600	1700	1800	1900	2000
1000	1.356	1.210	0.718	0.386	0.291	0.197	0.061
1200	0.493	0.253	0.319	0.498	0.470	0.267	0.115
1400	0.402	0.839	1.149	1.003	0.628	0.354	0.194
1600	1.564	1.614	1.231	0.811	0.577	0.416	0.201
1800	0.981	0.718	0.578	0.566	0.479	0.225	0.035
2000	0.422	0.582	0.747	0.691	0.397	0.171	0.091
2200	0.868	1.066	0.999	0.699	0.483	0.379	0.236
2400	1.158	1.115	0.899	0.770	0.689	0.451	0.167
2600	0.984	0.887	0.902	0.862	0.568	0.225	0.053
2800	0.570	0.756	0.831	0.564	0.258	0.126	0.091
3000	0.901	1.030	0.782	0.559	0.491	0.403	0.218
3200	1.128	0.891	0.844	0.890	0.755	0.458	0.190
3400	0.684	0.935	1.099	0.903	0.539	0.221	0.051
3600	0.998	1.094	0.827	0.516	0.275	0.138	0.084
3800	0.861	0.683	0.608	0.547	0.466	0.368	0.215
4000	0.687	0.884	0.950	0.859	0.706	0.457	0.181
4200	1.143	1.172	1.076	0.931	0.645	0.292	0.086
4400	0.840	0.859	0.847	0.615	0.271	0.076	0.046
4600	0.805	0.894	0.710	0.438	0.329	0.335	0.221
4800	0.883	0.760	0.679	0.746	0.786	0.541	0.211
5000	0.791	0.983	1.201	1.177	0.743	0.261	0.050
5200	1.155	1.295	1.102	0.594	0.151	0.036	0.066
5400	0.822	0.658	0.360	0.170	0.274	0.369	0.218
5600	0.562	0.568	0.660	0.925	0.947	0.555	0.188
5800	1.020	1.232	1.509	1.310	0.679	0.222	0.080
6000	1.140	1.340	0.986	0.366	0.061	0.056	0.060
6200	0.894	0.532	0.161	0.176	0.378	0.389	0.202
6400	0.371	0.389	0.793	1.121	0.957	0.519	0.198
6600	0.963	1.569	1.686	1.177	0.569	0.213	0.080
6800	1.620	1.309	0.718	0.302	0.153	0.125	0.078
7000	0.376	0.144	0.167	0.304	0.390	0.322	0.159
7200	0.386	0.768	1.055	1.095	0.869	0.509	0.218
7400	1.436	1.561	1.429	1.066	0.619	0.274	0.103
7600	1.135	1.026	0.756	0.423	0.187	0.092	0.044
7800	0.554	0.433	0.321	0.297	0.335	0.309	0.174
8000	0.469	0.641	0.867	0.994	0.878	0.533	0.222
8200	1.251	1.538	1.518	1.180	0.650	0.249	0.086
8400	1.343	1.133	0.788	0.374	0.142	0.114	0.078
8600	0.333	0.287	0.204	0.238	0.363	0.312	0.140
8800	0.608	0.755	0.966	1.129	0.913	0.501	0.219
9000	1.271	1.498	1.546	1.092	0.546	0.249	0.118
9200	1.192	1.132	0.668	0.279	0.183	0.159	0.063
9400	0.559	0.273	0.224	0.427	0.495	0.318	0.138
9600	0.352	0.689	1.128	1.125	0.740	0.400	0.204
9800	1.468	1.785	1.430	0.870	0.525	0.330	0.148
10000	1.231	0.765	0.455	0.392	0.356	0.207	0.061
10200	0.153	0.298	0.559	0.635	0.447	0.216	0.095

L3\L2	1400	1500	1600	1700	1800	1900	2000
10400	0.843	1.168	1.160	0.868	0.583	0.410	0.240
10600	1.356	1.248	1.005	0.795	0.639	0.400	0.151
10800	0.873	0.794	0.743	0.669	0.435	0.170	0.033
11000	0.565	0.670	0.727	0.568	0.339	0.205	0.129
11200	0.757	0.938	0.856	0.676	0.553	0.402	0.207
11400	1.267	1.172	1.036	0.935	0.724	0.426	0.169
11600	0.813	0.822	0.863	0.698	0.411	0.166	0.044
11800	0.632	0.839	0.740	0.518	0.337	0.199	0.100
12000	0.988	0.869	0.762	0.681	0.541	0.380	0.218
12200	0.835	0.944	1.014	0.875	0.670	0.428	0.174
12400	1.005	1.102	0.937	0.753	0.518	0.226	0.050
12600	0.840	0.738	0.728	0.613	0.345	0.152	0.093
12800	0.640	0.852	0.829	0.568	0.392	0.328	0.200
13000	1.111	1.039	0.823	0.757	0.737	0.518	0.212
13200	0.810	0.805	0.956	0.983	0.652	0.219	0.027
13400	0.817	1.093	1.059	0.630	0.200	0.070	0.078
13600	1.011	0.869	0.527	0.292	0.335	0.387	0.235
13800	0.641	0.576	0.650	0.873	0.887	0.531	0.176
14000	0.917	1.177	1.396	1.216	0.638	0.187	0.050
14200	1.111	1.197	0.916	0.375	0.073	0.071	0.088
14400	0.770	0.602	0.292	0.254	0.419	0.414	0.205
14600	0.629	0.556	0.800	1.082	0.930	0.503	0.191
14800	0.854	1.338	1.549	1.123	0.543	0.190	0.058
15000	1.400	1.300	0.741	0.288	0.114	0.097	0.076
15200	0.616	0.271	0.218	0.352	0.457	0.394	0.203
15400	0.300	0.662	1.009	1.077	0.845	0.471	0.182
15600	1.420	1.627	1.455	1.061	0.604	0.257	0.094
15800	1.130	0.911	0.658	0.357	0.136	0.066	0.048
16000	0.438	0.449	0.373	0.336	0.380	0.358	0.195
16200	0.658	0.741	0.876	0.999	0.891	0.526	0.207
16400	1.106	1.377	1.476	1.170	0.626	0.223	0.068
16600	1.294	1.200	0.795	0.327	0.079	0.066	0.066
16800	0.470	0.272	0.157	0.220	0.395	0.389	0.193
17000	0.421	0.666	0.962	1.166	0.955	0.487	0.179
17200	1.416	1.631	1.618	1.130	0.530	0.220	0.112
17400	1.115	1.016	0.585	0.182	0.091	0.113	0.057
17600	0.478	0.267	0.174	0.372	0.514	0.373	0.162
17800	0.471	0.704	1.148	1.231	0.846	0.434	0.201
18000	1.307	1.728	1.503	0.889	0.452	0.246	0.112
18200	1.359	0.903	0.433	0.278	0.272	0.193	0.068
18400	0.135	0.094	0.356	0.557	0.476	0.270	0.127
18600	0.610	1.138	1.306	1.047	0.698	0.431	0.221
18800	1.645	1.475	1.101	0.788	0.552	0.329	0.137
19000	0.768	0.640	0.585	0.514	0.351	0.154	0.031
19200	0.446	0.587	0.635	0.540	0.374	0.241	0.139
19400	0.819	0.961	0.968	0.839	0.671	0.454	0.227
19600	1.222	1.257	1.119	0.910	0.622	0.324	0.115
19800	0.975	0.864	0.757	0.566	0.344	0.176	0.067
20000	0.420	0.548	0.560	0.469	0.362	0.223	0.106

Table 3.4: Relationship between the length of L2 and corresponding full branching angle for d=15 μm ($2.0 \times tan^{-1}(10.5/L2)$)

Length of L2 (μm)	Full Branching Angle 2θ (degree)
100	11.99
150	8.01
200	6.01
300	4.01
400	3.01
500	2.41
600	2.01
700	1.72
800	1.50
900	1.34
1000	1.20
1100	1.09
1200	1.00
1300	0.93
1400	0.86
1500	0.80
1600	0.75
1700	0.71
1800	0.67
1900	0.63
2000	0.60

3.3 Appendices

3.3.1 Vector Helmholtz Equations in Isotopic Media

We begin with the basic Maxwell's equations in a linear, nonconducting, nonmagnetic and isotropic medium:

$$\nabla \times \vec{H} = j\omega\epsilon\vec{E} \tag{3.15}$$

$$\nabla \times \vec{E} = -j\omega\mu_0\vec{H} \tag{3.16}$$

$$\nabla \cdot (\epsilon\vec{E}) = 0 \tag{3.17}$$

$$\nabla \cdot \vec{H} = 0 \tag{3.18}$$

and also assuming a time dependent term $exp(j\omega t)$ for both electric and magnetic fields. Do curl on (3.16) and make use of (3.15), we have

$$\nabla \times (\nabla \times \vec{E}) = -j\omega\mu_0(\nabla \times \vec{H}) = -j\omega\mu_0(j\omega\epsilon\vec{E})$$

$$\nabla \times (\nabla \times \vec{E}) = \omega^2\mu_0\epsilon\vec{E} \tag{3.19}$$

Using vector identity

$$\nabla \times (\nabla \times \vec{E}) = \nabla(\nabla \cdot \vec{E}) - \nabla^2\vec{E} \tag{3.20}$$

$$\nabla \cdot (\epsilon\vec{E}) = \epsilon\nabla \cdot \vec{E} + \nabla\epsilon \cdot \vec{E}$$

By equation (3.17), we can get

$$\nabla \cdot \vec{E} = -\frac{\nabla\epsilon}{\epsilon} \cdot \vec{E} = -\nabla \ln\epsilon \cdot \vec{E} \tag{3.21}$$

Using (3.19), (3.20) and (3.21), we get

$$\nabla(\nabla \ln\epsilon \cdot \vec{E}) + \nabla^2\vec{E} + \omega^2\mu_0\epsilon\vec{E} = 0 \tag{3.22}$$

with $\epsilon = \epsilon_0 n^2$, and $k_0^2 = \omega^2\mu_0\epsilon_0$, (3.22) could be rewritten as

$$\nabla^2\vec{E} + n^2k_0^2\vec{E} = -\nabla(\nabla \ln\epsilon \cdot \vec{E}) \tag{3.23}$$

If the refractive index varies slowly along z-axis (refer to Fig. 2.1 for the co-ordinate system used) and so does $\vec{E}$, then only the transverse field components are of interest and (3.23) becomes

$$\nabla^2\vec{E}_t + n^2k_0^2\vec{E}_t = -\nabla_t(\nabla_t \ln n^2 \cdot \vec{E}_t) \tag{3.24}$$

where $\vec{E}_t = E_x\hat{i} + E_y\hat{j}$ and $\nabla_t = \frac{\partial}{\partial x}\hat{i} + \frac{\partial}{\partial y}\hat{j}$. Seperating (3.24) into x and y components, we have

$$\nabla^2 E_x + n^2k_0^2E_x = -\frac{\partial}{\partial x}(\frac{\partial \ln n^2}{\partial x}E_x) - \frac{\partial}{\partial x}(\frac{\partial \ln n^2}{\partial y}E_y) \tag{3.25}$$

$$\nabla^2 E_y + n^2k_0^2E_y = -\frac{\partial}{\partial y}(\frac{\partial \ln n^2}{\partial x}E_x) - \frac{\partial}{\partial y}(\frac{\partial \ln n^2}{\partial y}E_y) \tag{3.26}$$

Now assume that these transverse fields can be represented by plane waves travelling in a homogeneous medium where n_0 is a reference refractive index.

$$\vec{E}_t = \vec{\psi}_t e^{-jk_0n_0z} \tag{3.27}$$

For the x component:

$$E_x = \psi_x e^{-jk_0n_0z}$$

$$\frac{\partial E_x}{\partial x} = \frac{\partial \psi_x}{\partial x}e^{-jk_0n_0z}; \quad \frac{\partial E_x}{\partial y} = \frac{\partial \psi_x}{\partial y}e^{-jk_0n_0z}; \quad \frac{\partial E_x}{\partial z} = \frac{\partial \psi_x}{\partial z}e^{-jk_0n_0z} - jk_0n_0\psi_x e^{-jk_0n_0z}$$

$$\frac{\partial^2 E_x}{\partial z^2} = \frac{\partial^2 \psi_x}{\partial z^2}e^{-jk_0n_0z} - jk_0n_0\frac{\partial \psi_x}{\partial z}e^{-jk_0n_0z} - jk_0n_0\frac{\partial \psi_x}{\partial z}e^{-jk_0n_0z} - k_0^2n_0^2\psi_x e^{-jk_0n_0z}$$

$$\frac{\partial^2 E_x}{\partial z^2} = (\frac{\partial^2 \psi_x}{\partial z^2} - 2jk_0n_0\frac{\partial \psi_x}{\partial z} - k_0^2n_0^2\psi_x)e^{-jk_0n_0z}$$

Making use of the slowly varying envelope approximation:

$$|\frac{\partial^2 \psi_x}{\partial z^2}| \ll 2k_0n_0|\frac{\partial \psi_z}{\partial z}| \tag{3.28}$$

We have:

$$\frac{\partial^2 E_x}{\partial z^2} = (-2jk_0n_0\frac{\partial \psi_x}{\partial z} - k_0^2n_0^2\psi_x)e^{-jk_0n_0z} \tag{3.29}$$

Substituting (3.29) into (3.25) and cancelling out the $exp(-jk_0n_0z)$ terms on both sides, we have

$$\frac{\partial^2 \psi_x}{\partial x^2} + \frac{\partial^2 \psi_x}{\partial y^2} - 2jk_0n_0\frac{\partial \psi_x}{\partial z} - k_0^2n_0^2\psi_x + n^2k_0^2\psi_x = -\frac{\partial}{\partial x}(\frac{\partial \ln n^2}{\partial x}\psi_x) - \frac{\partial}{\partial x}(\frac{\partial \ln n^2}{\partial y}\psi_y) \tag{3.30}$$

Note that

$$\frac{\partial}{\partial x}(n^2\psi_x) = \frac{\partial n^2}{\partial x}\psi_x + n^2\frac{\partial\psi_x}{\partial x}$$

$$\frac{\partial}{\partial x}(\frac{1}{n^2}\frac{\partial n^2}{\partial x}\psi_x) = \frac{\partial}{\partial x}(\frac{1}{n^2}\frac{\partial}{\partial x}(n^2\psi_x)) - \frac{\partial}{\partial x}(\frac{1}{n^2}n^2\frac{\partial\psi_x}{\partial x})$$

$$\frac{\partial}{\partial x}(\frac{1}{n^2}\frac{\partial n^2}{\partial x}\psi_x) = \frac{\partial}{\partial x}(\frac{1}{n^2}\frac{\partial}{\partial x}(n^2\psi_x)) - \frac{\partial}{\partial x}(\frac{\partial\psi_x}{\partial x})$$

Similarly,

$$\frac{\partial}{\partial x}(\frac{1}{n^2}\frac{\partial n^2}{\partial y}\psi_y) = \frac{\partial}{\partial x}(\frac{1}{n^2}\frac{\partial}{\partial y}(n^2\psi_y)) - \frac{\partial^2\psi_y}{\partial x\partial y}$$

Thus (3.30) becomes

$$j\frac{\partial\psi_x}{\partial z} = \frac{1}{2n_0k_0}[\frac{\partial^2\psi_x}{\partial y^2} + (n^2 - n_0^2)k_0^2\psi_x + \frac{\partial}{\partial x}(\frac{1}{n^2}\frac{\partial}{\partial x}(n^2\psi_x)) + \frac{\partial}{\partial x}(\frac{1}{n^2}\frac{\partial}{\partial y}(n^2\psi_y)) - \frac{\partial^2\psi_y}{\partial x\partial y}] \tag{3.31}$$

Similarly (3.26) becomes

$$j\frac{\partial\psi_y}{\partial z} = \frac{1}{2n_0k_0}[\frac{\partial^2\psi_y}{\partial x^2} + (n^2 - n_0^2)k_0^2\psi_y + \frac{\partial}{\partial y}(\frac{1}{n^2}\frac{\partial}{\partial y}(n^2\psi_y)) + \frac{\partial}{\partial y}(\frac{1}{n^2}\frac{\partial}{\partial x}(n^2\psi_x)) - \frac{\partial^2\psi_x}{\partial x\partial y}] \tag{3.32}$$

When TM-like or TE-like waves are concerned, which means either the y component or the x component is zero ($\psi_x \neq 0, \psi_z \neq 0, \psi_y = 0$ or $\psi_y \neq 0, \psi_z \neq 0, \psi_x = 0$, refer to Fig. 2.1 for the co-ordinate system used), the above two paraxial-wave Helmholtz equations in isotropic media could be simplified to

$$TM: \quad j\frac{\partial\psi_x}{\partial z} = \frac{1}{2n_0k_0}[\frac{\partial^2\psi_x}{\partial y^2} + (n^2 - n_0^2)k_0^2\psi_x + \frac{\partial}{\partial x}(\frac{1}{n^2}\frac{\partial}{\partial x}(n^2\psi_x))] \tag{3.33}$$

$$TE: \quad j\frac{\partial\psi_y}{\partial z} = \frac{1}{2n_0k_0}[\frac{\partial^2\psi_y}{\partial x^2} + (n^2 - n_0^2)k_0^2\psi_y + \frac{\partial}{\partial y}(\frac{1}{n^2}\frac{\partial}{\partial y}(n^2\psi_y))] \tag{3.34}$$

In a 3-D problem like diffused channel waveguides, the above n should be written as $n(x, y, z)$. If we use the Effective Index Method to reduce a 3-D problem to a 2-D problem, the above two Helmholtz equations could be further simplified (assuming that the coordinates are chosen so that y is the depth direction and $\partial/\partial y = 0$):

$$TM: \quad j\frac{\partial\psi_x}{\partial z} = \frac{1}{2n_0k_0}[(n_{eff}^2(x,z) - n_0^2)k_0^2\psi_x + \frac{\partial}{\partial x}(\frac{1}{n_{eff}^2(x,z)}\frac{\partial}{\partial x}(n_{eff}^2(x,z)\psi_x))] \tag{3.35}$$

$$TE: \quad j\frac{\partial \psi_y}{\partial z} = \frac{1}{2n_0k_0}[\frac{\partial^2\psi_y}{\partial x^2} + (n_{eff}^2(x,z) - n_0^2)k_0^2\psi_y] \tag{3.36}$$

3.3.2 Vector Helmholtz Equations in Anisotopic Media

In a number of technologically important materials, such as $LiNbO_3$, responses to fields with different orientations can differ; that is, they are anisotropic [37]. This anisotropy may be either in the response to the electric field or to the magnetic field. In the former case, the permittivity must be represented by a matrix, an array of nine scalar quantities. This can be called *electrical anisotropy* [38]. In such crystals, since permittivity is no longer a constant, the material equation $\vec{D} = \epsilon\vec{E}$ will no longer hold. Consequently, while in isotropic media it can be deduced from $\nabla \cdot \vec{D} = 0$ that $\nabla \cdot \vec{E} = 0$, in anisotropic media such conclusion can not be drawn.

We assume the relation between $\vec{D}$ and $\vec{E}$ to have the simplest form which can account for anisotropic behaviour, namely one in which each component of $\vec{D}$ is linearly related to the components of $\vec{E}$:

$$\left\{ \begin{array}{lcl} D_x & = & \epsilon_{xx}E_x + \epsilon_{xy}E_y + \epsilon_{xz}E_z \\ D_y & = & \epsilon_{yx}E_x + \epsilon_{yy}E_y + \epsilon_{yz}E_z \\ D_z & = & \epsilon_{zx}E_x + \epsilon_{zy}E_y + \epsilon_{zz}E_z \end{array} \right. \tag{3.37}$$

The nine quantities $\epsilon_{xx}, \epsilon_{yy}, \ldots$ are constants of the medium, and constitute the *dielectric tensor*; the vector $\vec{D}$ is the product of this tensor with $\vec{E}$ [38]. It can be proved that the dielectric tensor must be symmetric and there exists a coordinate system fixed in the crystal called the *principal dielectric axes* such that the material equations take the simple forms

$$D_x = \epsilon_x E_x; \quad D_y = \epsilon_y E_y; \quad D_z = \epsilon_z E_z \tag{3.38}$$

ϵ_x, ϵ_y, ϵ_z are called the *principal dielectric constants* (or *principal permittivities*). It may be seen from the formula that $\vec{D}$ and $\vec{E}$ will have different directions, unless $\vec{E}$ coincides in direction with one of the principal axes, or the principal dielectric constants are all equal [38].

In practical use, either Y-cut (or X-cut) Z propagation or Z-cut Y propagation (or X propagation) crystals of $LiNbO_3$ are chosen which means coincidence between actual geometric coordinates and principal dielectric axes is always satisfied. The electrical field $\vec{E}$ is also deliberately polarized along one of the principal axes. In such cases, it could be considered that the wave is travelling in an isotropic medium. Nevertheless, more general and exact formulas of paraxial Helmholtz equations are sometimes needed for waves travelling in an anisotropic medium. The final result will show that for the specific case where we only have E_y in a 2D waveguide, the equation will end up to be the same as that in an isotropic medium.

Use $\tilde{\epsilon}$ to represent the dielectric tensor, and assume the crystal axis orientation are arranged properly:

$$\tilde{\epsilon} = \begin{pmatrix} n_x^2 & 0 & 0 \\ 0 & n_y^2 & 0 \\ 0 & 0 & n_z^2 \end{pmatrix} \tag{3.39}$$

From the Maxwell's equations:

$$\nabla \times \vec{E} = -j\omega\mu_0\vec{H}$$

$$\nabla \times \vec{H} = j\omega\tilde{\epsilon}\epsilon_0\vec{E}$$

a full-vectorial wave equation can be derived as [14] (details in Section 3.3.1):

$$\nabla^2\vec{E} + \tilde{\epsilon}k_0^2\vec{E} = \nabla(\nabla \cdot \vec{E})$$

The transverse component of the above equation is:

$$\nabla^2\vec{E_t} + \tilde{\epsilon_t}k_0^2\vec{E_t} = \nabla_t(\nabla_t \cdot \vec{E_t} + \frac{\partial E_z}{\partial z}) \tag{3.40}$$

where the subscript "t" stands for the transvers components and

$$\tilde{\epsilon_t} = \begin{pmatrix} n_x^2 & 0 \\ 0 & n_y^2 \end{pmatrix} \tag{3.41}$$

is the transverse components of the dielectric tensor. Using the Gauss's law:

$$\nabla \cdot (\tilde{\epsilon}\vec{E}) = 0$$

we can get:

$$\nabla_t \cdot (\bar{\epsilon}_t \vec{E}_t) + \frac{\partial}{\partial z}(n_z^2 E_z) = \nabla_t \cdot (\bar{\epsilon}_t \vec{E}_t) + \frac{\partial n_z^2}{\partial z} E_z + n_z^2 \frac{\partial E_z}{\partial z} = 0 \tag{3.42}$$

If the refractive index $n_z(x, y, z)$ varies slowly along the propagating direction z, which is valid for most photonic guided-wave devices, then $(\partial n_z^2 / \partial z) E_z$ is much smaller than the other two terms in the above equation. Thus,

$$\frac{\partial E_z}{\partial z} \simeq -\frac{1}{n_z^2} \nabla_t \cdot (\bar{\epsilon}_t \vec{E}_t) \tag{3.43}$$

By substituting (3.43) into (3.40), the wave equation for the transverse electric fields can be derived:

$$\nabla^2 \vec{E}_t + \bar{\epsilon}_t k_0^2 \vec{E}_t = \nabla_t [\nabla_t \cdot \vec{E}_t - \frac{1}{n_z^2} \nabla_t \cdot (\bar{\epsilon}_t \vec{E}_t)] \tag{3.44}$$

Writing out the x component:

$$\nabla^2 E_x + n_x^2 k_0^2 E_x = \frac{\partial}{\partial x}[(\frac{\partial}{\partial x}\hat{i} + \frac{\partial}{\partial y}\hat{j}) \cdot (E_x \hat{i} + E_y \hat{j}) - \frac{1}{n_z^2}(\frac{\partial}{\partial x}\hat{i} + \frac{\partial}{\partial y}\hat{j}) \cdot (n_x^2 E_x \hat{i} + n_y^2 E_y \hat{j})]$$

$$\nabla^2 E_x + n_x^2 k_0^2 E_x = \frac{\partial}{\partial x}[\frac{\partial E_x}{\partial x} + \frac{\partial E_y}{\partial y} - \frac{1}{n_z^2}\frac{\partial}{\partial x}(n_x^2 E_x) - \frac{1}{n_z^2}\frac{\partial}{\partial y}(n_y^2 E_y)]$$

$$\frac{\partial^2 E_x}{\partial x^2} + \frac{\partial^2 E_x}{\partial y^2} + \frac{\partial^2 E_x}{\partial z^2} + n_x^2 k_0^2 E_x = \frac{\partial^2 E_x}{\partial x^2} + \frac{\partial^2 E_y}{\partial x \partial y} - \frac{\partial}{\partial x}[\frac{1}{n_z^2}\frac{\partial}{\partial x}(n_x^2 E_x)] - \frac{\partial}{\partial x}[\frac{1}{n_z^2}\frac{\partial}{\partial y}(n_y^2 E_y)] \tag{3.45}$$

Assume that the transverse electric fields can be represented as plane waves travelling in a homogeneous medium where n_0 is a reference refractive index: $\vec{E}_t = \vec{\psi}_t e^{-jk_0 n_0 z}$, and for the x component: $E_x = \psi_x e^{-jk_0 n_0 z}$, as in Section 3.3.1, substituting all the derivatives of E_x into (3.45), we have:

$$\frac{\partial^2 \psi_x}{\partial y^2} e^{-jk_0 n_0 z} + (-2jk_0 n_0 \frac{\partial \psi_x}{\partial z} - k_0^2 n_0^2 \psi_x) e^{-jk_0 n_0 z} + n_x^2 k_0^2 \psi_x e^{-jk_0 n_0 z}$$

$$= \frac{\partial^2 \psi_y}{\partial x \partial y} e^{-jk_0 n_0 z} - \frac{\partial}{\partial x}[\frac{1}{n_z^2}\frac{\partial}{\partial x}(n_x^2 \psi_x)] e^{-jk_0 n_0 z} - \frac{\partial}{\partial x}[\frac{1}{n_z^2}\frac{\partial}{\partial y}(n_y^2 \psi_y)] e^{-jk_0 n_0 z}$$

Cancelling all the $exp(-jk_0 n_0 z)$ terms on both sides

$$\frac{\partial^2 \psi_x}{\partial y^2} - 2jk_0 n_0 \frac{\partial \psi_x}{\partial z} - k_0^2 n_0^2 \psi_x + n_x^2 k_0^2 \psi_x = \frac{\partial^2 \psi_y}{\partial x \partial y} - \frac{\partial}{\partial x}[\frac{1}{n_z^2}\frac{\partial}{\partial x}(n_x^2 \psi_x)] - \frac{\partial}{\partial x}[\frac{1}{n_z^2}\frac{\partial}{\partial y}(n_y^2 \psi_y)]$$

Rearranging the above equation

$$2jk_0n_0\frac{\partial\psi_x}{\partial z} = \frac{\partial^2\psi_x}{\partial y^2} + (n_x^2 - n_0^2)k_0^2\psi_x + \frac{\partial}{\partial x}[\frac{1}{n_z^2}\frac{\partial}{\partial x}(n_x^2\psi_x)] + \frac{\partial}{\partial x}[\frac{1}{n_z^2}\frac{\partial}{\partial y}(n_y^2\psi_y)] - \frac{\partial^2\psi_y}{\partial x\partial y} \tag{3.46}$$

Following the same procedure, we get

$$2jk_0n_0\frac{\partial\psi_y}{\partial z} = \frac{\partial^2\psi_y}{\partial x^2} + (n_y^2 - n_0^2)k_0^2\psi_y + \frac{\partial}{\partial y}[\frac{1}{n_z^2}\frac{\partial}{\partial y}(n_y^2\psi_y)] + \frac{\partial}{\partial y}[\frac{1}{n_z^2}\frac{\partial}{\partial x}(n_x^2\psi_x)] - \frac{\partial^2\psi_x}{\partial x\partial y} \tag{3.47}$$

When TM-like or TE-like waves are concerned, which means either the y field component or the x field component is zero ($\psi_x \neq 0, \psi_z \neq 0, \psi_y = 0$ or $\psi_y \neq 0, \psi_z \neq 0, \psi_x = 0$, refer to Fig. 2.1 for the co-ordinate system used), the above two paraxial-wave Helmholtz equations in anisotropic media could be simplified to

$$TM: \quad 2jk_0n_0\frac{\partial\psi_x}{\partial z} = \frac{\partial^2\psi_x}{\partial y^2} + (n_x^2 - n_0^2)k_0^2\psi_x + \frac{\partial}{\partial x}[\frac{1}{n_z^2}\frac{\partial}{\partial x}(n_x^2\psi_x)] \tag{3.48}$$

$$TE: \quad 2jk_0n_0\frac{\partial\psi_y}{\partial z} = \frac{\partial^2\psi_y}{\partial x^2} + (n_y^2 - n_0^2)k_0^2\psi_y + \frac{\partial}{\partial y}[\frac{1}{n_z^2}\frac{\partial}{\partial y}(n_y^2\psi_y)] \tag{3.49}$$

In a 3-D problem like diffused channel waveguides, the above n_x, n_y and n_z should be written as $n_x(x,y,z)$, $n_y(x,y,z)$ and $n_z(x,y,z)$. If we use the Effective Index Method to reduce a 3-D problem to a 2-D problem, the above two Helmholtz equations could be further simplified (assuming that the coordinates are chosen so that y is the depth direction and $\partial/\partial y = 0$):

$$TM: \quad 2jk_0n_0\frac{\partial\psi_x}{\partial z} = (n_x^2(x,z) - n_0^2)k_0^2\psi_x + \frac{\partial}{\partial x}[\frac{1}{n_z^2(x,z)}\frac{\partial}{\partial x}(n_x^2(x,z)\psi_x)] \tag{3.50}$$

$$TE: \quad 2jk_0n_0\frac{\partial\psi_y}{\partial z} = \frac{\partial^2\psi_y}{\partial x^2} + (n_y^2(x,z) - n_0^2)k_0^2\psi_y \tag{3.51}$$

It should also be noted that $LiNbO_3$ is a so called *uniaxial* crystal, and there exists a relation $n_x = n_z \neq n_y$ and also $n_y = n_e$, when a Z-cut Y-propagation crystal is chosen (here x, y, z are used to represent the coordinate and X, Y, Z are used to represent the axes of the crystal, refer to Fig. 2.1).

3.3.3 Finite-Difference Schemes

In Section 3.3.1 , we have derived the paraxial-wave vector Helmholtz equations in isotropic media. Now we develop a finite–difference scheme for solving these equations. Since in our particular case, only the y component of a field is concerned, only the FD solution of equation (3.36) in Section 3.3.1 will be derived in full detail. This corresponds to a TE_0 mode in a 2D problem with an effective refractive index profile $n_{eff}(x, z)$.

Rewrite equation (3.36) in Section 3.3.1 and move all terms to the left hand side, we have

$$-j2n_0k_0\frac{\partial\psi_y}{\partial z}+\frac{\partial^2\psi_y}{\partial x^2}+[n^2(x_i,z)-n_0^2]k_0^2\psi_y=0 \tag{3.52}$$

Since it would be a numerical solution, we discretize a window in the xz surface into a mesh. Let the step size in the x and z direction be Δx and Δz and use m and l as the index in x and z coordinate grid respectively. We can write the above equation into an implicit weighted finite-difference formula (with a weight ω)

$$\begin{aligned}&-j2n_0k_0\{\frac{\psi_y^{l+1}(m)-\psi_y^l(m)}{\Delta z}\}+\{\frac{(1-\omega)\delta_x^2(\psi_y^l(m))+\omega\delta_x^2(\psi_y^{l+1}(m))}{(\Delta x)^2}\}\\&+\{(1-\omega)[n^2(m,l)-n_0^2]k_0^2\psi_y^l(m)+\omega[n^2(m,l+1)-n_0^2]k_0^2\psi_y^{l+1}(m)\}=0\end{aligned} \tag{3.53}$$

where

$$\delta_x^2(\psi_y^l(m))=\psi_y^l(m-1)-2\psi_y^l(m)+\psi_y^l(m+1) \tag{3.54}$$

if the TE_0 mode is considered [7] [8]. Rearrange (3.53)

$$\begin{aligned}&\{\frac{-j2n_0k_0}{\Delta z}+\omega[n^2(m,l+1)-n_0^2]k_0^2-\frac{2\omega}{(\Delta x)^2}\}\psi_y^{l+1}(m)+\frac{\omega}{(\Delta x)^2}[\psi_y^{l+1}(m+1)+\psi_y^{l+1}(m-1)]\\&=\{\frac{-j2n_0k_0}{\Delta z}+\frac{2(1-\omega)}{(\Delta x)^2}-(1-\omega)[n^2(m,l)-n_0^2]k_0^2\}\psi_y^l(m)-\frac{(1-\omega)}{(\Delta x)^2}[\psi_y^l(m+1)+\psi_y^l(m-1)]\end{aligned} \tag{3.55}$$

Devide the two sides of (3.55) by $-j2n_0k_0/\Delta z$, we finally obtain the implicit weighted finite-difference scheme which will lead to a tridiagonal system of linear equations:

$$A_m^{l+1}\psi_y^{l+1}(m)+A_{m+1}^{l+1}\psi_y^{l+1}(m+1)+A_{m-1}^{l+1}\psi_y^{l+1}(m-1)$$

$$= A_m^l \psi_y^l(m) + A_{m+1}^l \psi_y^l(m+1) + A_{m-1}^l \psi_y^l(M-1) \tag{3.56}$$

where

$$A_m^{l+1} = 1 - j\frac{\omega\Delta z}{2n_0 k_0}\{\frac{2}{(\Delta x)^2} - [n^2(m, l+1) - n_0^2]k_0^2\}$$

$$A_{m\pm 1}^{l+1} = j\frac{\omega\Delta z}{2n_0 k_0(\Delta x)^2}$$

$$A_m^l = 1 + j\frac{(1-\omega)\Delta z}{2n_0 k_0}\{\frac{2}{(\Delta x)^2} - [n^2(m, l) - n_0^2]k_0^2\}$$

$$A_{m\pm 1}^l = -j\frac{(1-\omega)\Delta z}{2n_0 k_0(\Delta x)^2}$$

If $\omega = 1/2$, the above scheme is equal to a standard Crank–Nicholson method. Formulae for TM modes are more complicated since the reflections of the field at dielectric interface of refractive index discontinuities have to be taken care of. The exact FD equation could be found in [7].

Bibliography

[1] M. C. Feit and J. A. Fleck, Jr. "Light propagation in graded-index optical fibers", *Applied Optics*, Vol. 17, No. 24, pp. 3990–3998, 1978

[2] D. Marcuse, *Theory of Dielectric Optical Waveguides*, Academic Press, 1991, Chapter 8. Approximate and Numerical Methods

[3] J. Van Roey, *et al.*, "Beam Propagation Method: Analysis and Assessment", *J. Opt. Soc. Am.*, Vol. 71, No. 7, pp. 803–810, 1981

[4] Weiping Huang, Chenglin Xu, S. T. Chu, and S. K. Chaudhuri, "The Finite-Difference Vector Beam Propagation Method: Analysis and Assessment", *J. of Lightwave Tech.*, Vol. 10, No. 3, pp. 295–305, 1992

[5] W. P. Huang, C. L. Xu, S. T. Chu, and S. K. Chaudhuri, "A Vector Beam Propagation Method for Guided-Wave Optics", *IEEE Photonics Technology Letters*, Vol. 3, No. 10, pp. 910–913, 1991

[6] W. P. Huang, C. L. Xu, and S. K. Chaudhuri, "A Vector Beam Propagation Method Based on H Fields", *IEEE Photonics Technology Letters*, Vol. 3, No. 12, pp. 1117–1120, 1991

[7] G. L. Yip and P. C. Noutsios, "An Improved Finite-Difference Vector Beam Propagation Formulation for Graded–Index Waveguides", *IEEE Photonics Technology Letters*, Vol. 6, No. 4, pp. 543–545, 1994

[8] L. Sun and G. L. Yip, "Modified Finite-Difference Beam-Propagation Method Based on the Douglas Scheme", *Optics Letters*, Vol. 18, No. 15, pp. 1229–1231, 1993

[9] M. S. Stern, "Semivectorial Polarised Finite Difference Method for Optical Waveguides with Arbitrary Index Profiles", *IEE Proceedings*, Vol. 135, Pt. J, No. 1, pp. 56–63, 1988

[10] W. P. Huang, *et al.*, "A Scalar Finite-Difference Time–Domain Approach to Guided–Wave Optics", *IEEE Photonics Tech. Letters*, Vol. 3, No. 6, pp. 524–526, 1991

[11] W. P. Huang, *et al.*, "A Semivectorial Finite-Difference Time-Domain Method", *IEEE Photonics Tech. Letters*, Vol. 3, No. 9, pp. 803-806, 1991

[12] P. Kaczmarski and P. E. Lagasse, "Bidirectional Beam Propagation Method", *Electron. Lett.*, Vol. 24, pp. 675–676, 1988

[13] S. T. Chu and S. K. Chaudhuri, "A Finite-Difference Time-Domain Method for the Design and Analysis of Guided-Wave Optical Structures", *J. of Lightwave Tech.*, Vol. 7, pp. 2033–2038, 1989

[14] C. L. Xu, W. P. Huang, *et al.*, "A Full-Vectorial Beam Propagation Method for Anisotropic Waveguides", *J. of Lightwave Technology*, Vol. 12, No. 11, pp. 1926–1931, 1994

[15] Y. Chung and N. Dagli, "An Assessment of Finite Difference Beam Propagation Method", *IEEE J. of Quantum Electronics*, Vol. 26, No. 8, pp. 1335–1339, 1990

[16] P. Danielsen, "Two–Dimentional Propagating Beam Analysis of an Electrooptic Waveguide Modulator", *IEEE J. of Quantum Electronics*, Vol. QE–20, No. 9, pp. 1093–1097, 1984

[17] A. Neyer, *et al.*, "A Beam Propagation Method Analysis of Active and Passive Waveguide Crossings", *J. of Lightwave Tech.*, LT–3, No. 3, pp. 635–642, 1985

[18] W. Huang, C. Xu, and S. K. Chaudhuri, "Application of the Finite-Difference Vector Beam Propagation Method to Directional Coupler Devices", *IEEE Journal of Quantum Electronics*, Vol. 28, No. 6, pp. 1527–1532, 1992

[19] L. Sun and G. L. Yip, "Analysis of metal-clad optical waveguide polarizers by the vector beam propagation method", *Applied Optics*, Vol. 33, No. 6, pp. 1047–1050, 1994

[20] N. Goto, M. A. Sekerka-Bajbus, and G. L. Yip, "BPM Analysis of Y-Branch TE-TM Mode Splitter in $LiNbO_3$ by Proton-Exchange and Ti-Diffusion", *Electronics Letters*, Vol. 25, No. 25, pp. 1732–1734, 1989

[21] M. A. Sekerka-Bajbus, G. L. Yip and N. Goto, "BPM Design Optimization and Experimental Improvement of a Ti : $LiNbO_3$ Ridge Waveguide Linear-Mode Confinement Modulator", *Journal of Lightwave Technology*, Vol. 8, No. 11, pp. 1742–1749, 1990

[22] Y. Chung and N. Dagli, "Explicit Finite Difference Beam Propagation Method: Application to Semiconductor Rib Waveguide Y–Junction Analysis", *Electronics Letters*, Vol. 26, No. 11, pp. 711–713, 1990

[23] F. Xiang and G. L. Yip, "An Explicit and Stable Finite Difference 2–D Vector Beam Propagation Method", *IEEE Photonics Tech. Letters*, Vol. 6, No. 10, pp. 1248–1250, 1994

[24] W. P. Huang and C. L. Xu, "A Wide-Angle Vector Beam Propagation Method", *IEEE Photonics Technology Letters*, Vol. 4, No. 10, pp. 1118–1120, 1992

[25] Y. Chung and N. Dagli, "A Wide Angle Propagation Technique using an Explicit Finite Difference Scheme", *IEEE Photonics Technology Letters*, Vol. 6, No. 4, pp. 540–542, 1994

[26] C. M. Kim and R. V. Ramaswamy, "Overlap Integral Factors in Integrated Optic Modulators and Switches", *Journal of Lightwave Technology*, Vol. 7, No. 7, pp. 1063–1070, 1989

[27] G. R. Hadley, "Transparent Boundary Condition for Beam Propagation", *Optics Letters*, Vol. 16, No. 9, pp. 624–626, 1991

[28] G. R. Hadley, "Transparent Boundary Condition for the Beam Propagation Method", *IEEE J. of Quantum Electronics*, Vol. 28, No. 1, pp. 363–370, 1992

[29] P. G. Suchoski and R. V. Ramaswamy, "Minimum–Mode–Size Low–loss T_i : $LiNbO_3$ Channel Waveguides for Efficient Modulator Operation at 1.3 μm", *IEEE Journal of Quantum Electronics*, Vol. QE–23, No. 10, pp. 1673–1679, 1987

[30] I. Mansour and F. Caccavale, "Theoretical waveguide optimization in a $Ti : LiNbO_3$ Mach-Zehnder modulator by Mg diffusion", *Applied Optics*, Vol. 35, No. 9, pp. 1492–1499, 20 March 1996

[31] M. Rangaraj, M. Minakata and S. Kawakami, "Low Loss Integrated Optical Y-Branch", *Journal of Lightwave Technology*, Vol. 7, No. 5, pp. 753–758, 1989

[32] M. Fukuma and J. Noda, "Optical Properties of Titanium-Diffused $LiNbO_3$ Strip Waveguides and Their Coupling-to-a-Fiber Characteristics", *Applied Optics*, Vol. 19, No. 4, pp. 591–597, 1980

[33] D. Yap and L. M. Johnson, "Coupling between successive $Ti : LiNbO_3$ waveguide bends and branches", *Applied Optics*, Vol. 23, No. 17, pp. 2991–2999, 1 September 1984

[34] M. J. Taylor and H. F. Taylor, "Coherent Mode Coupling at Waveguide Bends", in *Digest of Meeting on Integrated and Guided Wave Optics* (Optical Society of America, Washington, D.C., 1977), paper WD4

[35] D. A. M. Khalil, P. Benech and S. Tedjini, "Asymmetric Excitation of Symmetric Single-Mode Y-Junction: The Radiation Mode Effects", in *IEEE MTT-S International Microwave Symposium Digest* (IEEE Service Center, Piscataway, NJ, USA, 92CH3141-9), Vol. 1, pp. 441–444, 1992

[36] D. A. M. Khalil and S. Tedjini, "Coherent Coupling of Radiation Modes in Mach-Zehnder Electrooptic Modulators", *IEEE Journal of Quantum Electronics*, Vol. 28, No. 5, pp. 1236–1238, 1992

[37] Simon Ramo, John R. Whinnery, Theodore Van Duzer, *Fields and Waves in Communication Electronics*, John Willey & Sons, pp. 689–703, 1984

[38] M. Born and E. Wolf, *Principles of Optics*, Pergamon, NY, pp. 665–681, 1980

Chapter 4

Investigation of Loss Reduction

4.1 Literature Review of Methods to Reduce Propagation Loss

There are various methods in the literature to reduce propagation losses introduced by either the waveguide bends or branchings in Y junction structures (power dividers, modulators, etc.). Ref. [1] to [18] represent most of these typical schemes. In this review, these different methods have been classified into five major categories according to their basic principles of design.

The first category tries to make further use of the coherent coupling effect as mentioned above. Instead of just optimizing the length of L_2 and L_3 in a conventional Y-branch to take advantage of the beat between the radiation modes and the guided mode, the two methods in Ref. [1] and [2] both redesigned the geometry of the branching part so as to control the power conversion and reconversion of the radiation wave with the guided waves to reduce loss. Ref. [1] used coherently coupled bends (the branching section is divided into three sections with two more bends, in other words, the branching is split into 2 steps), and Ref. [2] goes to the extreme by designing the branching part in a serpentine shape. While this type of method may be efficient in reducing loss, the geometric complexity that is involved will make the design procedure very complicated. Further more, the higher requirement to fabrication torlerance that may arise puts this kind of method in doubt.

The second category involves the double diffusion or extra diffusion of Mg. Ref. [3] shows a reduction of mainly the coupling loss between the channel guide and the optical fiber by double diffusing Ti and Mg during the waveguide fabrication (the waveguide depth index profile is symmetrized). Ref. [4] further apply the Mg diffusion to several selected areas beside the channel waveguides to increase the bend radius of curvature without extra bending losses, and decrease seperation of the modulator arms (a S-bend branching structure is also employed). It is obvious that this type of method brings about more steps and control requirement to the fabrication process, and also the simulation becomes difficult to perform (especially the modelling of refractive index distribution).

The third category replaces the conventional angle bends of a Y junction structure with some kind of S-bend profile to try to make the bending more smooth and giving less radiation loss. There are primarily three kinds of S-bend profiles, the sine-generated S-curve, the cosine-generated S-curve, and the S-curves generated by two circular arcs. Ref. [5] deals with the sine-generated curve, while Refs. [6] and [7] show that in fact a cosine-generated curve will be the best choice. Ref. [6] has even developed an optimized S-bend structure and showed that the cosine-generated one is the closest to the optimal design. Ref. [8] combines the cosine S-curve with the application of the coherent coupling effect (simultaneous optimization of the lengths of L_2 and L_3). While this type of method may only have limited efficiency in improving the propagation loss, its simplicity both geometrically and experimentally makes it a good choice, especially when it is combined with the coherent coupling effect.

The fourth category can be called notched Y-junctions. A square notch as in Ref. [9] is made at the branching area for better mode confinement. In this type of design, the branches are linear (according to the author, in the curved-branch Y-junction the retilting of the branches to the original signal flow direction will cause an additional radiation loss) and the Y-junction is based on a two-refractive-index structure that can be fabricated in a single-step process. Although it has benifits to have several degrees of freedom (both the width and the depth of the notch can be adjusted) in the design, it will also make the modeling and the optimization process more complicated.

The fifth category is the largest and consists of many slightly different approaches [10]–[18]. But their basic principle is the same, by introducing a third or even fourth refractive index area in an appropriate position, to try to get a better control of the wavefront at the junction and thus reduce loss. Among these methods, several typical ones are: phase-front accelarator, antenna coupled Y-junction, integrated microprism and a combination of the first two. This type of method is both complicated in design and requires two or even more steps of fabrication process. According to the reported results, improvement may be significant for large branching angles (usually by several dB), but the lowest achievable loss at small angles is not that attractive.

As suggested in the above descriptions, each of the five kinds of methods has its advantages and disadvantages. When a large angle operation is definitely necessary, the third and fouth category seem to be better choices because they require less fabrication and design complexities compared to the other three categories. Acturally for a M-Z modulator instead of a power divider, this necessity is much less urgent because of its unique structure, especially when the coherent coupling effect has been used and an overall propagation loss of around $0.1 - 0.3dB$ can be achieved with no difficulty.

4.2 Effect of a Cosine-Generated S-Bend Y-Branch

In the literature, there are several S-bend Y-branches which are used in place of the sharp-bend straight Y-branch (the traditional structure). Among them the cosine-generated and sine-generated S-bends are the most popular ones, and sometimes people use double arc bends as well. Fig. 4.1 shows a simple comparison of the branching part structural variation of a conventional Y-branch, a cosine-generated Y-branch and a sine-generated Y-branch. From the figure, it looks very obvious that if the traditional Y-branch is called a linear structure, the cosine-generated Y-branch

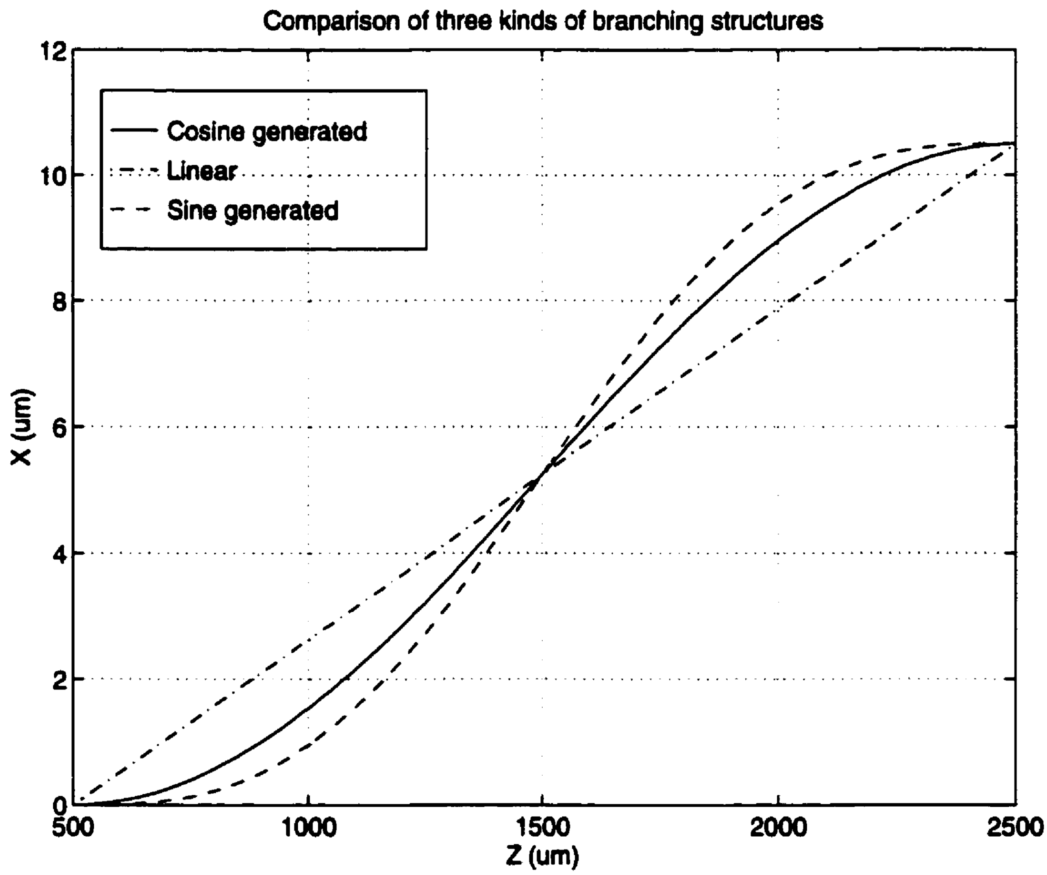

Figure 4.1: Comparison of different S-bend branching structures

would then have a medium degree of non-linearity, and the sine-generated Y-branch has the largest degree of non-linearity. According to Ref. [9], because of such a constant change of the wave path in the branching region, the constant retilting of the branches (to the original wave propagation direction) can cause an additional loss.

Although several publications have shown that in certain cases, the use of a cosine-generated Y-branch can be beneficial in reducing loss and also a cosine bend is always better than a sine bend (Refs. [5] to [8]), they are only helpful when the branching angle is relatively large (like that in a power divider case). However, none of the reports studied the weakly guided gradient index channel waveguide fabricated by titanium diffusion in lithium niobate. Hence, this kind of structure seems to have inherent disadvantages in dealing with a small angle structure which has a gradient index.

In this section, a cosine-generated Y-branch will be studied to determine whether it will be of any help or it will do any harm in reducing the propagation loss in the structure of our interest. First, the longitudinal refractive index distribution will be modelled for this specific branching structure and then wave propagation through the whole waveguide will be simulated and propagation loss calculated.

4.2.1 Modelling of Refractive Index Variations

Fig. 4.2 is a schematic diagram of a cosine-generated Y-branch. The whole branching region can be divided into two parts called l_{21} and l_{22}, respectively. The relationship between x and z is:

$$x = \frac{d'}{2}[1 - cos(\frac{\pi(z - l_1)}{l_2})] \tag{4.1}$$

To determine at what point section l_{21} stops, we let $x = w/2$ and substitute into the above equation to get:

$$l_{21} = \frac{l_2}{\pi} cos^{-1}(1 - \frac{w}{d'}) \tag{4.2}$$

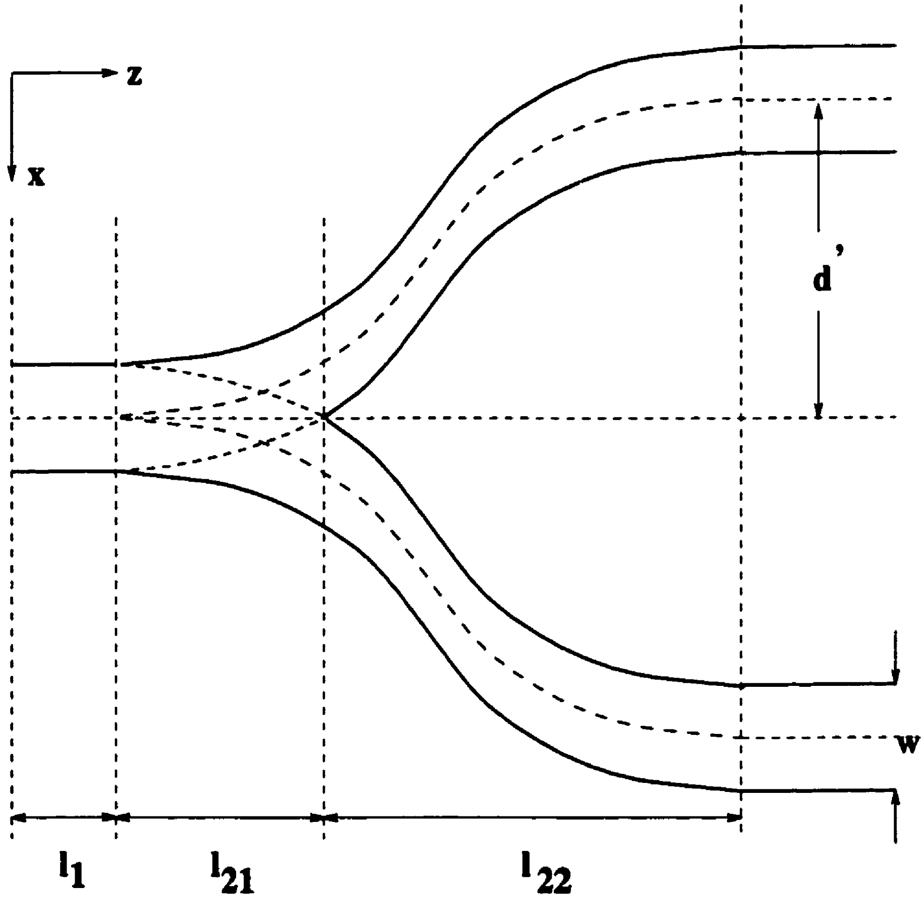

Figure 4.2: Schematic diagram of a cosine generated Y-branch

Using the very similar modelling technique as we used when modelling the refractive index distribution of a conventional structure, we can find different expressions for the function $g(x)$ for section l_{21} and section l_{22} seperately.

For section l_{21}:

$$g(x) = \frac{1}{2}[erf(\frac{\frac{w}{2} + \frac{d}{2}(1 - cos(\frac{\pi(z-l_1)}{l_2})) + x}{D_S}) + erf(\frac{\frac{w}{2} + \frac{d}{2}(1 - cos(\frac{\pi(z-l_1)}{l_2})) - x}{D_S})] \tag{4.3}$$

For section l_{22}:

$$g(x) = \frac{1}{2}[erf(\frac{\frac{w}{2} + x - \frac{d}{2}(1 - cos(\frac{\pi(z-l_1)}{l_2}))}{D_s}) + erf(\frac{\frac{w}{2} - x + \frac{d}{2}(1 - cos(\frac{\pi(z-l_1)}{l_2}))}{D_S})$$

$$+ erf(\frac{\frac{w}{2} + x + \frac{d}{2}(1 - cos(\frac{\pi(z-l_1)}{l_2}))}{D_S}) + erf(\frac{\frac{w}{2} - x - \frac{d}{2}(1 - cos(\frac{\pi(z-l_1)}{l_2}))}{D_S})] \tag{4.4}$$

The expression for the function $f(y)$ which is a Gaussian will not change. The same technique based on the Runge-Kutta method has been applied here again to get the effective index along the x-direction for each step along the z-direction.

4.2.2 Effect on Propagation Loss

Three different lengths of L_2 ($L_2 = l_{21} + l_{22}$) have been tried: 600, 1000 and 2000 μm. A comparison of loss results is shown in Table 4.1.

It is seen that a cosine-generated Y-branch will not improve propagation loss for any branching length in this study (all of which actually correspond to relatively small total branching angles). On the contrarary, very significant deteriorations have been observed for all three cases in comparison with the results of corresponding conventional Y-branches.

This result is in a sense much expected, although it is somewhat different to those in some publications. As already stated above, the constant retilting of the branches will definitely cause excessive loss for any S-bend Y-branch. While for a step-index case which involves a large branching angle and relatively long branching length, this effect may not seem to be significant, for a gradient-index case which involves a relatively short branching length and small branching angle, it can be very serious. It is imaginable that with a constant change in the propagation path, more radiated modes can be excited, especially for a weakly guiding gradient-index structure, which will obviously cause more loss than usual.

Figures 4.3 to 4.8 show some wave patterns in both the cosine-generated Y-branches and conventional Y-branches. These are BPM simulation results. From these 3D figures, we can see very clearly that compared to linear branches, cosine ones generate more radiation and thus the wave forms look more irregular. The beating of radiation modes are more obvious for the cosine-generated Y-branches.

We can thus draw such a conclusion that for our gradient-index channel waveguide structure in the M-Z intensity modulator on a lithium niobate substrate which has a typical total branching angle of around 1°, the effort to reduce propagation loss using a cosine-generated S-bend Y-branching will cause a totally contrary result and a S-bend should not be considered in future design work.

4.3 Effect of a Notched Y-Branch

The idea of a notched branching structure was first brought up in Ref. [9]. It was stated in that paper that there are two basic mechanisms which contribute to the radiation loss in the vicinity of the Y-junction: a wave-front mismatch due to the sudden tilt and the change of the modal field distribution along the seperating branches. The first mechanism dominates at small branching angles and depends on the guiding strength. The weaker the guidance the more significant this loss mechanism is, owing to the longer exponential mode tails. In the paper, to reduce the tilt effect on the modal tails the junction region is tapered and furthermore the two branches run parallel to each other along some distance before being tilted, thus a better modal

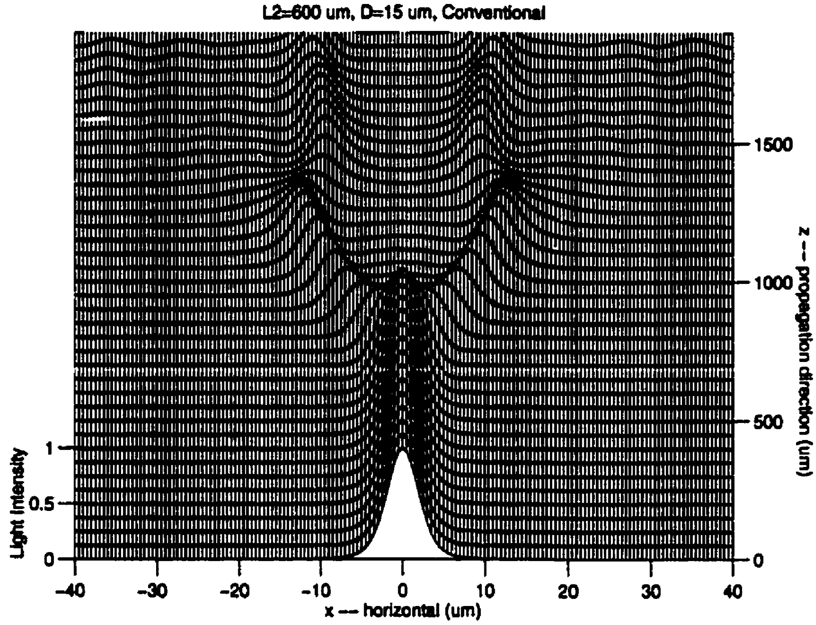

Figure 4.3: Field pattern at the first branching region of a conventional Y-branch of length 600 μm, $2\theta = 2°$

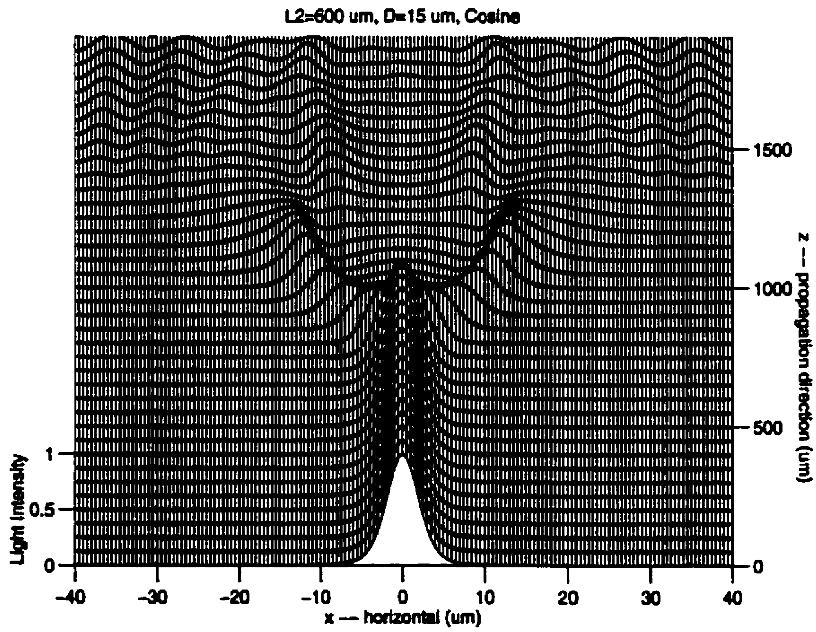

Figure 4.4: Field pattern at the first branching region of a cosine-generated Y-branch of length 600 μm

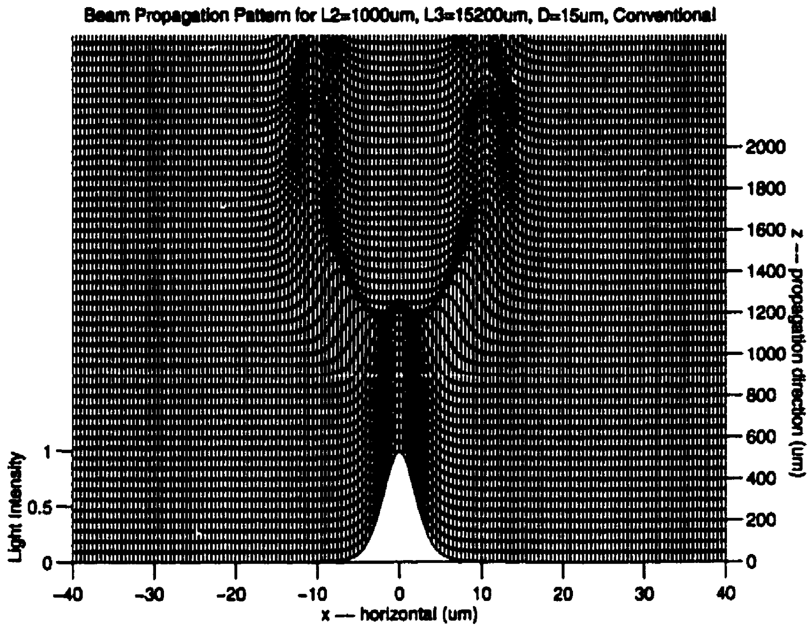

Figure 4.5: Field pattern at the first branching region of a conventional Y-branch of length 1000 μm, $2\theta = 1.2°$

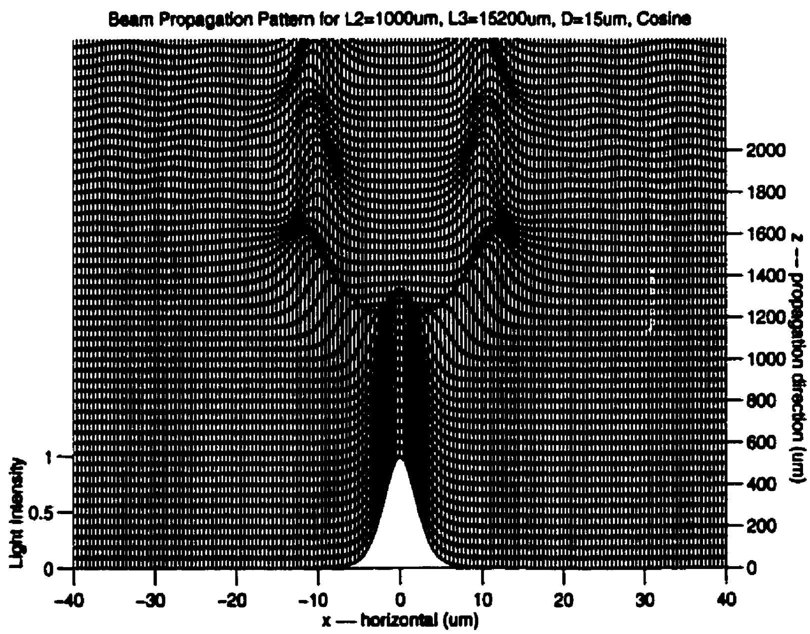

Figure 4.6: Field pattern at the first branching region of a cosine-generated Y-branch of length 1000 μm

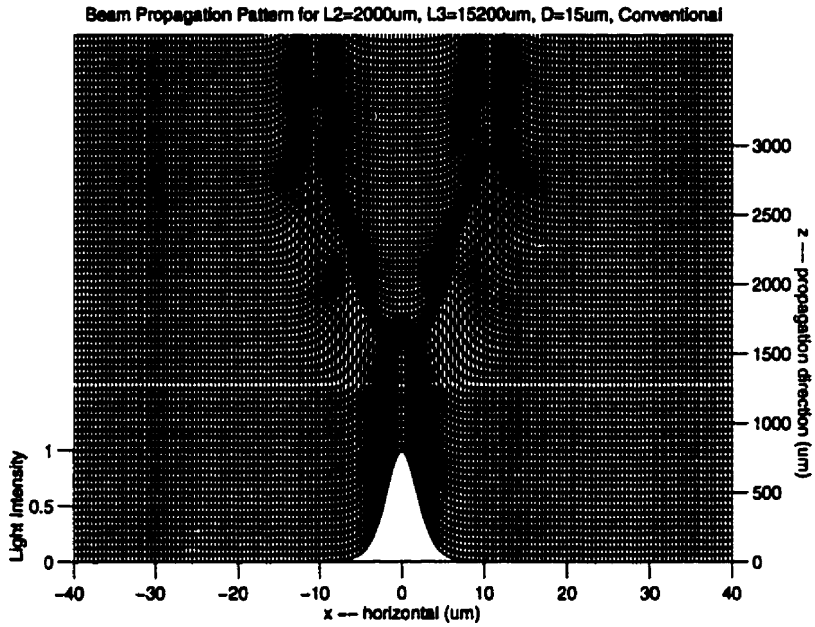

Figure 4.7: Field pattern at the first branching region of a conventional Y-branch of length 2000 μm, $2\theta = 0.6°$

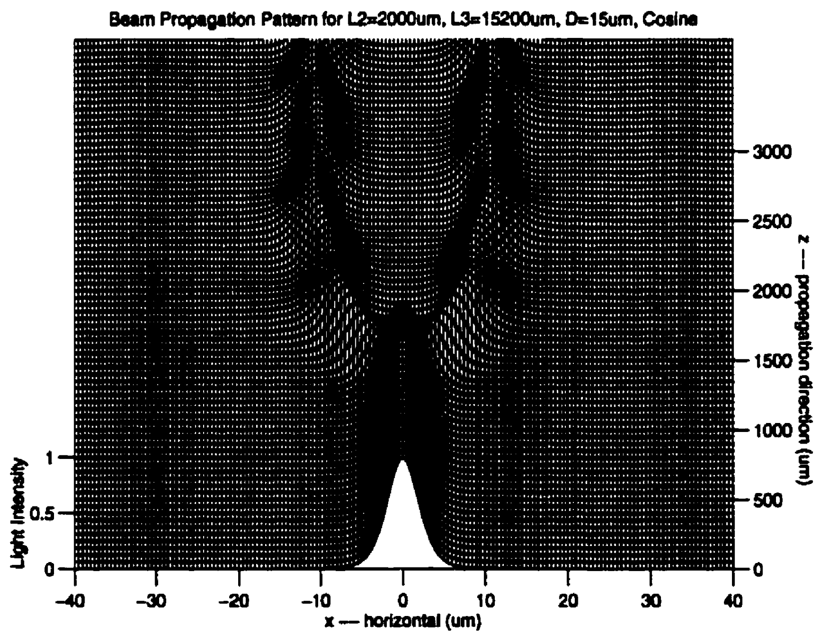

Figure 4.8: Field pattern at the first branching region of a cosine-generated Y-branch of length 2000 μm

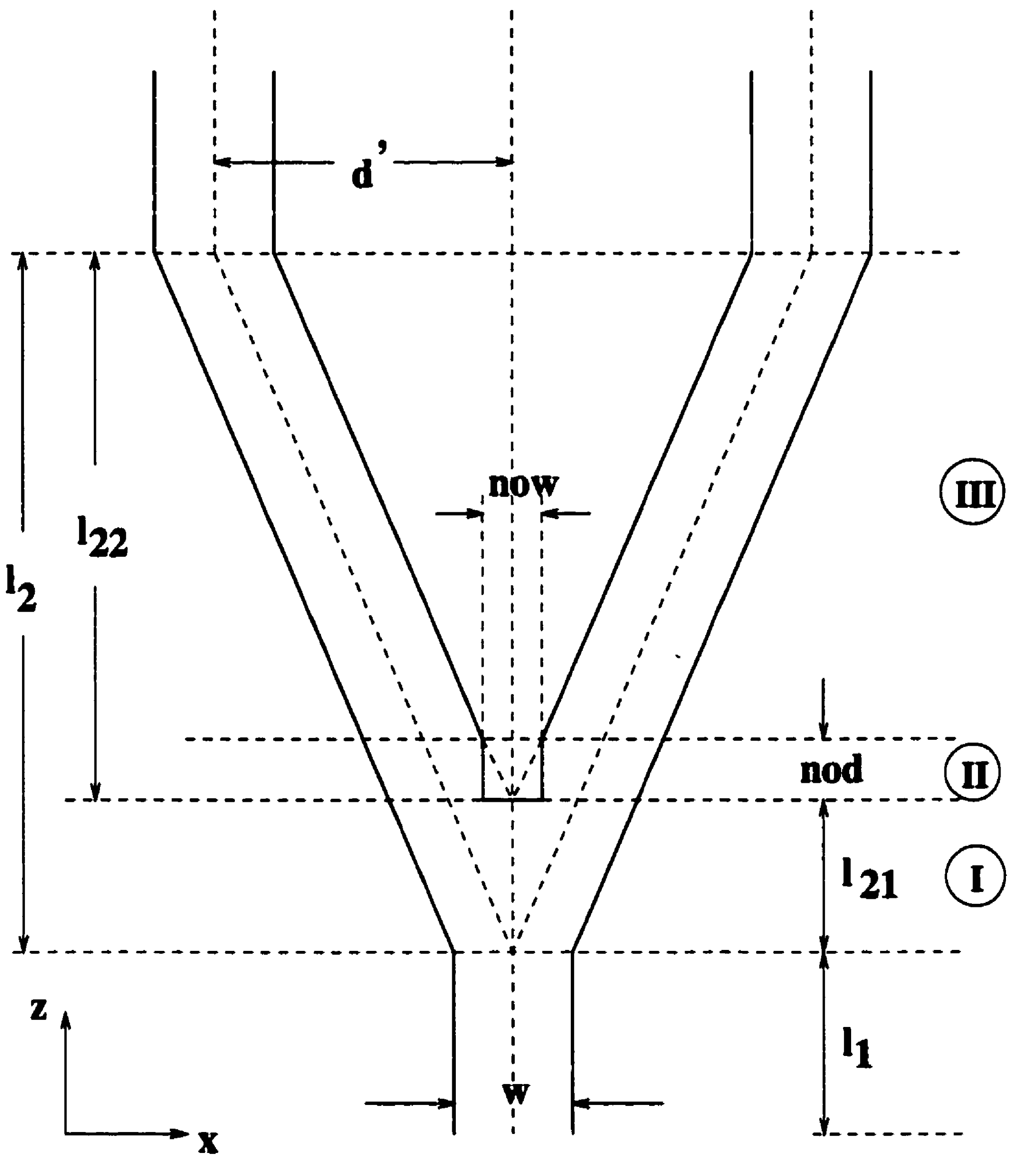

Figure 4.9: Schematic diagram of a notched Y-branch

confinement (and consequently a lower device loss) is achieved in each of the two branches before tilting takes place.

The structure studied in that reference is a dual mode Y-branch power divider (planar) with an input waveguide width of 6 μm and a branch width of 3 μm and no original taper region before the tilting. It is somewhat different from the structure which is studied in this project: a single mode Y-branch (gradient-index channel guide) for an intensity modulator with both an input waveguide width and a branch width of 6 μm and there exists a taper region before the tilting. Taking into consideration this difference, no other taper structure will be introduced because the construction can be complicated and no significant contribution in loss reduction can be expected. Only a notch will be formed at the point of the Y-junction in a way that its bottom rests at the point where the internal boundaries of the two tilted branches of a conventional Y-branch meet, as shown in Fig. 4.9. It is expected to give a better wavefront confinement and thus fewer radiation modes will be excited.

4.3.1 Modelling of Refractive Index Variations

The width of the notch is named *now* and the depth of the notch is named *nod*. Since the bottom of the notch is place at the specific point described above, there is actually only one degree of freedom, which is the width of the notch. By simple geometry, we can find that the depth of the notch is related to the width of the notch by the following expression:

$$nod = now \cdot \frac{l_2}{2d'} \tag{4.5}$$

where $l_2 = l_{21} + l_{22}$ is the total length of the taper/branching region as indicated in the figure, and $l_{21} = \frac{l_2 W}{2d'}$ is the same as that of the conventional structure. The whole region between the input part and the active part is divided into three sections instead of two as has been done for a conventional structure, namely I, II and III, each in a circle as shown in Fig. 4.9.

Using the very similar modelling technique as we used when modelling the refractive index distribution of a conventional structure, we can find different expressions for function $g(x)$ for section I, II and section III seperately.

For section I:

$$g(x) = \frac{1}{2}[erf(\frac{\frac{w}{2} + (z - l_1)\frac{d}{l_2} + x}{D_S}) + erf(\frac{\frac{w}{2} + (z - l_1)\frac{d}{l_2} - x}{D_S})] \tag{4.6}$$

For section II:

$$g(x) = \frac{1}{2}[erf(\frac{x - \frac{now}{2}}{D_S}) + erf(\frac{\frac{w}{2} - x + (z - l_1)\frac{d}{l_2}}{D_S}) + erf(\frac{\frac{w}{2} + x + (z - l_1)\frac{d}{l_2}}{D_S}) + erf(\frac{-x - \frac{now}{2}}{D_S})] \tag{4.7}$$

For section III:

$$g(x) = \frac{1}{2}[erf(\frac{\frac{w}{2} + x - (z - l_1)\frac{d}{l_2}}{D_S}) + erf(\frac{\frac{w}{2} - x + (z - l_1)\frac{d}{l_2}}{D_S}) + erf(\frac{\frac{w}{2} + x + (z - l_1)\frac{d}{l_2}}{D_S}) + erf(\frac{\frac{w}{2} - x - (z - l_1)\frac{d}{l_2}}{D_S})] \tag{4.8}$$

The expression of function $f(y)$ which is a Gaussian will not change. The same technique based on the Runge-Kutta method has been applied here again to get the effective index along x direction for each step along z direction.

4.3.2 Effect on Propagation Loss

Since it has been found by previous work that the average (for different lengths of L_3, Fig. 3.23 and Table 4.2) propagation loss is at a minimum near $L_2 = 1000\mu m$ for a conventional Y-branch due to the coherent coupling effect of radiation modes, this length of L_2 has been chosen to test the notched structure to see if there can be any further improvement. According to Table 4.2, at certain notch widths, the propagation loss has been lowered considerablly. But if the notch is too wide or too narrow, it will result in a contrary effect, i.e., the loss will actually increase. Hence, the optimization of the notch width is of the utmost importance in the design process of a notched Y-branch.

It is very natural to think of using this notched Y-branch to bring down the loss as much as possible for even larger branching angles. Based on this consideration, a structure with $L_2 = 600\mu m$ was also tested and the result is shown in Table 4.3. We can see that compared with the loss of a conventional Y-branch, although the loss of a notched Y-branch can be smaller when the notch width is chosen properly, this reduction is far from being enough to bring the loss quantity to a comparable range with that of a $L_2 = 1000\mu m$ structure. As a conclusion, although the notched Y-branch is a relatively effective way of improving propagation loss, nothing very drastic can be expected for larger angle branchings. Of course this conclusion is again based on our gradient index, weakly guiding channel waveguide structure used for M-Z modulators.

Fig. 4.10 shows loss variation according to the change of the active region length L_3 from $14500\mu m$ to $15500\mu m$, length $L_2 = 1000\mu m$. The loss curves of several structures with different notch widths as well as that of a conventional Y-branch have been shown at the same time for comparison. The significance of studying this range of active length extensively is that from the electrode design work done by a previous graduate student Mr. F. Y. Gan [19], an active length of around $15000\mu m$ is needed to achieve a $80GHz$ bandwidth device with a $1.2\mu m$ buffer layer, a $10\mu m$ electrode thickness, a $15\mu m$ central electrode width and an electrode gap of $6\mu m$. Detailed loss data can be found in Table 4.4.

While the minimum achievable loss in this range of L_3 of a conventional Y-branch is about $0.182dB$ ($L_3 = 15100\mu m$), the minimum achievable loss for a notched Y-branch of a notch width of $1.5\mu m$ can be as low as $0.145dB$ ($L_3 = 15080\mu m$). What is more important, with a $1.5\mu m$ notched structure, the coherent coupling is less significant. This is reflected by less vibration of its corresponding loss curve. This can make the fabrication process of the waveguide have a better tolerance of the fabrication error in the active length.

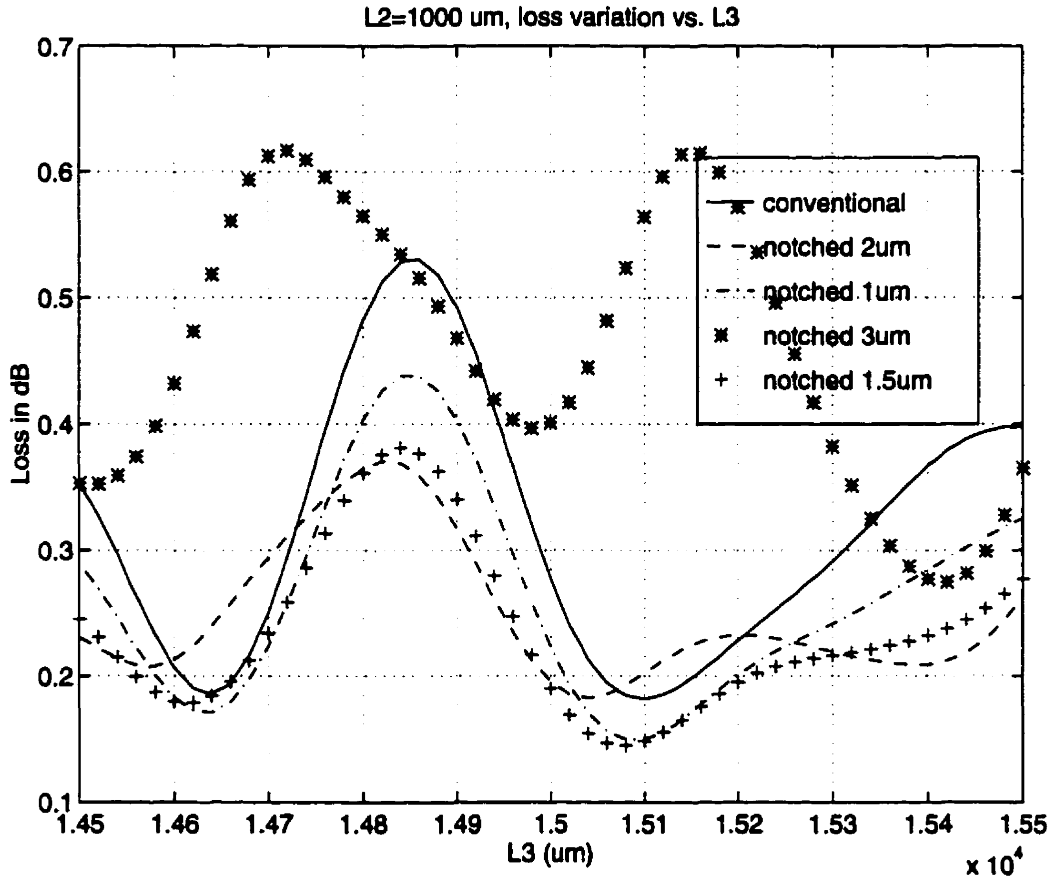

Figure 4.10: Comparison of losses of conventional Y-branch and notched Y-branches with notch width of 1 μm, 1.5 μm, 2 μm and 3 μm

Table 4.1: Comaprison of propagation losses of conventional Y-branches and cosine generated S-bends of different lengths

L2 (μm)	Loss for Conventional Y-Branch (dB)	Loss for Cosine S-Bend (dB)
600	4.697	17.004
1000	0.228	1.442
2000	0.203	9.484

Table 4.2: Propagation loss for notched Y-branches of total taper/branching length 1000 μm with different notch widths (L1=500 μm, L3=1000 μm)

	Loss (dB)
Conventional Y-Branch	0.602
Notch Width 1 μm	0.507
Notch Width 1.5 μm	0.448
Notch Width 2 μm	0.436
Notch Width 3 μm	0.624
Notch Width 4 μm	1.033
Notch Width 6 μm	1.822

Table 4.3: Propagation loss for notched Y-branches of total length 600 μm with different notch widths (L1=500 μm, L3=1000 μm)

	Loss (dB)
Conventional Y-Branch	3.666
Notch Width 2 μm	2.995
Notch Width 3 μm	2.577
Notch Width 4 μm	2.353
Notch Width 5 μm	2.391
Notch Width 6 μm	2.718

Table 4.4: Propagation loss (dB) vs. L3 ranging from 14500 to 15500 μm for a conventional Y-Branch and several notched structures of different notch widths, all with L1=L5=500 μm, L2=L4=1000 μm

L3	Conventional Y	Notched 1um	Notched 1.5 um	Notched 2um	Notched 3um
14500	0.353	0.289	0.245	0.231	0.353
14520	0.327	0.269	0.231	0.222	0.353
14540	0.296	0.246	0.215	0.214	0.359
14560	0.263	0.222	0.2	0.209	0.374
14580	0.232	0.2	0.187	0.208	0.398
14600	0.207	0.183	0.18	0.213	0.432
14620	0.19	0.173	0.179	0.224	0.473
14640	0.186	0.171	0.184	0.24	0.519
14660	0.194	0.18	0.196	0.258	0.561
14680	0.216	0.197	0.212	0.277	0.593
14700	0.251	0.224	0.234	0.295	0.612
14720	0.295	0.258	0.259	0.311	0.617
14740	0.344	0.296	0.286	0.327	0.609
14760	0.395	0.335	0.313	0.341	0.596
14780	0.443	0.372	0.34	0.355	0.58
14800	0.483	0.404	0.361	0.365	0.565
14820	0.513	0.427	0.376	0.371	0.55
14840	0.529	0.438	0.382	0.369	0.535
14860	0.531	0.438	0.377	0.359	0.516
14880	0.518	0.426	0.363	0.342	0.493
14900	0.492	0.403	0.34	0.317	0.468
14920	0.456	0.372	0.312	0.29	0.442
14940	0.413	0.336	0.28	0.261	0.419
14960	0.366	0.297	0.247	0.234	0.403
14980	0.32	0.258	0.217	0.212	0.397
15000	0.277	0.223	0.19	0.196	0.401

L3	Conventional Y	Notched 1 um	Notched 1.5 um	Notched 2 um	Notched 3 um
15020	0.241	0.193	0.169	0.186	0.417
15040	0.213	0.171	0.154	0.182	0.445
15060	0.195	0.156	0.147	0.185	0.482
15080	0.184	0.15	0.145	0.193	0.524
15100	0.182	0.15	0.148	0.203	0.564
15120	0.185	0.156	0.155	0.213	0.596
15140	0.193	0.165	0.165	0.221	0.614
15160	0.204	0.177	0.176	0.227	0.615
15180	0.216	0.19	0.186	0.231	0.599
15200	0.228	0.201	0.195	0.233	0.572
15220	0.241	0.211	0.202	0.232	0.536
15240	0.253	0.22	0.208	0.23	0.496
15260	0.265	0.227	0.211	0.227	0.456
15280	0.278	0.234	0.214	0.223	0.417
15300	0.292	0.242	0.216	0.219	0.382
15320	0.306	0.249	0.219	0.216	0.352
15340	0.322	0.258	0.221	0.213	0.325
15360	0.338	0.267	0.224	0.21	0.304
15380	0.353	0.276	0.228	0.209	0.287
15400	0.367	0.285	0.232	0.209	0.277
15420	0.379	0.294	0.237	0.212	0.275
15440	0.388	0.303	0.245	0.219	0.282
15460	0.394	0.311	0.254	0.23	0.299
15480	0.398	0.319	0.265	0.245	0.328
15500	0.398	0.325	0.277	0.263	0.365

Bibliography

[1] F. S. Chu and Pao-Lo Liu, "Low-loss coherent-coupling Y branches", *Optics Letters*, Vol. 16, No. 5, pp. 309–311, March 1, 1991

[2] M. Tsuji, O. Tanaka and H. Shigesawa, "Low-Loss Design Method for a Planar Dielectric-Waveguide Y Branch: Effect of a Taper of Serpentine Shape", *IEEE Transactions on Microwave Theory and Techniques*, Vol. 39, No. 1, pp. 6–13, 1991

[3] K. Komatsu, *et al.*, "Low-Loss Broad-Band $LiNbO_3$ Guided-Wave Phase Modulators Using Titanium/Magnesium Double Diffusion Method", *Journal of Lightwave Technology*, Vol. LT-5, No. 9, pp. 1239–1245, 1987

[4] I. Mansour and F. Caccavale, "Theoretical waveguide optimization in a $Ti : LiNbO_3$ Mach-Zehnder modulator by Mg diffusion", *Applied Optics*, Vol. 35, No. 9, pp. 1492–1499, 20 March 1996

[5] G. A. Bogert and Y. C. Chen, "Low-loss Y-branch power dividers", *Electronics Letters*, Vol. 25, No. 25, pp. 1712–1714, 1989

[6] F. J. Mustieles, E. Ballesteros and P. Baquero, "Theoretical S-Bend Profile for Optimization of Optical Waveguide Radiation Losses", *IEEE Photonics Technology Letters*, Vol. 5, No. 5, pp. 551–553, 1993

[7] K. T. Koai and Pao-lo Liu, "Modelling of $Ti : LiNbO_3$ Waveguide Devices: Part II — S-Shaped Channel Waveguide Bends", *Journal of Lightwave Technology*, Vol. 7, No. 7, pp. 1016–1021, 1989

[8] M. Munowitz and D. J. Vezzetti, "Numerical Modeling of Coherent Coupling and Radiation Fields in Planar Y-Branch Interferometers", *Journal of Lightwave Technology*, Vol. 10, No. 11, pp. 1570–1573, 1992

[9] Z. Weissman, E. Marom and A. Hardy, "Very low-loss Y-junction power divider", *Optics Letters*, Vol. 14, No. 5, 293–295, 1989

[10] W. Y. Hung, H. P. Chan and P. S. Chung, "Novel Design of Wide-angle Single-mode Symmetric Y-junctions", *Electronics Letters*, Vol. 24, No. 18, pp. 1184–1185, 1988

[11] K. Tsutsumi, *et al.*, "Analysis of Single-Mode Optical Y-Junctions by the Bounded Step and Bend Approximation", *Journal of Lightwave Technology*, Vol. 6, No. 4, pp. 590–600, 1988

[12] O. Hanaizumi, M. Miyagi and S. Kawakami, "Wide Y-Junctions with Low Losses in Three-Dimensional Dielectric Optical Waveguides", *IEEE Journal of Quantum Electronics*, Vol. QE-21, No. 2, pp. 168–173, 1985

[13] M. Rangaraj and M. Minakata, "A New Type of $Ti-LiNbO_3$ Integrated Optical Y-Branch", *IEEE Photonics Technology Letters*, Vol. 1, No. 8, pp. 230–231, 1989

[14] M. Rangaraj, M. Minakata and S. Kawakami, "Low Loss Integrated Optical Y-Branch", *Journal of Lightwave Technology*, Vol. 7, No. 5, pp. 753–758, 1989

[15] H. Hatami-Hanza, *et al.*, "A Novel Wide-Angle Low-Loss Dielectric Slab Waveguide Y-Branch", *Journal of Lightwave Technology*, Vol. 12, No. 2, pp. 208–213, 1994

[16] H. Hatami-Hanza, P. L. Chu and M. J. Lederer, "A New Low-Loss Wide-Angle Y-Branch Configuration for Optical Dielectric Slab Waveguides", *IEEE Photonics Technology Letters*, Vol. 6, No. 4, pp. 528–530, 1994

[17] H. Lin, R. Cheng and W. Wang, "Wide-Angle Low-Loss Single-Mode Symmetric Y-Junctions", *IEEE Photonics Technology Letters*, Vol. 6, No. 7, pp. 825–827, 1994

[18] S. Safavi-Naeini, *et al.*, "Wide Angle Phase-Corrected Y-Junction of Dielectric Waveguides for Low Loss Applications", *Journal of Lightwave Technology*, Vol. 11, No. 4, pp. 567–576, 1993

[19] F. Y. Gan, *Traveling Wave Electrode Design For High Speed $LiNbO_3$ Intensity Modulators*, Master's Thesis, McGill University, 1996

Chapter 5

Design Characterization of the Active Aspect

In order to make an active modulator, after the fabrication of the titanium diffused waveguide, a buffer layer as well as the electrodes have to be deposited on the substrate. Schematic diagrams can be found in the *Introduction* and *Chapter 2* of this thesis with certain notations that have been used. Relatively thick buffer layer and electrodes are necessary in order to increase the bandwidth of the device [1]. For a Z-cut $LiNbO_3$ substrate, the center electrode has to be deposited just above one waveguide in the active region and the other waveguide is underneath the ground electrode, being aligned near the edge. First, a narrow center electrode structure with a wide gap will be studied with the width of the center electrode the same as the width of a waveguide arm (6 μm in our case). Then, a wide center electrode structure with a narrow gap will be design-tested in the third section of this chapter.

5.1 Determination of Minimum Seperation of Two Waveguide Arms

It is known that when two waveguide arms are close enough, energy coupling can happen between them. When the refractive index distribution of these two arms and thus the propagation constants of them are different due to electro-optic effect, energy can be expected to exchange from one arm to the other if they are close enough because of their different abilities to retain light inside them. To effectively use a M-Z modulator, we would like to have approximately equal energy inside each arm at the point when they are combined, so a minimum seperation between the two waveguide arms has to be decided in order to prevent significant coupling. Based on design parameters in Refs. [2] [3] [4], two different values of the seperation of 10 and 15 microns between the two inner edges of the branching arms will be examined.

The simulation of the electrooptic effect of a Mach-Zehnder interferometric intensity modulator could be done either by considering the spatial variation of the modulation field or by using the uniform field approximation [5]. The uniform field approximation is accurate if its strength is calculated from the overlap interal [6]. The uniform field can also be evaluated at the peak of the optical mode, but the accuracy will be sacrificed. It has been proved that the most computer-efficient method is to incorporate the spatially varying modulation field directly into 2D BPM [5].

5.1.1 Calculation of Electric Field Distribution

In order to understand what effect the electric field generated by the electrodes will have on the refractive index of our waveguides, the distribution of the electric field has to be known. A scheme based on Fourier Series Method has been applied here [7] (program developed by F. Y. Gan in his M.Eng. thesis [1]). The field component and also its first order derivative and second order derivative can be calculated by the following formulae:

$$E_y(x,y) = \sum_{n=1}^{200} n \cdot s(n) \cdot e^{-n\pi k_1 y/R} \cdot sin(\frac{n\pi x}{R}) \cdot (\frac{\pi k_1}{R}) \tag{5.1}$$

$$\frac{dE_y}{dy}\Big|_{(x,y)} = -\sum_{n=1}^{200} n^2 \cdot s(n) \cdot e^{-n\pi k_1 y/R} \cdot sin(\frac{n\pi x}{R}) \cdot (\frac{\pi k_1}{R})^2 \tag{5.2}$$

$$\frac{d^2E_y}{dy^2}\Big|_{(x,y)} = \sum_{n=1}^{200} n^3 \cdot s(n) \cdot e^{-n\pi k_1 y/R} \cdot sin(\frac{n\pi x}{R}) \cdot (\frac{\pi k_1}{R})^3 \tag{5.3}$$

where $R = G_1 + G_2 + W_1 + W_2 + W_3$, W_2 (width of the center electrode) is taken to be $6\mu m$ (the same as that of a single waveguide), $W_1 = W_3 = 100\mu m$, and $G_1 = G_2$ is taken to be $10\mu m$ or $15\mu m$ in later computations. Also, $k_1 = \sqrt{q_x/q_y}$, where $q_x = 43.0$ and $q_y = 28.0$ are two dielectric constants of lithium niobate. The origin of the coordinate is at the very left end of the total width R on the buffer layer and substrate boundary. To incorporate this computation into the effective refractive index calculation where the center of the x axis is at $W_1 + G_1 + W_2 + G_2/2$ away from the very left end of the total width R, some arrangement to shift the coordinate has been made.

The electric field distribution will be substituted into the refractive index expression with external perturbation (see Chapter 2, Eqn. 2.9), and by using the effective index method (also see Chapter2) the effecitve index distribution of the active region will be obtained under a certain center electrode voltage.

5.1.2 Extinction Ratio Evaluation

Based upon the re-modelling of the effective index distribution of the active region (the index distributions in the input, output, taper and branching regions remain the same), the 2D-FD-VBPM method is used once again to simulate beam propagation under a specific modulation voltage. A modulation curve can thus be obtained by changing the voltage from zero to a certain value in steps (it should be a cosine like curve in the end) and the output power percentage corresponding to each discrete voltage value can be calculated. The extinction ratio can be evaluated as:

$$ER = -10log(\frac{Pout_{minimum}}{Pout_{maximum}}) = Loss_{maximum}(dB) - Loss_{minimum}(dB) \qquad (5.4)$$

where the way of ouput power evaluation has been introduced in Section 3.2.1. The maximum power output obviously occurs at zero voltage, and the minimum power output occurs at a certain voltage called the on-off voltage V_π (causes a 180° phase shift between the optical beams in the two branching arms before they re-combine, so that they cancel each other [9]). In order to compare the effects of different seperation widths between two waveguide arms, two seperation values $10\mu m$ and $15\mu m$ have been

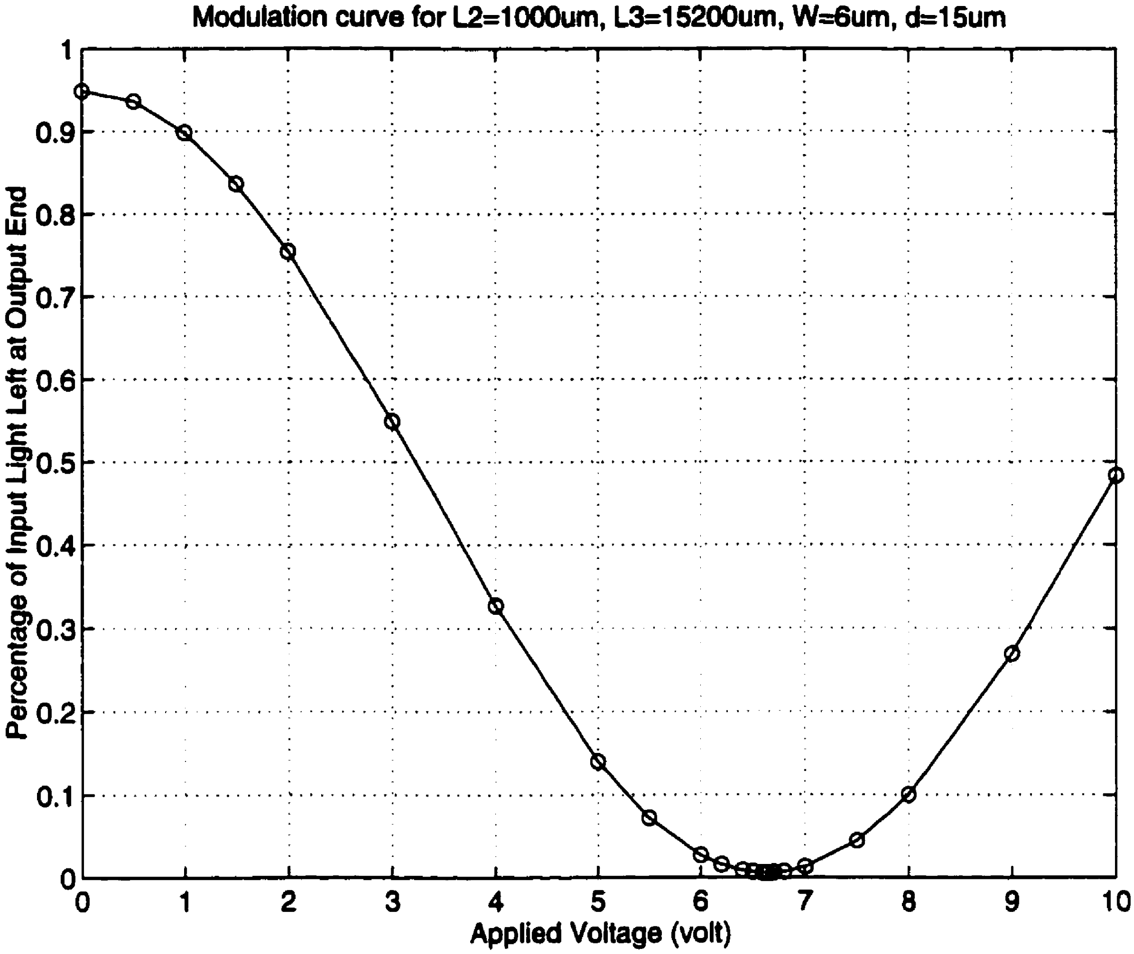

Figure 5.1: Output end percentage of light under different voltages in a conventional Y-branch structure of L1=L5=500 μm, L2=L4=1000 μm, L3=15200 μm, W=6 μm and d=15 μm

chosen in the calculation of the modulation curve. For the structure with a $15\mu m$ gap width, Fig. 5.1 and Fig. 5.2 show the modulation curves in percentage output and in dB loss respectively. Fig. 5.3 is the simulation result of the beam propagation inside this structure. Loss data have been listed in Table 5.1. For the structure with a $10\mu m$ gap width, results are shown in Fig. 5.4 to Fig. 5.6 and Table 5.2.

From the figures, we can see very clearly that for a separation width of $15\mu m$, the modulation depth is very satisfying and the extinction ratio can be seen in Table 5.4 to be as high as 22 dB under a 6.64 volt voltage for an active length of $15200\mu m$ (L_2 =

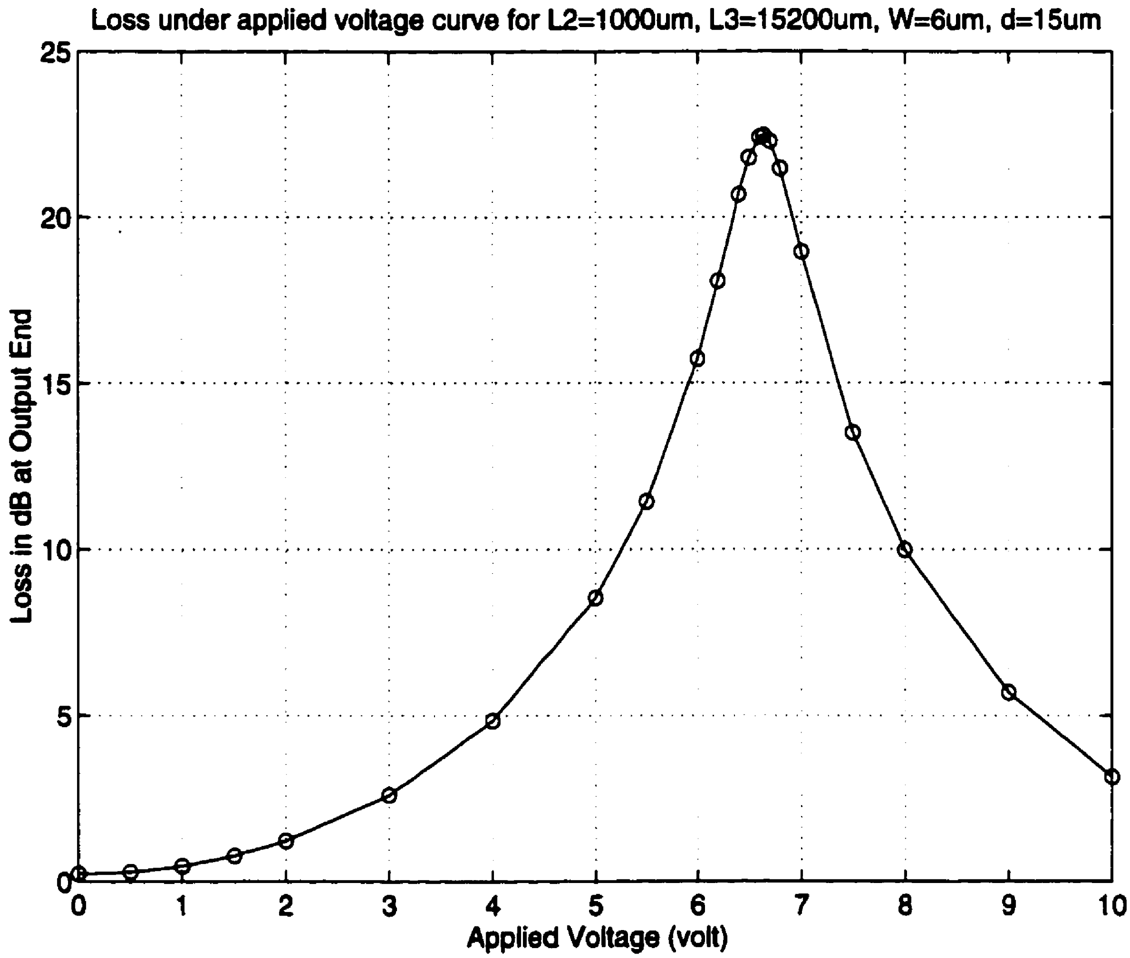

Figure 5.2: Output end loss in dB under different voltages in a conventional Y-branch structure of L1=L5=500 μm, L2=L4=1000 μm, L3=15200 μm, W=6 μm and d=15 μm

Table 5.1: Propagation loss vs. different applied voltages for L1=L5=500 μm, L2=L4=1000 μm, L3=15200 μm, W=6 μm, and d=15 μm, conventional Y-branch structure

Voltage (v)	Output Percentage (P_o/P_i)	Attenuation ($-10log(P_o/P_i)$) (dB)
0.0	0.9488	0.228
0.5	0.9366	0.285
1.0	0.8984	0.466
1.5	0.8366	0.775
2.0	0.7546	1.223
3.0	0.5489	2.605
4.0	0.3273	4.850
5.0	0.1398	8.546
5.5	7.19e-2	11.432
6.0	2.67e-2	15.733
6.2	1.56e-2	18.078
6.4	8.55e-3	20.680
6.5	6.61e-3	21.795
6.6	5.73e-3	22.417
6.64	5.67e-3	22.461
6.7	5.91e-3	22.288
6.8	7.13e-3	21.467
7.0	1.27e-2	18.951
7.5	4.47e-2	13.501
8.0	0.1004	9.981
9.0	0.2699	5.688
10.0	0.4834	3.156

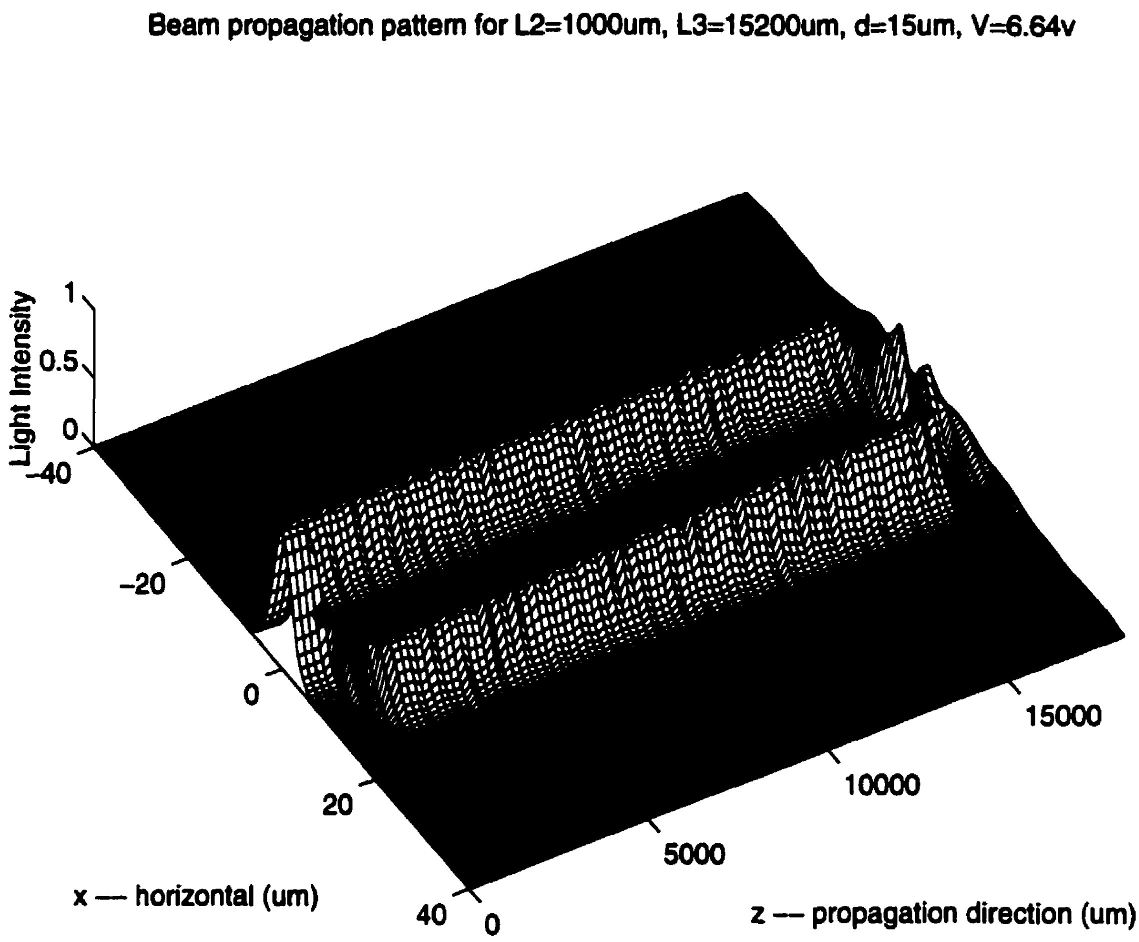

Figure 5.3: Beam propagation loss under 6.64V voltage in a conventional Y-branch structure of L1=L5=500 μm, L2=L4=1000 μm, L3=15200 μm, W=6 μm and d=15 μm

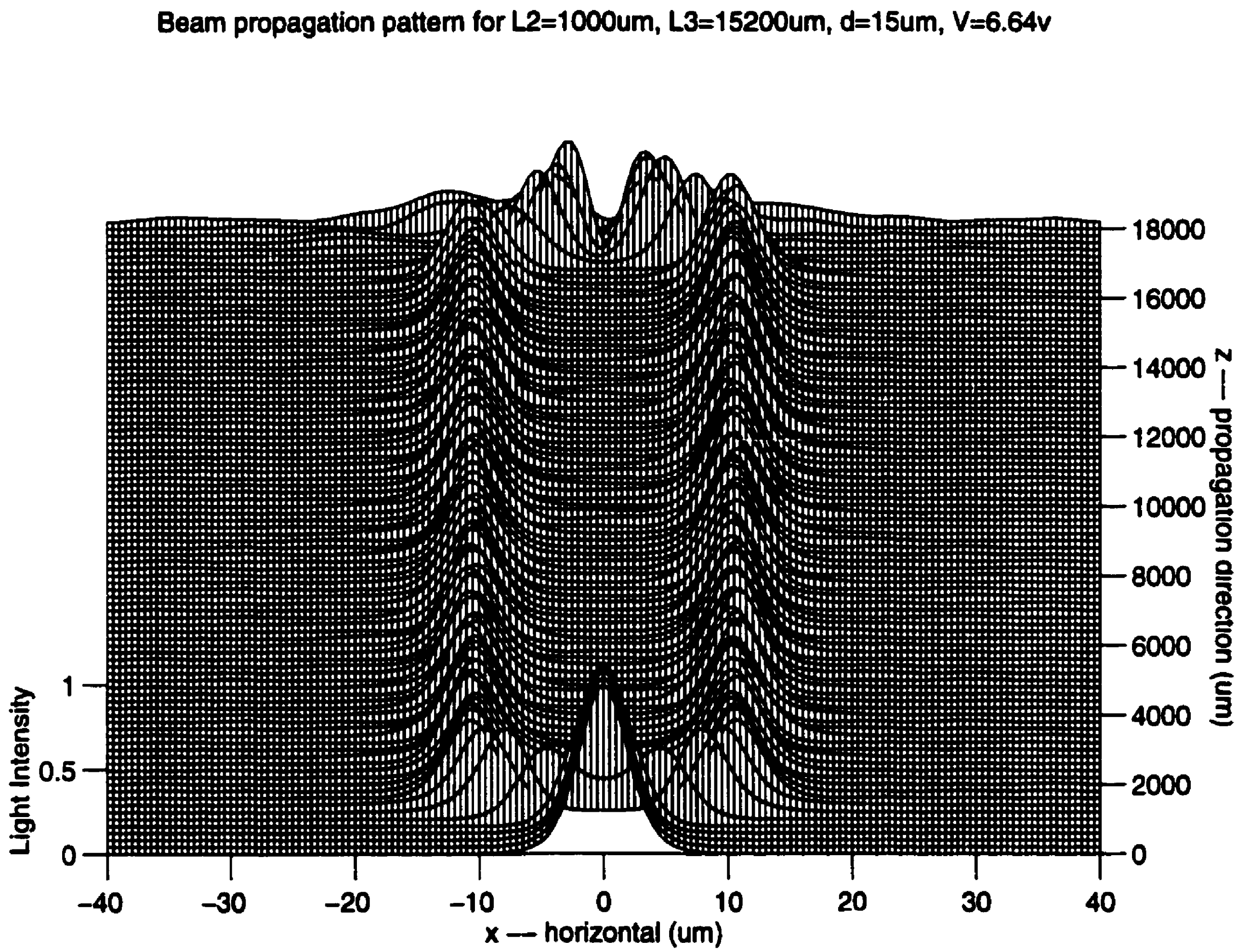

Figure 5.3: continued from the proceding page

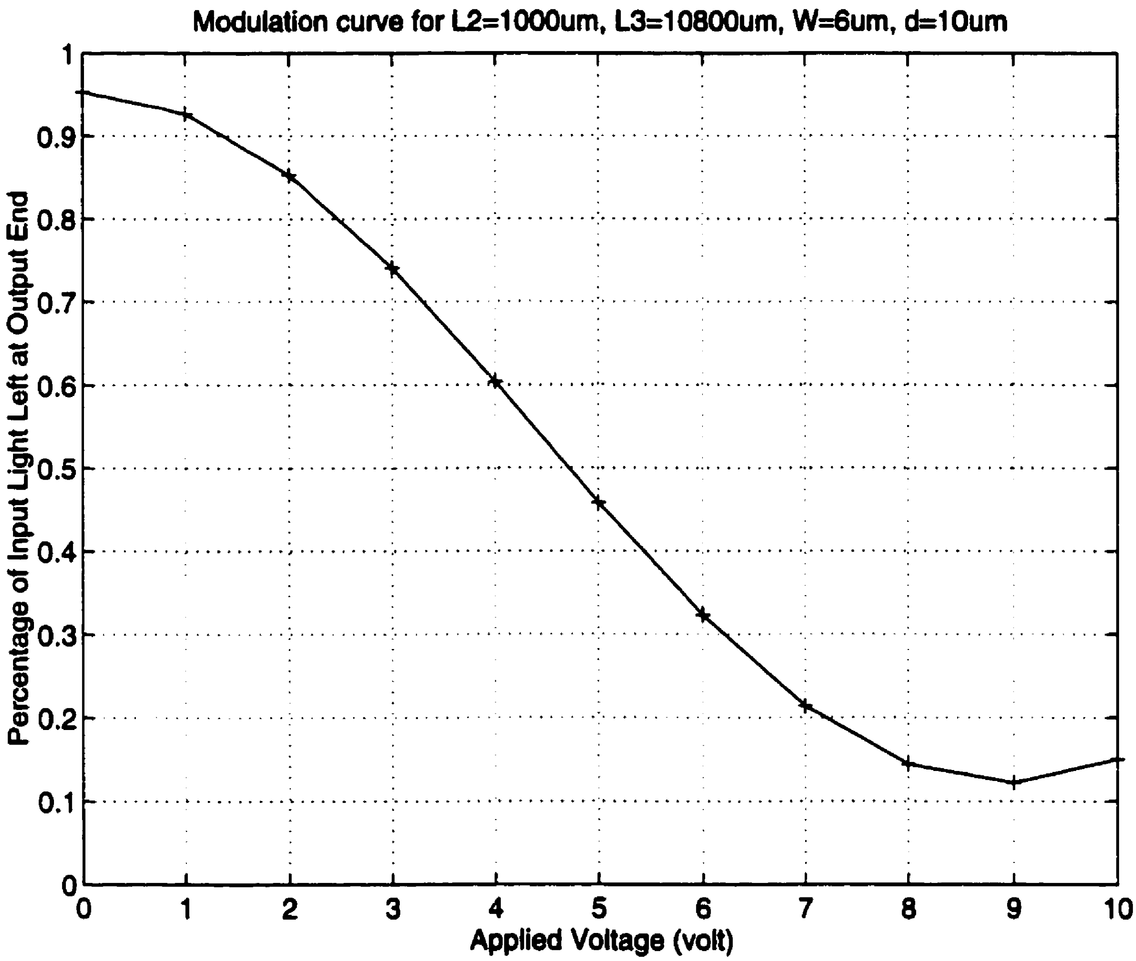

Figure 5.4: Output end percentage of light under different voltages in a conventional Y-branch structure of L1=L5=500 μm, L2=L4=1000 μm, L3=10800 μm, W=6 μm and d=10 μm

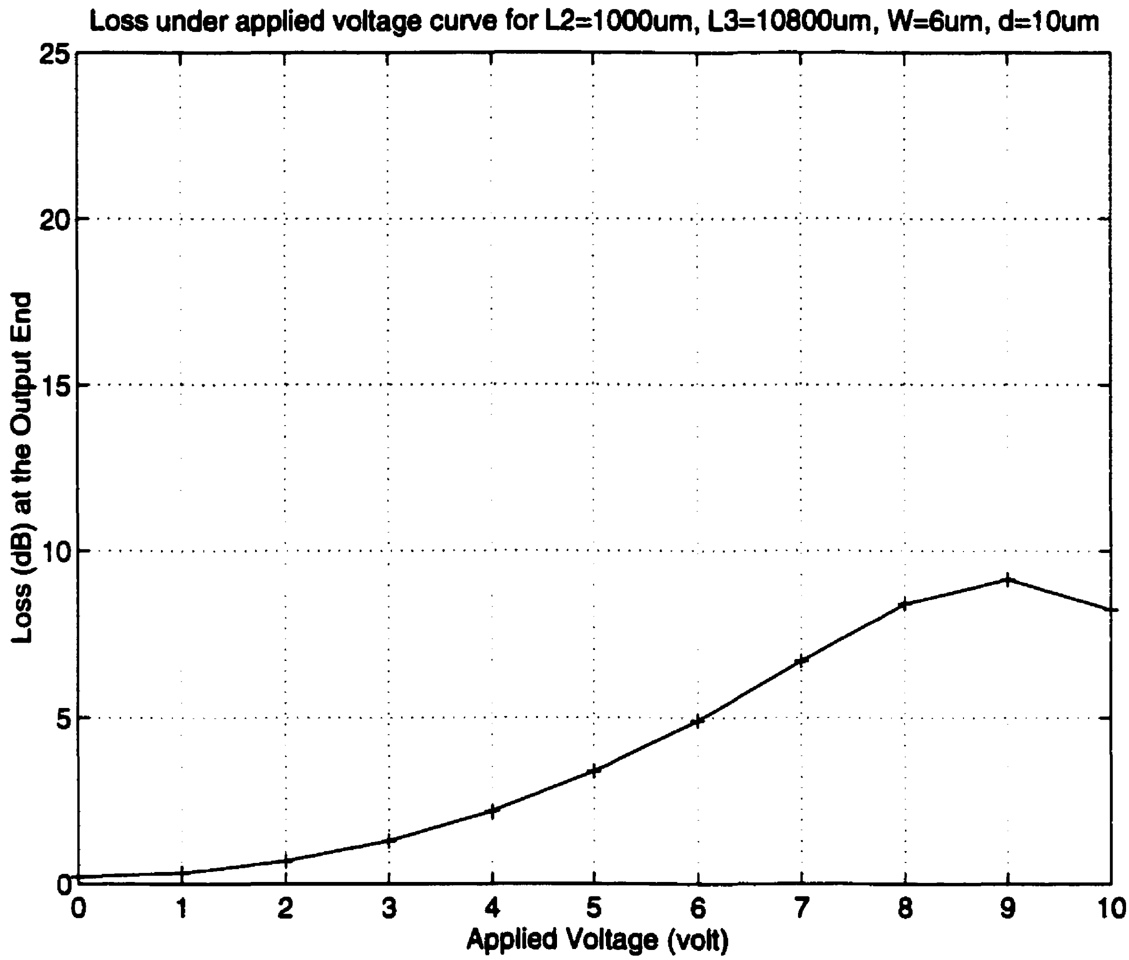

Figure 5.5: Output end loss in dB under different voltages in a structure of L1=L5=500 μm, L2=L4=1000 μm, L3=10800 μm, W=6 μm and d=10 μm

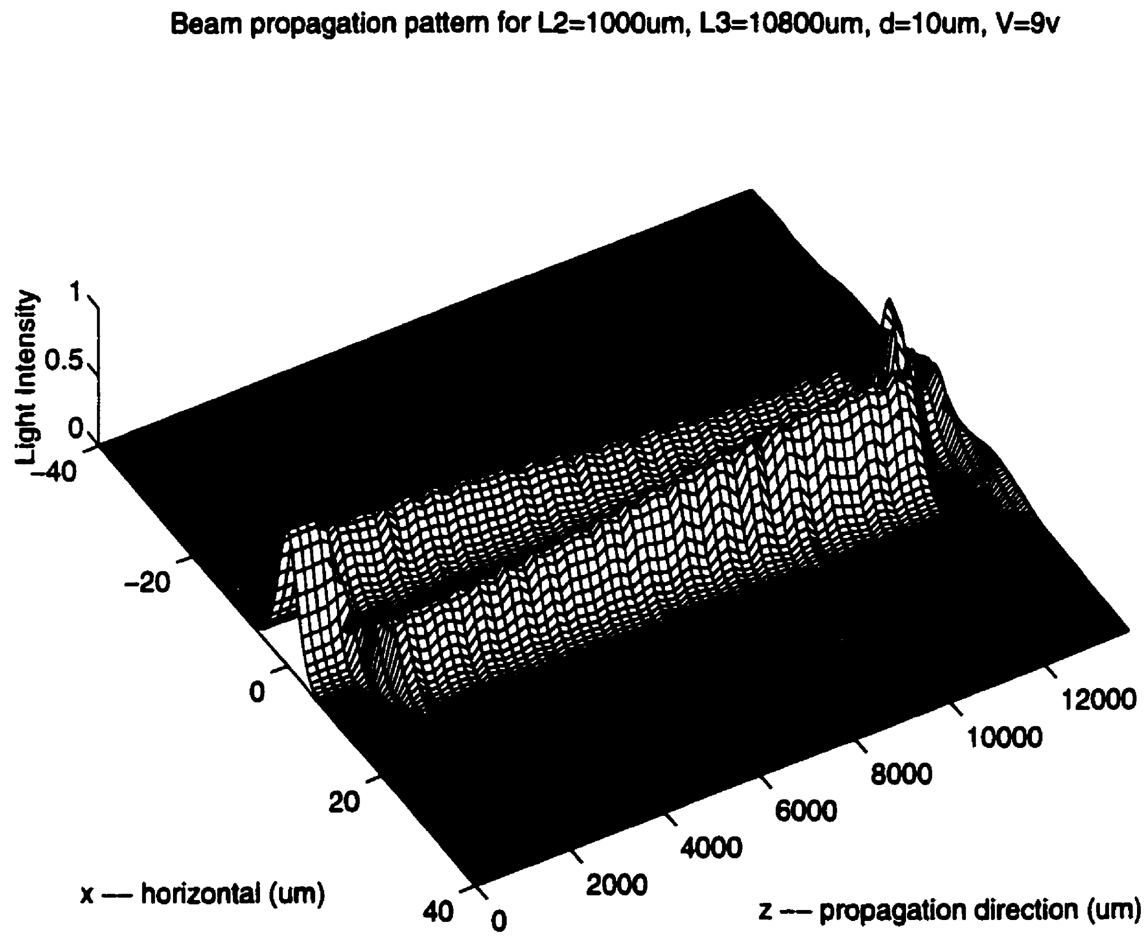

Figure 5.6: Beam propagation ~~poss~~ loss under 9V voltage in a conventional Y-branch structure of L1=L5=500 μm, L2=L4=1000 μm, L3=10800 μm, W=6 μm and d=10 μm

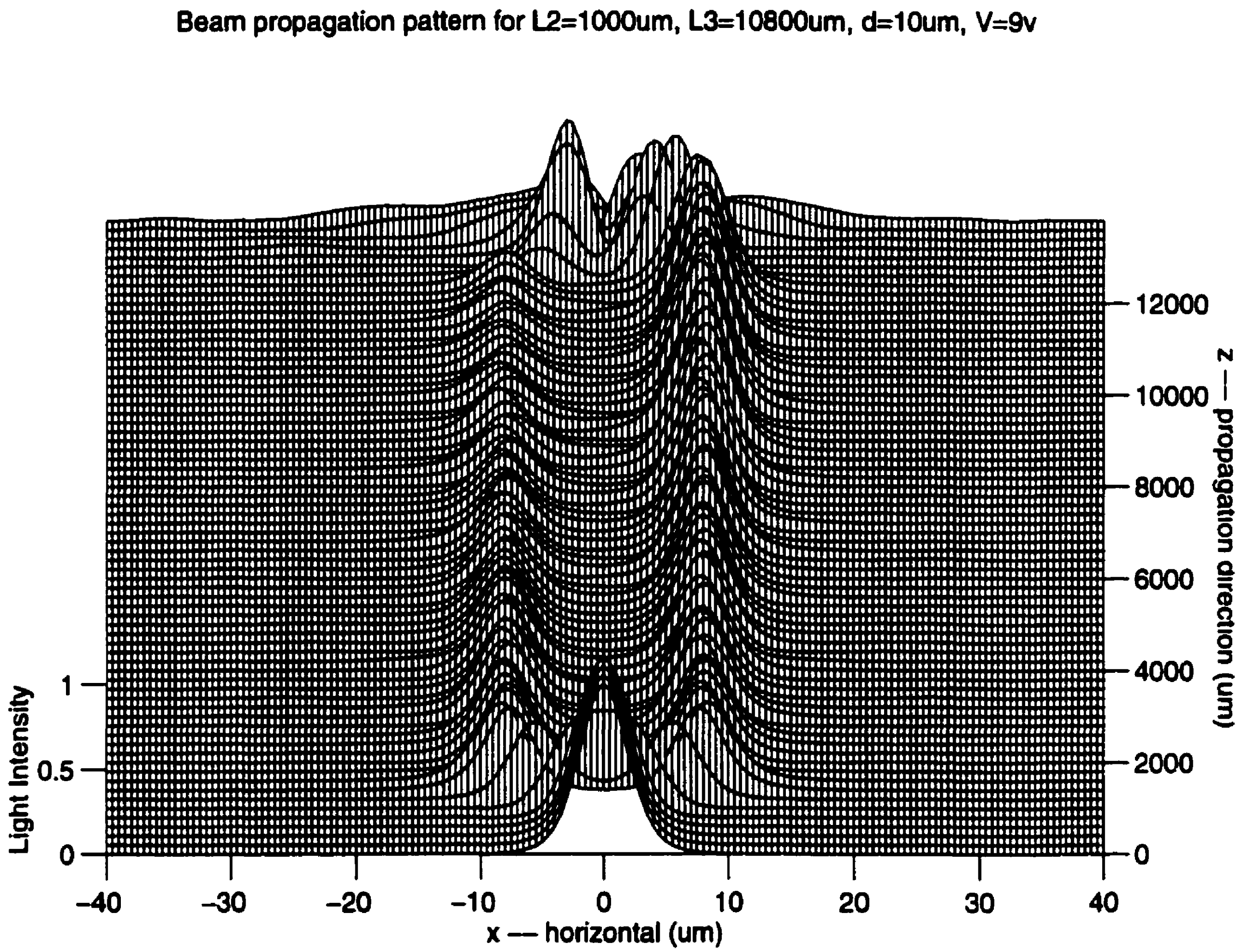

Figure 5.6: continued from the proceding page

Table 5.2: Propagation loss vs. different applied voltages for L1=L5=500 μm, L2=L4=1000 μm, L3=10800 μm, W=6 μm, and d=10 μm, conventional Y-branch structure

Voltage (v)	Output Percentage (P_o/P_i)	Attenuation ($-10log(P_o/P_i)$) (dB)
0.0	0.9531	0.209
1.0	0.9269	0.330
2.0	0.8531	0.690
3.0	0.7407	1.304
4.0	0.6036	2.192
5.0	0.4582	3.389
6.0	0.3230	4.908
7.0	0.2138	6.699
8.0	0.1440	8.418
9.0	0.1218	9.142
10.0	0.1501	8.236

$1000\mu m$, conventional Y-branch structure), while in the 3D visualization figures, there is virtually no significant coupling between the two arms and the cancellation at the output end is complete and clear. On the contrary, for a seperation width of $10\mu m$, the modulation depth is very shallow and the best extinction ratio is less than 10 dB (from Table 5.2, substract the loss at 9.0v by the loss at 0v), while in the 3D figures, there is very obvious coupling from one arm to the other, causing the recombination to be very incomplete.

From these simulation results, such a conclusion can be drawn that to ensure an extinction ratio of at least 20 dB, the seperation between two optical waveguide arms should be at least $15\mu m$. Theoretically, a wider seperation can give a higher extinction ratio, while demanding a higher on-off voltage and thus a higher drive power (which could be very critical), and also larger dimensions of the whole device. Since thereotically an extinction ratio of about 15 dB is generally acceptable [9], taking into consideration of the potential fabrication-induced deterioration, a design value of over 20 dB should be achieved. Based on this consideration, a seperation width of 15 to 20 μm will be reasonable (equal width of the two arms can not be ensured during fabrication and thus measured extinction ratio normally is expected to be worse than the design value).

Compared with the half-wave voltage given in F. Y. Gan's thesis [1], which is around 4.0 v for a similar structure of a $14.7\mu m$ gap width, a $5.9\mu m$ center electrode width and a $14962\mu m$ active length, the on-off voltage obtained by BPM simulation in this report is much higher (6.66 v). A very important reason is that a different approach has been taken in F. Y. Gan's thesis to evaluate the on-off voltage:

$$V_\pi = \frac{g\lambda}{n_e^3 r_{33} \Gamma L_3} \tag{5.5}$$

where g is the gap between electrodes on each optical channel waveguide, L_3 is the active electrode length, λ the optical wavelength, r_{33} and n_e the largest electrooptic coefficient and the extraordinary optical refractive index of $LiNbO_3$, respectively. The most important factor in the above formula is the overlap integral between the optical field and the modulation electric field Γ, whose calculated value heavily depends on the mode sizes w_x and w_y of the optical channel waveguide (Gaussian in x and Hermite-Gaussian in y direction of the optical field has been assumed). In his thesis, $w_x = 5.6$ and $w_y = 4.8\mu m$ have been used. According to results from the literature [10] [11] [12] [13] , a titanium diffused channel guide under the fabrication condition of 5 hours, $1050°C$ and a $6\mu m$ wide $600 - 700nm$ thick titanium strip does not have the above assumed mode sizes. Since relatively large deviation in Γ can be caused by not very large differences in the mode sizes, the difference between the two methods on the on-off voltage is natural because the BPM scheme does not involve the mode size evaluation step. It is estimated that the BPM simulation result may be closer to experimental results, though the 3D to 2D transformation can also cause errors.

5.2 Modulation Curve for the Optimized Notched Y-Branch Structure

In Section 5.1, it has been shown that for conventional Y-branch structures, a seperation between the inner edges of the two branching arms has to be at least $15\mu m$ in order to ensure a design-value of the extinction ratio to be greater than 20 dB. Since in Chapter 4, a notched Y-branch structure with an optimized width of 1.5 μm has been shown to have superior loss performance than a conventional Y-branch structure, it will be a favorite choice for real device fabrication. The modulation curves (one showing the light output percentages, the other showing the corresponding dB values) with external voltages ranging from 0.0 volt to 10.0 volts have been plotted as shown in Fig. 5.7 and Fig. 5.8. Detailed data are included in Table 5.3. The lengths of the waveguide sections (L2=L4=1000 μm, L3=15080 μm, L1=L5=500 μm) have been chosen to give a minimum propagation loss of 0.145 dB without modulation (refer to Table 4.4) for a bandwidth design-value of around 80 GHz.

From Table 5.3, we can observe that the minimum output power occur at a voltage of 6.64-volt which is thus the on-off voltage. By substracting the loss value at zero-voltage from the loss value at 6.64-volt, we can find the extinction ratio to be 21.7 dB for the above design parameters. The modulation curve shown in Fig. 5.7 is actually very much similar to Fig. 5.1 for a conventional Y-branch structure with quasi-optimized longitudinal section-lengths, with similar on-off voltage values and similar extinction ratio values. From this comparison, it is seen that while being able to give a relatively improved loss character, the optimized notched Y-branch structure will not significantly affect the modulation character of a device.

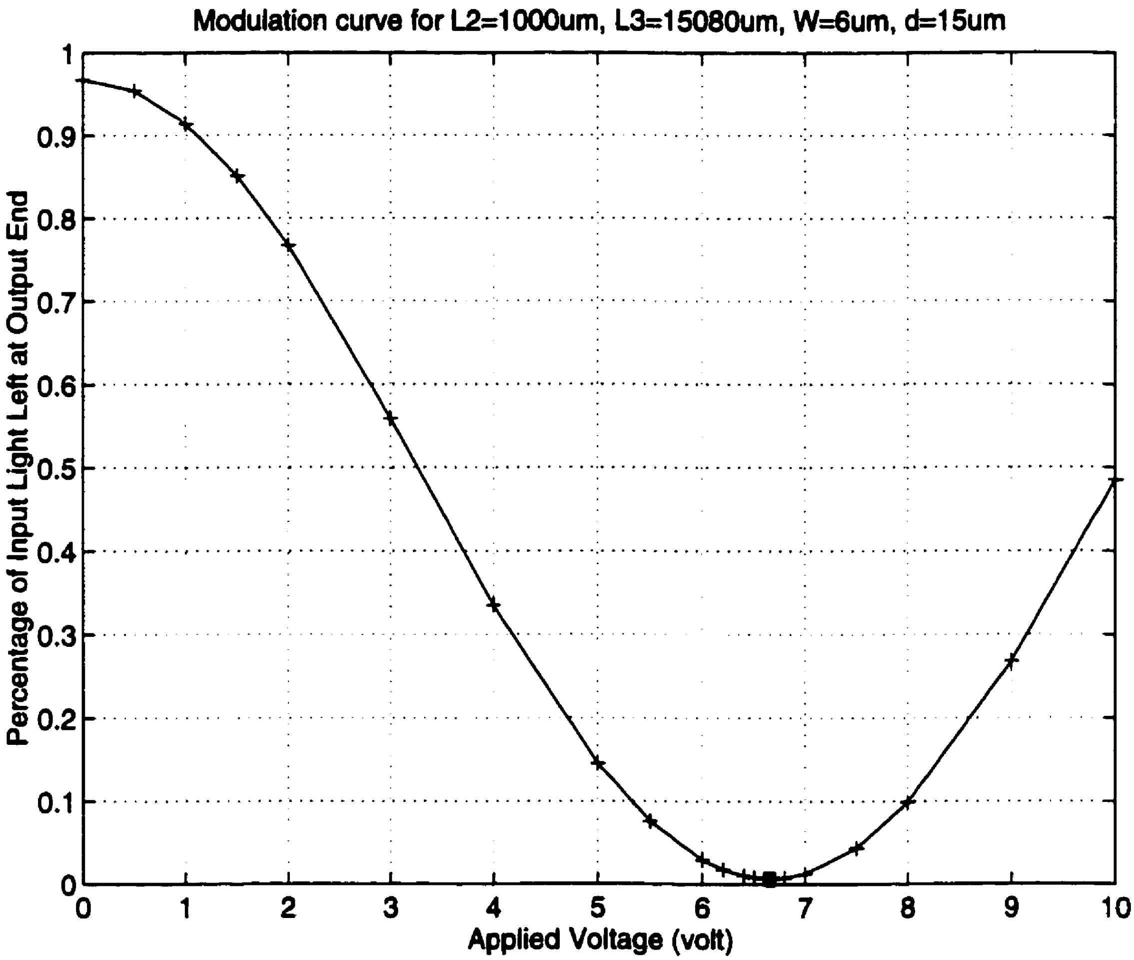

Figure 5.7: Output end percentage of light under different voltages in a 1.5μm wide notched Y-branch structure of L1=L5=500 μm, L2=L4=1000 μm, L3=15080 μm, W=6 μm and d=15 μm

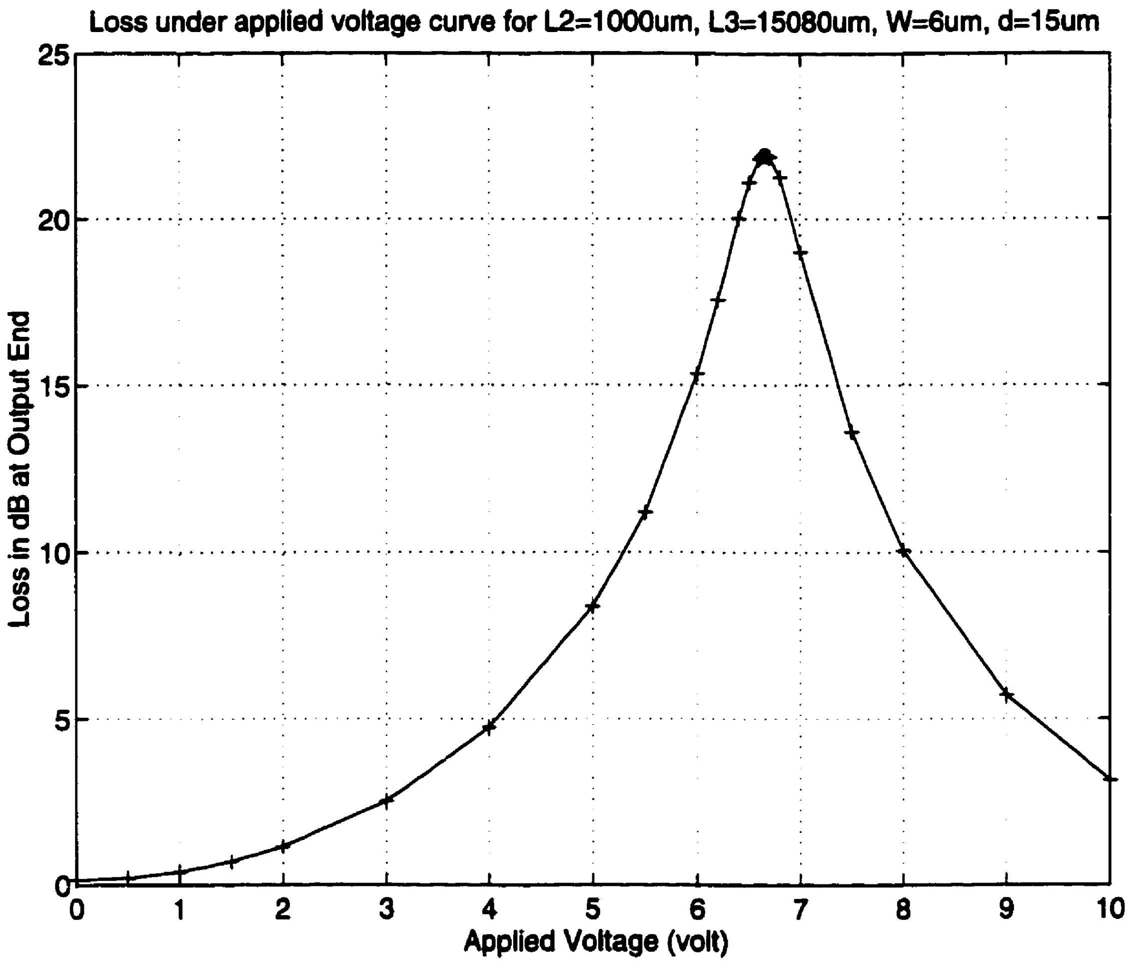

Figure 5.8: Output end loss in dB under different voltages in a 1.5μm wide notched Y-branch structure of L1=L5=500 μm, L2=L4=1000 μm, L3=15080 μm, W=6 μm and d=15 μm

Table 5.3: Propagation loss vs. different applied voltages for $L1 = L5 = 500\mu m$, $L2 = L4 = 1000\mu m$, $L3 = 15080\mu m$, $W = 6\mu m$, and $d = 15\mu m$, notched Y-branch structure with $1.5\mu m$ width

Voltage (v)	Output Percentage (P_o/P_i)	Attenuation ($-10log(P_o/P_i)$) (dB)
0.0	0.967	0.145
0.5	0.954	0.207
1.0	0.914	0.391
1.5	0.851	0.702
2.0	0.767	1.149
3.0	0.559	2.523
4.0	0.335	4.745
5.0	0.145	8.383
5.5	7.58e-2	11.200
6.0	2.92e-2	15.344
6.2	1.75e-2	17.569
6.4	9.93e-3	20.029
6.5	7.73e-3	21.119
6.6	6.58e-3	21.818
6.62	6.48e-3	21.885
6.64	6.42e-3	21.926
6.66	6.40e-3	21.936
6.68	6.43e-3	21.919
6.7	6.50e-3	21.873
6.8	7.47e-3	21.265
7.0	1.26e-2	18.999
7.5	4.35e-2	13.614
8.0	9.86e-2	10.060
9.0	0.268	5.713
10.0	0.485	3.145

5.3 Variation of ER and V_π with Longitudinal Structural Parameters

Considering the possible effect of the coherent coupling of radiation modes on the electro-optical aspect of the device, several different values of the active length have been tried for calculating the corresponding extinction ratio and on/off voltage. Table 5.4 shows the results for a conventional Y-branch and Table 5.4 shows the results for a notched Y-branch. It has been found that the on/off voltage is not affected much and the value of $V_\pi \cdot L_3$ is fairly constant as it should be for both cases. The extinction ratio can go up for certain active length values where the propagation loss also suffers a deterioration. Hence, there is a trade-off between the two parameters due to coherent coupling of radiation modes: for the lowest possible loss, the extinction ratio is the worst; for the best extinction ratio, the propagation loss is the worst.

Different taper/branching lengths have also been tried ($L_2 = 800\mu m, 2000\mu m$). Similar results as reported above have been obtained (see Table 5.6) showing that the shorter the active length L3, the higher the on-off voltage; the higher the loss without an electric field, the higher the extinction ratio for a specific active length.

This result is somewhat different from that reported in [14] (In that paper, it was found that by carefully chosing the length of the active region and the taper/branching region, a low on-off voltage as well as a short length can be achieved. This is an abnormal phenomenon.) probably because it was a *GaAs* step-index structure being studied (also a M-Z modulator) in that paper which has different performance than titanium-diffused gradient-index waveguide in lithium niobate studied here.

Table 5.4: Variation of on-off voltage (V_π) and extinction ratio (ER) for different active lengths (L_3) of a conventional Y-branch with L_2=1000 μm, W=6 μm and d=15 μm, $2\theta = 1.2°$

L_3 (μm)	V_π (volt)	ON loss (dB)	OFF loss (dB)	ER (dB)	$V_\pi \cdot L_3$
14600	6.88	0.207	21.872	21.665	100448
14640	6.88	0.186	22.055	21.869	100723
14860	6.70	0.531	26.212	25.681	99562
15100	6.64	0.182	21.548	21.366	100928
15200	6.64	0.228	22.461	22.233	100566

Table 5.5: Variation of on-off voltage (V_π) and extinction ratio (ER) for different active lengths (L_3) of a notched (notch width 1.5 μm) Y-branch with L_2=1000 μm, W=6 μm and d=15 μm, $2\theta = 1.2°$

L_3 (μm)	V_π (volt)	ON loss (dB)	OFF loss (dB)	ER (dB)	$V_\pi \cdot L_3$
14620	6.88	0.179	22.836	22.657	100586
14840	6.72	0.382	25.114	24.732	99725
15080	6.66	0.145	21.936	21.791	100433

Table 5.6: Variation of on-off voltage (V_π) and extinction ratio (ER) for different active lengths (L_3) of conventional Y-branches with $L_2 = 800\mu m$ and $L_2 = 2000\mu m$, d=15 μm, W=6 μm

L_2 (μm)	L_3 (μm)	V_π (volt)	ON loss (dB)	OFF loss (dB)	ER (dB)	$V_\pi \cdot L_3$
800	14760	6.84	0.288	19.171	18.883	100958
800	15080	6.66	0.984	27.566	26.582	100433
2000	14880	6.76	0.033	21.838	21.805	100589
2000	15200	6.60	0.203	24.113	23.910	100320

5.4 Comparison of Two Types of Electrode Structures

A structure with a wide center electrode and a narrow gap has also been design-tested in comparison with the above structure with a narrow center electrode and a wide gap. Fig. 5.9 shows a schematic diagram of a wide center electrode structure. Table 5.7 shows that the increase of the width of the center electrode (the gap width decreases to ensure that the width of the center electrode plus the total width of the two gaps remain the same which is $36\mu m$) has very little effect on the on/off voltage and virtually no effect on the extinction ratio. This means that there is little difference between the efficiency of a wide center electrode and narrow gap structure and that of a narrow center electrode and wide gap structure in the active region. The latter one is more promising and should be employed because a 50 Ω characteristic impedance can be achieved which is very important in obtaining a wide bandwidth [3].

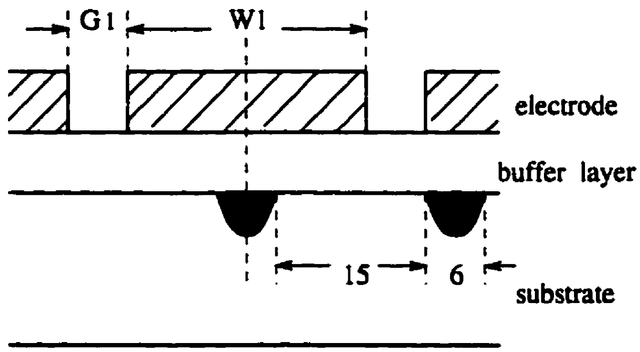

Figure 5.9: Schematic diagram of a wide center electrode narrow gap electrode stucture

5.5 Tolerance Study on the Electrode/Waveguide Alignment

We know that the design simulation process will serve as a good simulation and provide accurate guidance for real fabricaiton. Since during fabrication there will inevitably exist some misalignment between the optical waveguide and the traveling-wave electrodes from ideal designs when aluminum or gold electrodes are deposited, it is necessary to explore the tolerance of the alignment to make the design work complete.

Fig. 5.10 shows a certain shift δ from the ideal alignment between the waveguide and the electrodes (for a narrow center electrode structure only: one waveguide arm underneath the center electrode sharing the same symmetry axis (see the dotted line in Fig. 5.10), the other waveguide arm underneath the right-side ground electrode with their inner edges aligned). The value of δ can be either positive or negative. Several values have been tested ranging from -2 to +2 μm. Table 5.8 shows that the tolerance of alignment is around 1 to 2 microns for a 6 micron wide waveguide and center electrode to ensure no significant rise in the on/off voltage and drive power. The extinction ratio almost does not change at all even for a large shift. This result coincide well with that reported in [3] when the buffer layer is sufficiently thick. For a $\pm 2\mu m$ misalignment, we can see that the on-off voltage will increase by about 0.8 volt.

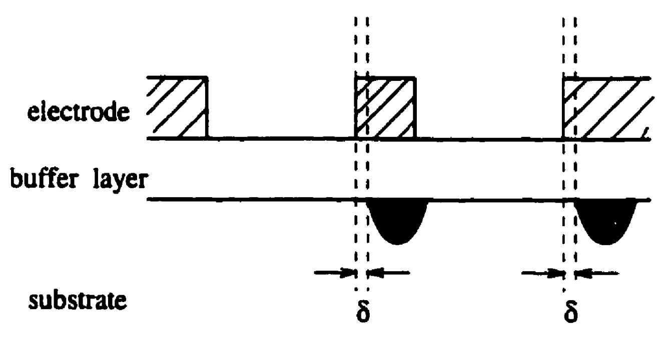

Figure 5.10: Schematic diagram of the mis-alignment between electrodes and waveguides

As a conclusion, we can predict based on the above simulation results that during the fabrication process, some misalignment between the optical waveguide and the deposited electrodes can be tolerated as long as the shift is within $\pm 1\mu m$ range.

Table 5.7: Effect on on-off voltage and extinction ratio of different central electrode widths and gaps (total width of central electrode and two gaps remains the same)

Central Electrode Width (μm)	Gap Width (μm)	V_π (volt)	ER (dB)
6	15	6.66	22.233
12	12	6.22	22.432
16	10	6.30	22.558

Table 5.8: Effect on on-off voltage and extinction ratio of different alignment shifts between electrodes and waveguides; waveguide dimensions: W=6μm, d=15μm, L_2=1000μm and L_3=15200μm

Alignment Shift δ (μm)	V_π (volt)	ER (dB)
0	6.66	22.233
1	6.80	22.225
2	7.38	22.228
-1	6.84	22.246
-2	7.50	22.271

Bibliography

[1] F. Y. Gan, *Traveling Wave Electrode Design For High Speed $LiNbO_3$ Intensity Modulators*, Master's Thesis, McGill University, 1996

[2] P. Danielsen, "Two–Dimentional Propagating Beam Analysis of an Electrooptic Waveguide Modulator", *IEEE J. of Quantum Electronics*, Vol. QE–20, No. 9, pp. 1093–1097, 1984

[3] N. Zhu and Z. Wang, "Comparison of two coplanar waveguide electrodes for $Ti : LiNbO_3$ interferometric modulators", *Optical and Quantum Electronics*, Vol. 67, pp. 607–615, 1995

[4] M. Rangaraj, T. Hosoi and M. Kondo, "A Wide-Band $Ti : LiNbO_3$ Optical Modulator with a Conventional Coplanar Waveguide Type Electrode", *IEEE Photonics Technology Letters*, Vol. 4, No. 9, pp. 1020–1022, 1992

[5] F. S. Chu and P. L. Liu, "Simulation of $Ti : LiNbO_3$ Waveguide Modulators — A Comparison of Simulation Techniques", *J. of Lightwave Tech.*, Vol. 8, No. 10, pp. 1492–1496, 1990

[6] C. M. Kim and R. V. Ramaswamy, "Overlap Integral Factors in Integrated Optic Modulators and Switches", *Journal of Lightwave Technology*, Vol. 7, No. 7, pp. 1063–1070, 1989

[7] W. Boyu, X. Guangjun and J. Xiaomin, "Travelling wave electrode optimization for high speed electro-optic modulators using the Fourier series method", *IEE Proc. -Optoelectron.*, Vol. 141, No. 6, pp. 381–390, 1994

[8] H. Jin, M. Belanger and Z. Jakubczyk, "General Analysis of Electrodes in Integrated-Optics Electrooptic Devices", *IEEE Journal of Quantum Electronics*, Vol. 27, No. 2, pp. 243–251, 1991

[9] R. C. Alferness, "Waveguide Electrooptic Modulators," *IEEE Transactions on Microwave Theory and Techniques*, vol. MTT–30, No. 8, pp. 1121–1137, 1982

[10] S. K. Korotky, *et al.*, "Mode Size and Method for Estimating the Propagation Constant of Single-Mode $Ti : LiNbO_3$ Strip Waveguides", *IEEE Journal of Quantum Electronics*, Vol. QE-18, No. 10, pp. 1796–1801, 1982

[11] R. Alferness, *et al.*, "Efficient Single-Mode Fiber to Titanium Diffused Lithium Niobate Waveguide Coupling for $\lambda = 1.32\mu m$", *IEEE Journal of Quantum Electronics*, Vol. QE-18, No. 10, pp. 1087–1813, 1982

[12] Haeyang Chung, William S. C. Chang, Eric L. Adler, "Modeling and Optimization of Traveling-Wave $LiNbO_3$ Interferometric Modulators," *IEEE J. of Quantum Electronics*, vol. 27, no. 3, pp. 608–617, 1991

[13] P. G. Suchoski and R. V. Ramaswamy, "Minimum–Mode–Size Low–loss T_i : $L_iN_bO_3$ Channel Waveguides for Efficient Modulator Operation at 1.3 μm", *IEEE Journal of Quantum Electronics*, Vol. QE–23, No. 10, pp. 1673–1679, 1987

[14] D. A. M. Khalil and S. Tedjini, "Coherent Coupling of Radiation Modes in Mach-Zehnder Electrooptic Modulators", *IEEE Journal of Quantum Electronics*, Vol. 28, No. 5, pp. 1236–1238, 1992

Chapter 6

Conclusion

To combine with the traveling-wave electrode design done previously in our laboratory to form a complete device design for high speed $Ti : LiNbO_3$ Mach-Zehnder electro-optical intensity modulators in long-haul wide-band optical fiber communication system applications, two major characteristics of the Y-branch Mach-Zehnder optical waveguide of such a device have been studied, namely the propagation loss and the extinction ratio under modulation, and optimization of structural parameters has been tried (in terms of each section length of the waveguide and under the condition that drive voltage is restricted to 6 to 7 volts which determines the 15 μm seperation between the two arms) in this paper.

The effective-index method combined with a 2D finite-difference beam propagation method have been used for the device simulation and proved effective. The refractive index distribution of the conventional Y-branch channel waveguide has first been modelled in a way that the values are continuous along the longitudinal direction (Instead of using one expression for function $g(x)$ for both the taper region and the branching region, two different expressions have been used. See Eqn. 2.11 and Eqn. 2.12 for reference.) and the effective-index distribution obtained for different sections of the device with and without an electric field. Aiming at reducing the propagation loss while keeping a short overall device length, the coherent coupling effect of radiation modes have been studied. By deliberately selecting both the length of the active region and the length of the taper/branching region, even for a conventional sharp-bend Y-branch structure, a propagation loss due to the axial variation of the waveguide of lower than 0.2 dB can be achieved for a length in the active region of around 1.5 cm and an overall length of around 1.8 cm. With a thickness of electrode and that of the buffer layer of 10 μm and 1.2 μm, respectively, a bandwidth of about 80 GHz can be achieved according to the electrode design. This non-classical scheme does not involve any geometric change in the structure nor any requirement for a two-step-fabrication, in comparison with the loss improvement methods that have been reviewed.

To further reduce the loss and stabilize the beat between the guided-mode and radiation modes, a notched Y-branch should be used in combination with the coherent coupling effect, which can result in a loss value of about 0.15 dB for a 1000 μm taper/branching region. Further, this structure helps to reduce the beating between guided modes and radiation modes and make the loss curve less sensitive to the change in the length in the active region. The key factor in the design of a notched structure is the optimization of the width of the notch. The widely used cosine-generated Y-branch has been proved to have a negative effect for our specific waveguide device, due to the constant change of the wave path in the branching region, leading to an increase in the number of radiation modes. Depending on the requirement of real application, more complicated loss reduction methods can be used to further improve the loss character of the device (refer to Section 4.1).

By increasing the modulation voltage and monitoring the output power, a modulation curve can be obtained from which we can get both the extinction ratio and the on-off voltage information. To get an extinction ratio of over 20 dB needed for practical applications while taking into consideration the fabrication tolerance, an inner edge seperation between the two waveguide arms at the active region has to be greater than 15 μm which can effectively prevent coupling. A larger seperation can result in a higher extinction ratio, but the drive-power requirement has to be increased correspondingly. The on-off voltage obtained will easily differ from the values predicted by estimating the overlap integral of the electric and the optical fields because the latter method is very sensitive to the mode sizes which can not be decided very accurately from the waveguide fabrication conditions. The abnormal effect of varying the active-region length and taper/branching length on the variation of the on/off voltage (i.e., getting a lower value of on/off voltage while reducing the length) which has been reported in other publications has not been observed in the simulations. It has also been established that there is virtually no difference in the resulting extinction ratio and on/off voltage values whether a narrow center electrode/wide gap electrode structure or a wide center electrode/narrow gap electrode structure is used. There is reasonable tolerance in the misalignment between the optical waveguide and the electrodes.

For future work, of course the experimental realization of a $Ti : LiNbO_3$ Mach-Zehnder interferometric intensity modulator should be done based upon both the electrode design and the optical waveguide design. To achieve certain specifications of a device, some parameter modifications and recalculations may be needed. After the device is fabricated, its bandwidth, drive power, insertion loss, extinction ratio and on-off voltage have to be measured in order to compare with the predicted design values to verify the effectiveness and accuracy of the initial design works. Since inevitably there are certain assumptions and approximations in the original design, it will be important to further improve the simulation process based on the experimental experience. For example, the effectiveness of BPM method in predicting the on-off voltage needs to be tested and see whether it should be used to replace the traditional overlap integral approach. For a device to be packed and function stably, some times its temperature characteristic has also to be taken into consideration because the DC drift of the bias point caused by an ambient temperature change (introduced mainly by the microwave source) can affect the modulation characteristics. Accessary temperature control can be added if necessary. During the fabrication process, the realization of a thick buffer layer and electrodes can also consume some effort and the limitations in the fabrication techniques may eventually make modifications to the original design parameters inevitable.